INFORMATION TO USERS

This manuscript has been reproduced from the microfilm master. UMI films the text directly from the original or copy submitted. Thus, some thesis and dissertation copies are in typewriter face, while others may be from any type of computer printer.

The quality of this reproduction is dependent upon the quality of the copy submitted. Broken or indistinct print, colored or poor quality illustrations and photographs, print bleedthrough, substandard margins, and improper alignment can adversely affect reproduction.

In the unlikely event that the author did not send UMI a complete manuscript and there are missing pages, these will be noted. Also, if unauthorized copyright material had to be removed, a note will indicate the deletion.

Oversize materials (e.g., maps, drawings, charts) are reproduced by sectioning the original, beginning at the upper left-hand corner and continuing from left to right in equal sections with small overlaps.

Photographs included in the original manuscript have been reproduced xerographically in this copy. Higher quality 6" x 9" black and white photographic prints are available for any photographs or illustrations appearing in this copy for an additional charge. Contact UMI directly to order.

Bell & Howell Information and Learning
300 North Zeeb Road, Ann Arbor, MI 48106-1346 USA
800-521-0600

Université d'Ottawa · University of Ottawa

Studies with B6-Cast Congenic Mice Bearing Mid-to-Distal Chromosome 7 Genes that Confer Resistance to Obesity: Mechanisms Involved

Manon Danielle Gagné

Thesis submitted to the Department of Biochemistry, Microbiology and Immunology in partial fulfillment of the requirements for the degree of Master of Science

Department of Biochemistry, Microbiology and Immunology
Faculty of Medicine
University of Ottawa
Ottawa, Ontario, Canada
June, 1999

ABSTRACT

The congenic mouse model studied herein is a mouse lineage in which a 26cM chromosomal segment on mid-to-distal chromosome 7, including the UCP2 and UCP3 genes from *Mus Castaneous* has been bred into the C57BL/6J background. The resulting congenic mice remain lean on a high fat diet. Control C57BL/6J mice on the same diet become almost twice as fat as the congenic mice. It was postulated that protection from obesity development could be due to functional differences in the UCP2 and/or UCP3 mapping in this region. The overall objective was to determine the metabolic basis for the observed differential susceptibility to fat deposition between congenic and control mice fed a high fat diet. We examined aspects of both energy intake and energy expenditure. Three separate studies were conducted with three sets of congenic and control mice. In the first study, the mice were fed a normal chow diet for 4.5 weeks. In the second and third studies they were fed a high fat diet for 6 weeks. Average daily energy intake was found to be similar in both groups of mice both on the normal chow diet and on the high fat diet. While the body weights of both groups remained fairly constant on the normal chow diet, high fat fed control mice gained significantly more body weight than congenic mice on the same diet. The metabolic efficiency (weight gain per unit of dietary energy ingested) of control mice is estimated to be nearly four fold greater than that of congenic mice. Indirect calorimetry assessments of resting metabolic rates and respiratory exchange ratios failed to reveal any significant differences between the two groups of mice fed either diet. Although total 24 hour energy expenditure and total 24 hour fasting energy expenditure of congenic and control mice fed a normal chow diet also failed to show differences between the two groups, these same analyses may reveal differences when the

mice are fed a high fat diet. These assessments are still underway in our laboratory. The presence of UCP2 and UCP3 in the congenic segment, two proteins that uncouple oxidative phosphorylation, led us to hypothesize that perhaps allelic variations in the *Ucp2* and/or *Ucp3* genes could be responsible for the decreased adiposity of the congenic mice. Top down elasticity analyses were thus conducted to examine possible differences in the putative function of these uncoupling proteins. The kinetics of the proton leak in skeletal muscle mitochondria were thereby examined. Experiments involving simultaneous measurements of mitochondrial oxygen consumption (with a Clarke-type oxygen electrode) and protonmotive force (using a $TPMP^+$-sensitive electrode) were performed. Although none of the three studies revealed a net increase in maximal proton leak-dependent oxygen consumption (*i.e.*, State 4 respiration) in congenic mice as compared to control mice, removing the BSA from the incubation conditions in the third study unveiled differences in the overall kinetics of the leak between the two groups. While these differences are significant, it is impossible to state unequivocally that they are sufficient to explain the resistance to obesity seen in the congenic mice. Other genes within the region of the congenic segment may contribute to the observed phenotype.

DEDICATION

This thesis is dedicated to my family and friends who have been there with me and for me throughout the years.

ACKNOWLEDGEMENTS

I would like to offer my thanks and appreciation to all of those who have contributed to the successful completion of this work and who have made my days here so enjoyable and memorable.

First and foremost, to my supervisor Dr. Mary-Ellen Harper for her never ending support, knowledge, optimism, assistance and guidance in every possible way

To the members of my advisory committee, Drs. Jean Himms-Hagen, and Alvin Chan for their helpful thoughts, advice and enlightening discussions

To Linda Jui for her technical assistance and for producing the wonderful histological work presented in this thesis

To Dr. Anna Melnyk for her advice and expertise, and for her patience in teaching me the ins and outs of Western blotting

To all past and present members of the Harper and Himms-Hagen labs, in particular Andreas Antoniou for their helping hand in the day to day activities, and for the necessary diversions

A very special thank you to Shadi Monemdjou, for her continuing help in the lab and for good times and comic relief, but most of all for her friendship during these past few years

My appreciation to Julie Normand, Joanne Barlow and Crystal Perry for their constant enthusiasm and administrative support over the years

I also wish to express my gratitude to the National Science and Engineering Research Council of Canada for financial support during my studies

Finally, I would like to thank Jeremy for his incessant support and encouragement, and for always putting up with the demands and circumstances of the student life.

It was greatly appreciated.

Thank you!!!

TABLE OF CONTENTS

LIST OF TABLES

LIST OF FIGURES

LIST OF ABBREVIATIONS

Symbols

~	approximately
$\Delta\Psi_m$	mitochondrial membrane potential
$\Delta\Psi_P$	plasma membrane potential
Δp	mitochondrial protonmotive force
ΔpH	pH gradient
ϵ	elasticity
°C	degrees Celsius
µCi	microcurie
µg	microgram
µL	microlitre
µm (filter)	micrometre
µM	micromole/litre

A

a_m	apparent mitochondrial $TPMP^+$ activity coefficient
Ab	antibody
ADP	adenosine 5'-diphosphate
Ag	antigen
ANOVA	analysis of variance
ATP	adenosine 5'-triphosphate

B

B6	C57BL/6J control mice
B6-CAST	B6 mice with a distal Chr. 7 CAST segment – congenic mice
BAT	brown adipose tissue
BMR	basal metabolic rate
bp	base pairs
BSA	bovine serum albumin
BWt	body weight

C

C	control coefficient
cAMP	adenosine 3',5'-cyclic monophosphate
$CaCl_2$	calcium chloride
CAST/Ei	Mus castaneous mouse strain
Chr.	chromosome
cm	centimetre
cM	centimorgan
CO_2	carbon dioxide
$CuSO_4 \cdot 5H_2O$	copper sulphate
C.V.	calorific value

D

DAB	3,3'-diaminobenzidine tetrahydrochloride

ddH_2O	deionized distilled water
DIO	diet-induced obesity
$DiOC_6$	3,3'-dihexyloxacarbocyanine iodide
DIT	diet-induced thermogenesis
DNA	deoxyribonucleic acid
dpm	disintegrations per min
E	
ECL	enhanced chemiluminescence
EDTA	ethylenediamine tetraacetic acid
EGTA	ethylene glycol-bis (β-aminoethyl ether) tetraacetic acid
EpiWAT	epididymal white adipose tissue
F	
f.c.	final concentration
FCCP	carbonyl cyanide p-trifluoromethoxyphenylhydrazone
FFA	free fatty acids
G	
g	centrifugal force
g	gram
GDP	guanine 5'-diphosphate
GTP	guanine 5'-triphosphate
H	
H&E	haematoxylin and eosin staining
h	hour
H_20_2	hydrogen peroxide
HCl	hydrocholoric acid
HEPES	N-2-hydroxyethylpiperazine-N'-2-ethanesulphonic acid
HF	high fat
hr	hour
I	
IBAT	interscapular brown adipose tissue
IgG	immunoglobulin G
IngWAT	inguinal white adipose tissue
J	
JAX	Jackson Laboratories
K	
$K_2C_4H_4O_6$	potassium tartrate
K_2HPO_4	dipotassium phosphate
kb	kilobase
kcal	kilocalorie
KCl	potassium chloride
kDa	kilodalton
KH_2PO_4	potassium dihydrogen orthophosphate
KI	potassium iodide
KOH	potassium hydroxide

L	
LBM	lean body mass
LiCl	lithium chloride
LiOH	lithium hydroxide
log	logarithm (base 10)
M	
M	mol/litre
MCA	metabolic control analysis
mg	milligram
$MgSO_4 \cdot 7H_2O$	magnesium sulphate
MIM	mitochondrial inner membrane
min	minute
mL	millilitre
mm	millimetre
mM	millimole/litre
mol	mole
mRNA	messenger ribonucleic acid
mtDNA	mitochondrial deoxyribonucleic acid
mV	millivolt
MV	mitochondrial matrix volume
N	
Na_2EDTA	ethylenediamine tetraacetic acid (disodium salt)
Na_2HPO_4	di-sodium hydrogen orthophosphate
NaCl	sodium chloride
NAD	nicotinamide dinucleotide
$NaHCO_3$	sodium carbonate
NaOH	sodium hydroxide
NCM	nitrocellulose membrane
NEFA	non-esterified fatty acids
ng	nanogram
$NiCl_2$	nickel chloride
NIDDM	non-insulin dependent diabetes mellitus
nm	nanometre
NST	non-shivering thermogensis
nuDNA	nuclear deoxyribonucleic acid
O	
O	monoatomic oxygen
O_2	molecular oxygen
P	
PAGE	polyacrylamide gel electrophoresis
PBS	phosphate buffered saline
PFV	physiological fuel value
Pi	inorganic phosphate
PMSF	phenylmethylsulfonyl fluoride
PUFA	polyunsaturated fatty acid

Q	
QTL	quantitative trait locus
R	
RbCl	rubidium chloride
RER	respiratory exchange ratio
RMR	resting metabolic rate
RNA	ribonucleic acid
rpm	revolutions per minute
RQ	respiratory quotient
S	
SDS	sodium dodecyl sulfate
SEM	standard error of the mean
SLB	sample loading buffer
SMR	standard metabolic rate
State 4	maximal non-phosphorylating (leak-dependent) respiration
State 3	maximal phosphorylating respiration
T	
TBS	Tris-buffered saline
TCA	Trichloroacetic acid
TCT	Tris buffer, 0.6% Carrageenan, 0.3% Triton X-100
TEF	thermic effect of food
TG	triacylglycerol
$TPMP^+$	methyltriphenylphosphonium cation
TPMP-Br	methyltriphenylphosphonium-bromide
Tris	2-amino 2-hydroxy-methylpropan-1,3-diol
Tween-20	polyoxyethylene sorbitan monolaurate
U	
Ucp	uncoupling protein gene
UCP	uncoupling protein
V	
v/v	volume/volume
v/w	volume/weight
VO_2	volume of oxygen
VCO_2	volume of carbon dioxide
vs.	versus
W	
w/v	weight/volume
WAT	white adipose tissue
wk	week
Z	
z	constant = $\frac{[(-2.3 \times \text{gas constant} \times \text{temperature (in kelvins)}]}{\text{Faraday constant}}$

1. INTRODUCTION

1.1 Obesity and Associated Health Risks

Obesity is a disorder with complex etiologies characterized by excessive accumulations of adipose tissue and associated with the development of some of the most prevalent diseases of our time. It is the most prominent risk factor for non-insulin-dependant diabetes mellitus (NIDDM), and is linked to such medical conditions as hypertension, hypercholesterolemia and other altered plasma lipoprotein profiles, coronary heart disease and to increased mortality (Brindley and Rolland, 1989; Jung, 1997; Lew and Garfinkel, 1979). Obesity also complicates the management of a number of other diseases like osteoarthritis, sleep apnea and chronic obstructive lung disease (Pi-Sunyer, 1993). In Western society, many efforts have been, and continue to be, directed towards the management of obesity, one of the most common health disorders with over one third of the population being afflicted (Kuczmarski *et al.*, 1994; Rosenbaum, 1997). Obesity is arguably the most costly nutritional problem in North–America with related health care costs representing 7-8% of total health care expenditures, which in 1996 amounted to $97 billion dollars. In Canada alone, the total direct cost of obesity in 1997 was estimated to be over 1.8 billion dollars (Birmingham *et al.*, 1999). This corresponds to 2.4% of the total health care expenditures for all diseases in 1997. Such a considerable proportion of health care dollars being devoted to the treatment and management of obesity-related comorbidities occurs not only in Canada, but also in many other industrialized nations (*i.e.*, 2.5% in New Zealand, 4% in the Netherlands, and 5.5%-6.8% in the United States) (Birmingham *et al.*, 1999).

1.2 Energy Balance: Intake vs. Expenditure

Obesity results from a chronic imbalance between energy intake and energy expenditure. When an individual's energy intake chronically exceeds his or her energy expenditure, a state of positive energy balance persists which, over time, leads to increased adipose tissue stores of triglyceride and body weight gain. The amount of triglyceride in adipose tissue is thus the cumulative sum over time of the differences between energy intake and its expenditure. The control of energy balance in humans is very complex, and as is the case for many regulated physiologic systems, the central nervous system plays an integral role. It coordinates energy intake and expenditure by mediating signals that emanate from adipose tissue (Flier, 1995) and the main endocrine (Figlewicz *et al.*, 1996), neurologic (Rohner-Jeanrenaud and Jeanrenaud, 1997), and gastrointestinal (Friedman *et al.*, 1986) systems.

In recent years, there have been significant advances in the understanding of energy intake regulation. These range from the discovery and understanding of mechanisms involved in hunger and satiety including multiple neural circuits with specific neuropeptides, neurotransmitters, their cognate receptors and various feedback loops, to the numerous and varied psychological aspects of appetite control, all of which are influenced by peripheral signals and input from higher cortical centers. When taken together, the multitude of players and pathway interactions involved in the control of energy intake indeed render it very complex. The redundancy and interactions within the involved systems make it unlikely that pharmacological or surgical manipulation of a single component will lead to long-term resolution of obesity (Rosenbaum, 1997). Consequently, the focus has been progressively shifting towards understanding the

regulation of energy expenditure, in the hope of elucidating potential causes of, and possible treatments for obesity.

1.2.1 Components of Overall Energy Expenditure

The field of bioenergetics involves the study of the many aspects of energy metabolism at the cellular and molecular levels in relation to whole animal energetics and has been the subject of extensive review (Blaxter, 1989; Rolfe and Brown, 1997). The energy contained in the body can be simplistically viewed, and indirectly approximated by calorimetric studies, as the difference between the energy ingested and the sum of the energy excreted and heat produced, which is in agreement with the first law of thermodynamics (reviewed by Blaxter, 1989). Therefore, unless it is saved as growth of an individual or passed on during birth or lactation, the majority of an individual's calorific intake is lost as heat (Rolfe and Brown, 1997). Heat production, or thermogenesis, thus plays a major role in the regulation of energy balance.

Thermogenesis is the result of a wide range of contributing processes, which generally fall under one of two main categories, namely obligatory and facultative thermogenesis.

Obligatory thermogenesis is that which occurs in all organs of the body and whose principal endocrine regulators are the thyroid hormones (reviewed by Silva, 1995). It includes heat production from all tissues occurring as a result of maintaining vital cellular metabolic processes and body temperature (or endothermy). When an individual is resting and is not digesting food, this heat production corresponds roughly to the basal metabolic rate (BMR) when measured at thermoneutrality, a temperature which elicits no thermoregulatory effect (Himms-Hagen, 1990). Since feeding is also a requirement in

the maintenance of a physiologic steady state, the thermic effect of food (TEF) occuring in the intestine, liver and white adipose tissue (WAT), and defined as the energy expenditure needed to process the food during ingestion, digestion, absorption and storage, also contributes to obligatory thermogenesis (Himms-Hagen, 1989).

On the other hand, facultative thermogenesis occurs almost exclusively in distinct tissues, namely, skeletal muscle and brown adipose tissue (BAT). Facultative thermogenesis is controlled mainly by the motor nerves (in the case of skeletal muscle) and the sympathetic nerves (in the case of BAT) of the nervous system (Himms-Hagen, 1990). It includes heat production by working muscles (exercise-induced thermogenesis), as well as heat production occurring as a result of thermoregulatory processes such as cold-induced shivering in muscles and cold-induced non-shivering in BAT. Facultative thermogenesis also includes diet-induced thermogenesis occurring in BAT and arguably, albeit to a lesser extent, in skeletal muscle in response to overfeeding. This phenomenon, first described by Rothwell and Stock (Rothwell and Stock, 1979), causes metabolic rate to increase, thereby reducing metabolic efficiency and attenuating the expected increase in body energy stores.

Apart from exercise-induced and cold-induced shivering thermogenesis, the other two processes contributing to facultative thermogenesis, namely cold-induced non-shivering thermogenesis and diet-induced thermogenesis, can be grouped under the subcategory of adaptive thermogenesis. This term refers to processes by which energy is dissipated in response to changing environmental conditions, such as exposure to cold or excessive caloric intake. The two major hormonal effectors regulating adaptive thermogenesis, β-adrenergic and thyroid hormones, exert their effect on energy dissipation by acting on the

number and function of mitochondria in skeletal muscle and BAT. These actions include, amongst others, the biogenesis of mitochondria and the expression of genes that control the rate of mitochondrial fuel-oxidation and ATP synthesis (Nicholls *et al.*, 1986).

1.3 Components of Cellular Energy Expenditure and their Contribution to Standard Metabolic Rate

As mentioned earlier, BMR (the term most commonly used in the case of humans) or standard metabolic rate (SMR: a term that is generally applicable to all mammals) is the steady-state rate of heat production by all mammalian tissues which occurs as a result of maintaining essential cellular metabolic processes and body temperature. BMR and SMR can be measured directly as heat production or indirectly as oxygen consumption from which heat production can be accurately derived (Schutz, 1995). The former approach is referred to as direct calorimetry, whereas the latter is appropriately called indirect calorimetry. In both cases, the animal must be in a post-absorptive state and resting in a stress free environment maintained at thermoneutrality. If the metabolic rate is measured while the animal is still digesting food, then it is generally referred to as resting metabolic rate or RMR.

As discussed by Rolfe and Brown (Rolfe and Brown, 1997), contributions to SMR can be quantified in terms of coupling to oxygen consumption, ATP turnover, or uncoupling. In the standard state, approximately 90% of mammalian cellular oxygen consumption is used by mitochondria, with the remaining 10% being used by various cellular oxidases. Of the mitochondrial O_2 consumption, roughly 80% is coupled to ATP synthesis whereas the other 20% is uncoupled by the mitochondrial proton leak (defined and discussed in detail below) (Note that these proportions vary tremendously depending

on cell type and the metabolic state of the cell). Of all the ATP produced, decreasing amounts are used by protein synthesis, the Na^+-K^+ ATPase, the Ca^{2+}-ATPase, actinomyosin ATPase, gluconeogenesis, ureagenesis, RNA synthesis and substrate cycling (Rolfe and Brown, 1997). The contribution to SMR of each of these components differs significantly from tissue to tissue.

Despite the details of the specific substrate oxidation processes involved and the specific ATP hydrolyzing reactions occurring at the cellular level, the energy released during substrate oxidation must ultimately be released as heat. Moreover, regardless of the efficiency of mitochondrial energy transduction, the heat that is produced is proportional to the oxygen being consumed, since oxygen is the final electron acceptor in the respiratory chain. And, since the total oxygen consumed by cellular mitochondrial and non-mitochondrial reactions is equal to the oxygen consumption at the whole animal level, measurement of the latter via indirect calorimetry accurately reflects SMR.

Although SMR remains fairly constant over time (Blaxter, 1989), changes do occur under various conditions. In the short term, causes of changes in SMR include cold exposure, feeding, and muscle use. As an animal ages or if its nutritional status changes (e.g., under- or overfeeding; certain nutrient deficiencies), SMR is also affected. These represent long-term changes (Rolfe and Brown, 1997). Nevertheless, except for small variations due to differences in percentage of lean body mass (Garby and Lammert, 1994a; Garby and Lammert, 1994b; Miller and Blyth, 1953), individuals of the same species, age and weight have a similar SMR. It has also long been known that thyroid status plays a large role in fixing a set point for SMR (Gustafsson *et al.*, 1965; Tata,

1964). Individuals with lower or higher than normal thyroid hormone levels have accordingly lower or higher than normal SMRs.

SMR has also been shown to be inversely related to body mass, with large animals having lower metabolic rates per unit of body mass than smaller animals. For example, the mouse has a metabolic rate which is approximately 25 times that of an elephant (Brody, 1945; Schmidt-Nielsen, 1984). Phylogeny also affects SMR. Animals of similar body mass but of different phyla have differing metabolic rates, with warm-blooded animals having an SMR 4 to 5 fold higher than cold-blooded reptiles (Hulbert, 1985).

A great deal of research has been devoted to the study of the molecular origin of the factors responsible for the aforementioned differences in SMR (reviewed extensively by Rolfe and Brown, 1997). The regulation of mammalian metabolic rate is indeed quite complex. Nonetheless, it is important to attempt to identify the cellular reactions that contribute significantly to SMR, since changes in the rates of these reactions could significantly affect heat production by SMR and thus ultimately energy balance.

Various aspects of the control of cellular respiration have been addressed in a number of reviews (Brand and Murphy, 1987; Brown, 1985; Himms-Hagen, 1976). Metabolic rate was originally thought to be solely controlled by the ATP-utilizing processes, to which the ATP-producing processes passively responded. However, extensive investigations of control within isolated mitochondria have shown that control is shared by a number of reactions in a given pathway, and that the distribution of control changes depending on metabolic conditions (Brown, 1992a; Groen *et al.*, 1982; Hafner *et al.*, 1990; Letellier *et al.*, 1993; Rolfe and Brown, 1997). For example, in isolated rat liver cells, control over mitochondrial oxygen consumption has been shown to be shared

between the "substrate oxidation" (29-35% of control), "proton leak" (22-25%) and "ATP turnover" (41-49%) pathways (Brown *et al.*, 1990b; Harper and Brand, 1993). A separate study on perfused rat skeletal muscle mitochondria unveiled a similar distribution of control where substrate oxidation reactions had 44 ± 28% of the control, proton leak reactions had 38 ± 21% of the control, and ATP turnover reactions, 21 ± 9% of the control (Rolfe and Brand, 1996b).

Any ambiguity between the concepts of "control" and "regulation", two terms which are too often confused, can be avoided by considering the following propositions. "*A controls B*" means that any change in *A* causes a significant change in *B*. On the other hand, "*A regulates* B", means that in vivo changes in *B* are brought about by changes in *A*. Of course, *A* can only regulate *B* if *A* has significant control over *B* in vivo (Rolfe and Brown, 1997). For example, normal blood glucose level is *regulated* by insulin and glucagon, two hormones which affect many different pathways such as glycogenolysis and gluconeogenesis by altering the specific *control* patterns within these pathways. Thus, regulation is a property at the whole organism level and is affected by hormonal and many environmental factors to maintain homeostasis. Control applies to properties within a specific metabolic system or series of pathways.

1.4 Origin of the Mitochondrial Proton Leak

The mitochondrial proton leak is a non-productive pathway for the return of protons to the mitochondrial matrix, which leads to heat production and a lowered efficiency of oxidative phosphorylation.

Simply put, oxidative phosphorylation is the process by which reduced substrates are oxidized by the respiratory electron transport chain, resulting in an electron flow from the reduced substrates to molecular oxygen, which ultimately fuels ATP synthesis by mitochondria. It requires the participation of several enzyme complexes embedded in the mitochondrial inner membrane, three of which (complexes I, III and IV) are capable of coupling electron transport to the pumping of protons out of the mitochondrial matrix, generating an electrochemical potential difference across the inner membrane, known as the protonmotive force (Δp). This proton concentration gradient serves as a reservoir of free energy. The energy is trapped as protons are channelled back into the matrix through the inner membrane enzyme complex ATP synthase and the combined action of the adenine nucleotide and phosphate carriers, resulting in the formation of extramitochondrial ATP (see Figure 1.1). If the electron transport reactions always led to proton pumping, and if all proton backflow was always through these phosphorylation reactions, then the processes of substrate oxidation and ADP phosphorylation would be perfectly coupled (Brand, 1994). However, as suggested initially by Mitchell and Moyle (Mitchell and Moyle, 1967) oxidative phosphorylation is never fully coupled. In order to assess the effective P/O ratio, all processes that consume the protonmotive force must be taken into account. It follows that the efficiency of oxidative phosphorylation is variable and strongly depends on the route of proton return into the mitochondrial matrix. Aside from the productive translocation of protons through the ATP synthase leading to the energy-conserving formation of ATP, other protonmotive force consuming processes include transport of substrates on the anion carriers, cycling of ions (Ca^{2+}, Na^{+}, K^{+}) across the membrane on the cation carriers and most importantly the passive leak of

Figure 1.1 Schematic illustration of the mitochondrial inner membrane showing the major components in the oxidative phosphorylation pathway and the proposed mechanism for the mitochondrial proton leak. Shown in turquoise are the different complexes of the electron transport chain. As reducing equivalents are being passed from one complex to the next, protons are being pumped from the mitochondrial matrix into the intermembrane space with the establishment of an electrochemical gradient, which serves as a reservoir of free energy. This energy, also known as the protonmotive force can be trapped as protons are channelled through the ATP synthase (pink) and the combined action of the adenine nucleotide (yellow) and phosphate (grey) carriers, resulting in the formation of ATP. The uncoupling protein mediated proton leak (shown in lavender) is a non-productive mode of proton translocation in which protons passively leak back into the matrix without being coupled to ATP synthesis or any other energy conserving reactions. The protonmotive force is dissipated and this energy is simply released as heat. The oxygen consumption occurring during cellular respiration therefore maintains both ATP turnover and proton leak reactions in varying proportions depending on cellular energy demands.

The Mitochondrial Inner Membrane

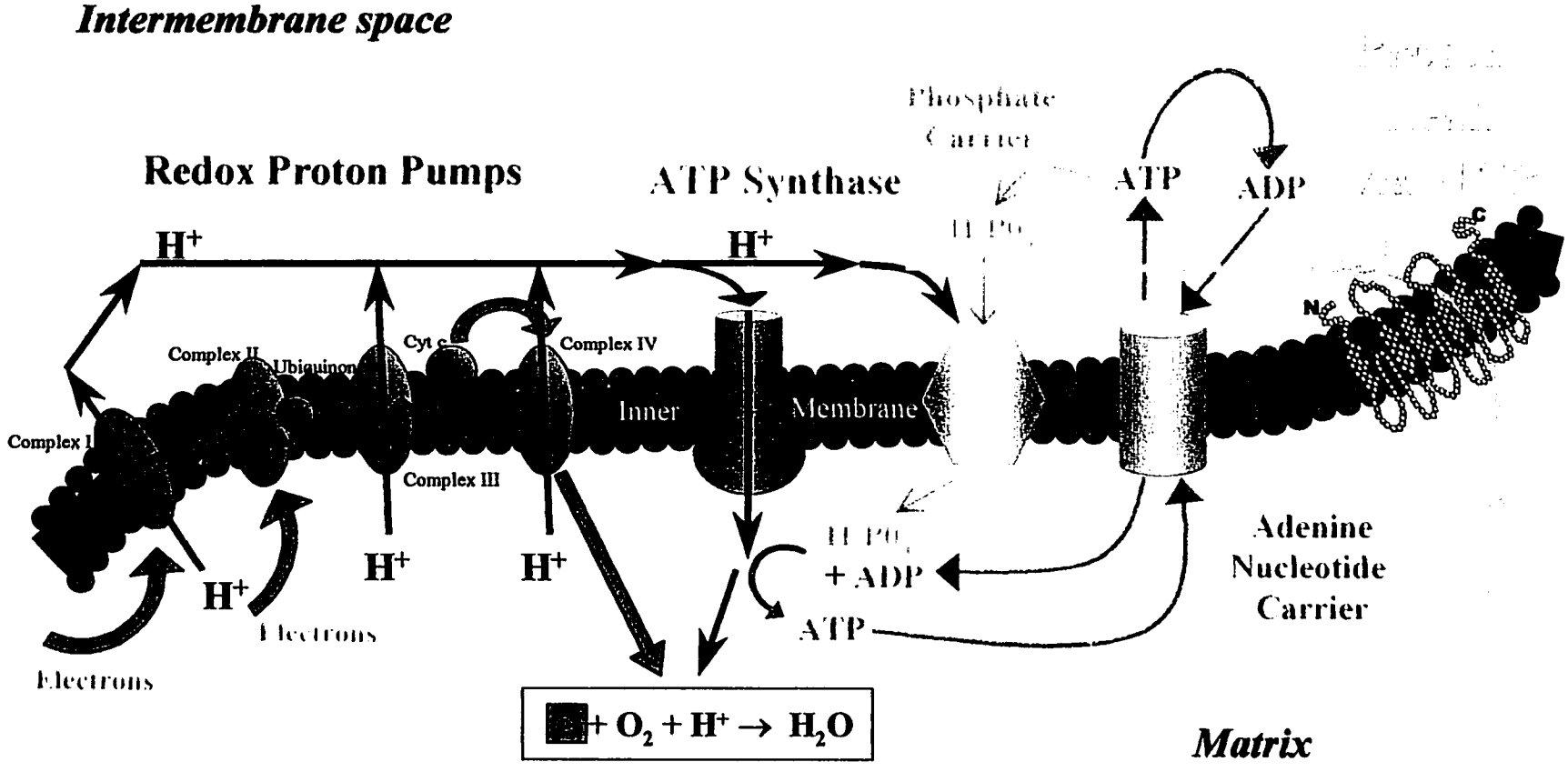

protons across the mitochondrial inner membrane. In fact, research conducted in the last decade, has demonstrated conclusively the existence of mitochondrial inner membrane proton permeability (Brown, 1992b; Brown and Brand, 1986). This proton leak is a non-productive mode of proton translocation in which protons leak back across the membrane without being coupled to ATP synthesis or any other energy conserving reaction. The energy of the protonmotive force is simply released as heat.

The presence of a proton leak across bioenergetic membranes was first measured by Mitchell and Moyle (Mitchell and Moyle, 1967), when after adding a small pulse of oxygen to anaerobic mitochondria or bacteria, protons were pumped out and detected with a pH electrode. When the oxygen was depleted, the protons leaked back across the membrane as evidenced by the increase in pH. Thereafter, measurements of mitochondrial proton leak rate were conducted by first inhibiting all known proton transport processes and then inducing an artificial membrane potential ($\Delta\Psi m$) with potassium gradients (Brown and Brand, 1986; Krishnamoorthy and Hinkle, 1984). Results showed that leak rate was much greater at high values of $\Delta\Psi m$ and that it had a roughly exponential dependence on $\Delta\Psi m$ (Brown, 1992b). Earlier experiments by Nicholls (Nicholls, 1974) on mitochondria respiring at State 4 (in the absence of ATP synthesis) had also shown a strong dependence of proton leak on $\Delta\Psi m$. Only small reductions in $\Delta\Psi m$ (induced by inhibiting the electron transport chain with malonate) were required to substantially inhibit the respiration rates of the mitochondria.

The above described experiments briefly summarize the theory and rationale underlying the techniques used to measure proton leak kinetics in this research. A more

detailed description of the techniques will however be provided and elaborated in sections 1.7 and 2.5.3.

1.4.1 Importance of the Mitochondrial Proton Leak

The question of whether mitochondrial proton leak is an artefact of the isolation process or a real physiological phenomenon has been answered by numerous studies in which leak has been shown to exist in intact cells and tissues. It has been demonstrated in mitochondria within isolated hepatocytes (Brand, 1990; Brand *et al.*, 1994; Brown *et al.*, 1990b; Harper and Brand, 1993; Nobes *et al.*, 1990), thymocytes (Buttgereit *et al.*, 1992), lymphocytes (Buttgereit *et al.*, 1991), perfused skeletal muscle (Rolfe and Brand, 1996a) and intact heart (Challoner, 1968). The results of these studies confirm that the quantitative importance of the proton leak in energy expenditure is substantial. In isolated hepatocytes, mitochondrial proton leak was shown to account for approximately 26% ± 7% of total cellular oxygen consumption rate or 33% ± 7% of mitochondrial respiration rate (Brand *et al.*, 1994). In resting perfused skeletal muscle, the mitochondrial proton leak was shown to account for up to 52% of the oxygen consumption (Brand *et al.*, 1994). Since such a high proportion of oxygen consumption is used to drive the proton leak, it has been hypothesized to be a significant contributor to mammalian energy expenditure and, specifically to SMR.

The study of mitochondrial proton leak and its contribution to cellular respiration rates in animals of various species and phyla has helped to establish the leak as having a true function in the regulation of SMR. Given that the proton leak activity of the isolated mitochondria from hepatocytes of various mammals shows a positive correlation with the

cellular oxygen consumption, it follows that proton leak is a variable property of the mitochondrial inner membrane and that it has some important function (Rolfe and Brand, 1997). In general, the smaller the mammal, the faster the respiration rate and the higher the proton leak; proton leak across the mitochondrial inner membrane is 5 x higher in the mouse than it is in the horse whose body mass is 7,500 fold greater. (Porter and Brand, 1993; Porter and Brand, 1995b). Thus proton leak is thought to contribute to differences in mass-specific metabolic rates in mammals.

Differences in mitochondrial proton leak are also thought to play an important role in the 5-fold higher SMR of homeotherms compared to poikilotherms. Isolated liver mitochondria of the rat (a mammal) have a 4-5 fold greater proton permeability than those of the bearded dragon (a reptile of the same body mass and temperature) (Brand *et al.*, 1991). Furthermore, the proportion of hepatocyte respiration used to drive proton leak, ATP turnover and non-mitochondrial oxygen use remains relatively constant, regardless of body mass and phylogeny (Brand *et al.*, 1991; Porter and Brand, 1995a). Taken together, these findings indicate that a balance between the rates of the various processes is maintained even though the metabolic rate of the cells differs widely. This balance may act to preserve a certain pattern of "control distribution" over oxidative metabolism. In addition to the aforementioned studies on different animal species and phyla, a number of other studies on isolated mitochondria, from different tissues of the same animal (Rolfe *et al.*, 1994) or even from plants (Diolez *et al.*, 1993; Kesseler *et al.*, 1992), reveal that the distribution of control amongst oxidative phosphorylation reactions is a conserved property. Maintenance of the balance between proton leak and the other mitochondrial metabolic pathways suggests useful physiologic functions for the leak,

rather than it being a useless and detrimental consequence of having an inner membrane with a very high protein content which cannot withstand the protonmotive force (Rolfe and Brand, 1997).

1.4.2 Postulated Functions of the Mitochondrial Proton Leak

Several different functions have been suggested for the proton leak in mammals, all of which closely correlate with those having been brought forward for the processes underlying SMR. These functions include: i) the production of heat to maintain body temperature, ii) the endowment of increased potential for control of metabolism, iii) the reduction of harmful free radical production, and iv) the regulation of carbon flux by maintaining a relatively high NAD^+/NADH ratio (reviewed by Rolfe and Brand, 1997). For the purposes of this research, the focus will lie mainly upon the first two functions listed above.

1.4.2.1 Proton Leak as a Means of Heat Production

In mammals at thermoneutral environmental temperatures, standard metabolic processes provide the heat required to maintain a body temperature of between 33°C and 39°C. In these conditions, the level of mitochondrial proton leak could be dictated by the need to match the rate of heat production to that of heat loss. However, at temperatures below thermoneutrality, the increased need for internal heat production exceeds the capacity of standard metabolism and, as a result, facultative thermogenesis is necessary. In rodents, brown adipose tissue largely fulfils this function since it is an organ specialized in the production of heat through the uncoupling of oxidative phosphorylation by a specialized uncoupling protein (UCP1)(see below). Although humans possess BAT

at birth, which does serve an important thermogenic function then, under normal circumstances (which excludes prolonged exposure to cold, or catecholamine producing tumors), adult humans are thought to possess very limited amounts of BAT. Therefore, activity of UCP1-containing BAT is unlikely to be quantitatively important in the facultative energy metabolism of adult humans (Garruti and Ricquier, 1992).

Nonetheless, a strong indication that proton leak is involved in thermoregulation during standard metabolism lies in the fact that, parallel to SMR, the leak is greater in homeotherms than in poikilotherms of equivalent size, and greater in smaller compared to larger mammals. In the latter case, smaller animals, because of their larger surface area to volume ratio, tend to lose larger amounts of heat which need to be balanced by an increased metabolic rate (Brand, 1990). Relative to their body size, both the mass and the metabolic activity of heat producing organs are relatively greater in small mammals as compared to larger mammals (Blaxter, 1989; Brand, 1990; Else and Hulbert, 1985; Krebs, 1950; Schmidt-Nielsen, 1984).

Since leak and other oxygen consuming processes in hepatocytes isolated from both homeotherms and poikilotherms show similar proportions in terms of control of oxidative metabolism, this suggests that heat production is not the only function of proton leak.

1.4.2.2 Proton Leak Increases the Potential for Regulation of Oxidative Metabolism

Because the oxygen consumption that is used to support the futile cycle of proton pumping and leak (coupling and uncoupling processes) across the mitochondrial membrane cannot be used to drive ATP synthesis, the occurrence of the proton leak in intact cells lowers the effective P/O ratio (the actual ATP produced/O_2 consumed) below

its maximum possible values (Brand *et al.*, 1994). It follows that the contribution of proton leak to total proton influx declines as ATP synthesis increases since a greater proportion of protons return through ATP synthase (Brown *et al.*, 1990a). In the latter case, the control by leak over respiration also declines correspondingly. Hence, the presence of the mitochondrial proton leak allows oxidative phosphorylation to vary its coupling efficiency depending on ATP demand, without large changes in oxygen consumption. Mitochondrial proton leak increases the sensitivity and decreases the response time to changes in ATP utilization in the cell. Thus, proton leak may provide a mechanism for increasing the sensitivity and rate of response of oxidative phosphorylation to effectors, since changes in the amount of leak due to hormones or other regulators will ultimately change the in vivo respiration rate and P/O ratio (Brown, 1992b).

1.4.3 Uncoupling Protein Mediated Proton Leak in Brown Adipocytes

A thermogenic function was first ascribed to BAT some 25 years ago by two researchers, Smith and Hock (Smith and Hock, 1963), who along with others later characterized its role as being important in the process of non-shivering thermogensis (NST) during arousal from hibernation and acclimation to cold or during the neonatal period (Chaffee and Roberts, 1971; Jansky, 1973; Smith and Horwitz, 1969). It was not until the late 1970s that the role of BAT in the development of obesity became an issue, when two publications showed that rodent BAT metabolism played a role in obesity development (Himms-Hagen and Desautels, 1978; Rothwell and Stock, 1979). Today, BAT thermogenesis is well recognised to be a quantitatively important component of overall energy expenditure in animals either living at temperatures below

thermoneutrality (where NST occurs) or in those having ingested excessive amounts of calories (where DIT occurs).

The molecular mechanisms responsible for BAT function have been well defined. Energy expenditure in this discrete and unique tissue is stimulated by the sympathetic nervous system which densely inervates it. Norepinephrine released from nerve terminals stimulates β-adrenergic receptors on the plasma membranes of brown adipocytes, which results in uncoupled mitochondrial respiration (reviewed by Flier and Lowell, 1997). That a transgenic mouse with decreased BAT is obese (Lowell *et al.*, 1993), and that this phenotype disappears at thermoneutrality (Melnyk *et al.*, 1997), strongly supports previous studies that provided indirect evidence that BAT plays an important role in the regulation of energy balance in rodents.

The key factor responsible for the thermogenic activity of BAT is a 32kDa protein, named uncoupling protein (UCP), which resides in the inner membrane of the mitochondria in brown adipocytes (Heaton *et al.*, 1978; Himms-Hagen *et al.*, 1978; Nicholls *et al.*, 1978; Ricquier and Kader, 1978). This uncoupling protein has generally been accepted as the major component of BAT that bestows upon them their particular thermogenic property (Himms-Hagen, 1990). UCP1, as it has now been called, was cloned in 1986 by Bouillaud and colleagues (Bouillaud *et al.*, 1986), nearly a decade after its identification in BAT. It is a type II transmembrane protein containing six transmembrane domains, and is a member of the mitochondrial carrier protein family, which also includes the ATP/ADP translocator, and the phosphate carrier (see Figure 1.2). Unlike the other members of this family, however, UCP1 is exclusive to mature brown adipocytes.

Figure 1.2 Membrane-spanning model illustrating the structure of the uncoupling protein (UCP1) specific to brown adipose tissue. This cross sectional view shows all six transmembrane domains of UCP1 spanning the mitochondrial inner membrane in BAT with both the N and C terminals facing the intermembrane space.

Structure of the Uncoupling protein 1 (UCP1)

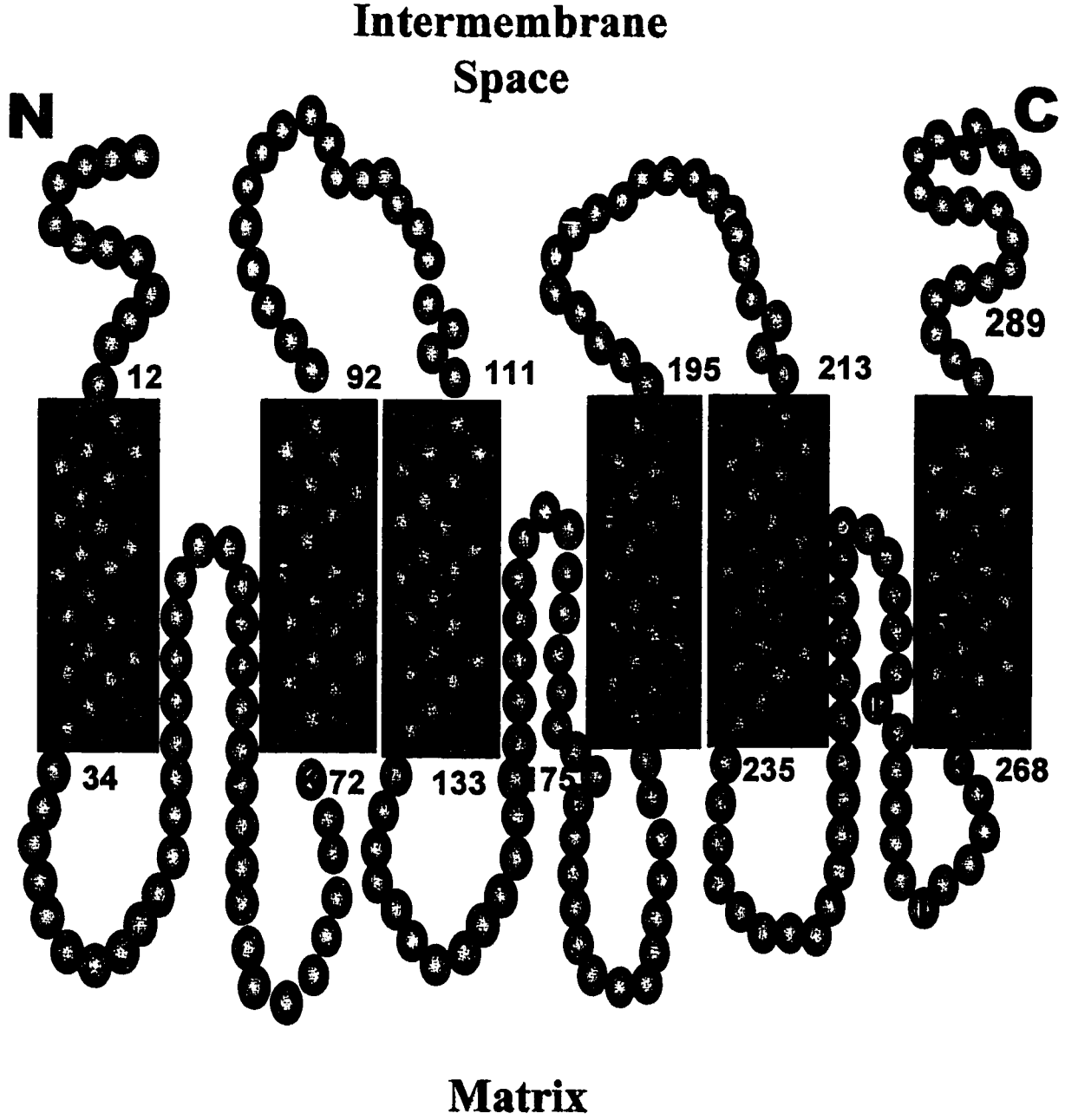

In these cells, UCP1 functions to dissipate the electrochemical potential gradient, thereby uncoupling fuel oxidation from ATP synthesis. Consequently, when BAT is stimulated, the proton gradient is dissipated by UCP1, and heat is the only product. The sympathetic regulation of BAT uncoupling activity occurs by both an increase in UCP1 abundance, and an acute increase in UCP1 activity. These two events respectively result from changes in the UCP1gene (*Ucp1*) transcription, and from the cAMP-induced elevation of intracellular free fatty acids (FFA) available for oxidation following lipolysis induced by the β3-adrenergic receptor stimulation of norepinephrine (Bukowiecki *et al.*, 1981) (LaNoue *et al.*, 1986; Locke *et al.*, 1982; Nicholls *et al.*, 1986; Rial *et al.*, 1983). Transcription of *Ucp1* is also mediated by the cAMP pathway (Cassard-Doulcier *et al.*, 1993; Kozak and Kozak, 1994; Ricquier *et al.*, 1986; Rohlfs *et al.*, 1995), as well as by thyroid hormones (Bianco *et al.*, 1988; Guerra *et al.*, 1996) and retinoic acid (Cassard-Doulcier *et al.*, 1994; Larose *et al.*, 1996; Rabelo *et al.*, 1996; Silva and Rabelo, 1997), both of which seem to be required for an efficient transcription process to take place.

The activity of UCP1 is also acutely regulated by the specific binding of purine nucleotides (*i.e.*, ADP, ATP GDP, GTP) which inhibit its proton translocating activity; a phenomenon that distinguishes UCP1 from other mitochondrial carrier proteins (Desautels *et al.*, 1978; Heaton *et al.*, 1978; Lin and Klingenberg, 1982).

1.4.4 Mechanism of Proton Leak in Tissues Other Than BAT

Until a few years ago the causes and mechanisms of proton leaks in tissues other than brown adipose tissue remained a mystery. In the early 1990s, in light of the rapidly accumulating evidence in support of the idea that a substantial amount of energy was

expended to support a mitochondrial proton leak in all cells of the body, the search for a mechanism started to intensify. Initial hypotheses involved the proportional relationship between leak and the total surface area of the mitochondrial inner membrane (MIM) and pointed toward the fatty acid composition of the MIM (reviewed by Harper, 1997). Research done in Martin Brand's laboratory at the University of Cambridge showed striking correlations between membrane proton permeability and fatty acid composition of the membrane phospholipids (Brand *et al.*, 1991; Brand *et al.*, 1992; Porter *et al.*, 1996). However, further studies with liposomes made from phospholipids of mitochondrial inner membrane led to the conclusion that the phospholipid leak accounted for only about 5% of the proton leak flux (Brookes *et al.*, 1997). These findings therefore led to attention being diverted towards a possible mechanism involving the action of a protein.

Since it had been well established that UCP1 in BAT plays an important role in energy balance and thermogenesis in small mammals (Nicholls and Locke, 1984), the search intensified for possible uncoupling proteins in tissues other than BAT. In 1991, Shinohara *et al.* (Shinohara *et al.*, 1991) reported the finding of the mRNA for an uncoupling protein similar to UCP1, but found in hepatocytes of newborn and cold-stressed adult rats. Since then, the search for other uncoupling proteins has been undying.

1.4.4.1 Uncoupling Protein Homologues

In the last two years, significant advances in the realm of proton leak mediated energy expenditure have been made possible thanks to the discovery of four novel uncoupling protein homologues which, unlike UCP1, are widely expressed throughout the body.

In 1997, Fleury and colleagues described the cloning of UCP2, which is 59% identical to UCP1 at the amino acid level, and also functions to uncouple mitochondrial respiration (Fleury *et al.*, 1997) (Gimeno *et al.*, 1997). UCP2 is ubiquitously expressed with the highest levels of expression being found in white adipose tissue (WAT), BAT, heart, kidney, spleen, thymus, macrophages, bone marrow and stomach in both mice and humans (Fleury *et al.*, 1997; Gimeno *et al.*, 1997). Noteworthy is the fact that human and mouse UCP2 are 95% identical, while human and mouse UCP1 are only 79% identical, suggesting a critical role for UCP2 in the well-being of an organism. Several protein motifs known to be important in UCP1 function are conserved in UCP2, as are the putative purine nucleotide binding sequences. By virtue of its wide expression and its uncoupling activity, UCP2 was quickly flagged as being a possible important determinant of SMR. Its expression throughout the immune system, also suggested a putative role for this protein in immunity and/or thermoregulatory responses to infection (fever) (Fleury *et al.*, 1997). Moreover, since its mRNA expression was found to be 5-fold higher in BAT of transgenic mice deficient in UCP1 (Enerback *et al.*, 1997), UCP2 was thought to be at the source of the essential compensatory mechanism which allows these mice to remain lean even on a high fat diet, further supporting a role for UCP2 in energy balance. In investigating the regulation of UCP2 as compared to that of UCP1, Fleury *et al.* reported that the expression of these two proteins was quite distinct. They found that the levels of mouse UCP2 mRNA in BAT and WAT were insensitive to both cold exposure and β3-adrenergic stimulation by CL 316,243 (which induce UCP1 in BAT), but were dramatically increased in obesity-resistant mice on a high-fat diet. Expression of UCP2 was also found to be lower in strains of mice susceptible to obesity. Given these

findings, it was logical to investigate the possibility that the UCP2 locus on mouse chromosome 7 and human chromosome 11 (11q13) is somehow linked to obesity. Several reports showed that this chromosomal mapping of UCP2 is co-incident with quantitative trait loci (QTLs) for obesity and hyperinsulinemia (DeBry and Seldin, 1996; Hashimoto *et al.*, 1994; Seldin *et al.*, 1994; Taylor and Phillips, 1996; Warden *et al.*, 1995).

Within six months of the cloning of UCP2, a third uncoupling protein was discovered. UCP3 has 57% and 73% identity to human UCP1 and human UCP2, respectively (Boss *et al.*, 1997; Gong *et al.*, 1997; Vidal-Puig *et al.*, 1997). In an attempt to better understand the biochemical events underlying non-shivering thermogenesis in muscle, Boss and colleagues screened a human skeletal muscle cDNA library and isolated three clones. One of these was found to be UCP2 while the others appeared to be two forms of a novel UCP3: one long (312 residues: $UCP3_L$) and one short (275 residues: $UCP3_S$). These differ only by the presence or absence of the 37 residues of the C-terminus, which contain the putative purine nucleotide binding domain. UCP3 is distinguished from other UCPs by its relatively selective and abundant expression in skeletal muscle in humans, and brown adipose tissue and skeletal muscle in rodents, making it a potential mediator of adaptive thermogenesis (Matsuda *et al.*, 1997; Vidal-Puig *et al.*, 1997). The chromosomal location of the UCP3 gene has been mapped to the distal segment of human chromosome 11 (11q13) and to murine chromosome 7, adjacent to UCP2. In fact, these two genes are located within 75-150 kilobases of each other and most likely result from a gene duplication event (Solanes *et al.*, 1997). Given its proximity to the UCP2 gene, the mouse UCP3 gene is also coincident with quantitative

trait loci for obesity in three mouse models, raising the possibility that abnormalities in one or both of these genes are responsible for obesity in these models (Seldin et al., 1994; Taylor and Phillips, 1996; Warden et al., 1993).

Very recently, two other mitochondrial proteins have been discovered, both having respiration uncoupling activity in recombinant yeast, and as such, become members of the uncoupling protein family. BMCP1 (or brain mitochondrial carrier protein-1), cloned in the fall of 1998, has 34%, 38% and 39% identity with UCP1, UCP2 and UCP3 respectively (Sanchis *et al.*, 1998). The gene expression of this novel protein occurs mainly in the brain of both rodents and humans, and maps to murine chromosome X and to Xq24 in man (Sanchis *et al.*, 1998). The most recent addition to the UCP family, characterized in January 1999, was termed UCP4. It is most related to UCP3, however its transcripts are exclusively found in fetal and adult brain tissues, and its gene maps to human chromosome 6p11.2-q12 (Mao *et al.*, 1999). Although these findings suggest that BMCP-1 and UCP4 may be involved in thermoregulatory heat production and metabolism in the brain, it is unknown whether or not they play a significant role in overall energy balance.

1.4.4.2 UCP Homologues: Importance in Overall Energy Metabolism

The contributions of the first two novel uncoupling protein homologues to both standard metabolic rate and adaptive thermogenesis are under active study. The hypothesis that UCP2 and UCP3 may be contributing to energy balance by mediating the mitochondrial proton leak be it either as compensatory mechanisms in BAT and/or as regulators of adaptive thermogenesis and SMR in tissues other than BAT is the focus of several laboratories. At this point, there is evidence in support, and evidence contrary to

the hypothesis that these UCPs cause the leak described by Brand's group. As research in the field progresses, new findings raise doubt on this being the main role of these homologues. One thing that is clear though is that their regulation differs from that of UCP1 whose sole purpose is heat production.

In agreement with their role as uncouplers, the expression of both UCP homologues in yeast causes significant decreases in membrane potential in contrast to strains containing empty expression vectors (Fleury *et al.*, 1997). Using the same method of flow cytometry of yeast labeled with the potential sensitive probe DiOC6, previous analyses by Nicholls accordingly demonstrated that UCP1 decreases the mitochondrial potential of transformed yeast (Nicholls and Locke, 1984). It appears from these findings that both homologues are able to uncouple respiration. In fact, the depolarizing effects of UCP2 were found to be even more potent than those of UCP1 (Fleury *et al.*, 1997).

However, recent studies looking at the differential mRNA expression of UCP2 and UCP3 in rat interscapular BAT and slow and fast twitch skeletal muscle in response to food deprivation and controlled refeeding unveiled results somewhat inconsistent with their role as uncouplers involved in thermogensis (Samec *et al.*, 1998). Although in BAT, the pattern of UCP mRNA expression closely followed that of UCP1 (a decrease during fasting and increase upon refeeding), in skeletal muscle this pattern was reversed so that the UCP mRNA expression increased during food deprivation and decreased upon transition to refeeding. Similar trends were observed in the fast- (gastrocnemius) and slow- (soleus) twitch muscles, however, changes in their mRNA expression contrast in that the magnitude of response to fasting was much lower, and the restoration to control levels much more rapid in the soleus (Samec *et al.*, 1998). These findings are consistent

with the capacity of these two muscle types to shift from lipids to glucose during refeeding and raise the possibility that free fatty acids (circulating levels of which are increased during the fasted state) might be a modulator of gene transcription of these UCP homologues in highly oxidative skeletal muscles (Samec *et al.*, 1998; Weigle *et al.*, 1998). An earlier study of similar nature, but conducted this time in humans, also revealed increased expression of UCP2/3 mRNA in skeletal muscle and WAT during fasting (Millet *et al.*, 1997). Also, recent findings by Argyropoulos *et al.* report polymorphisms in the UCP3 gene which cause a 50% reduction in basal fat oxidation rates and a marked increase in respiratory quotient (Argyropoulos *et al.*, 1998). Taken together, these results are suggestive of a role for UCP2 and UCP3 in the regulation of lipids as fuel substrate (metabolic fuel partitioning), and in the metabolic adaptation to fasting, rather than in a direct role in the mediation of thermogenesis. Alternatively, the increased expression of these uncoupling proteins in the fasted state could reflect an attempt to maintain normal body temperature. It must be kept in mind however, that in both of the aforementioned studies, only levels of mRNA were investigated, and that this does not necessarily reflect the level of actual expression of the proteins, which makes it difficult to draw valid conclusions. The expression of UCP1 protein correlates poorly with its mRNA under certain conditions (Kopecky *et al.*, 1997).

Consistent with their proposed role in energy balance is the discovery that a number of polymorphisms in the UCP2 gene and possibly in the UCP3 gene (still under investigation) have been associated with obese phenotypes in humans (Walder *et al.*, 1998). These researchers suggest a contribution from UCP2 (or UCP3) to variations in metabolism in young Pima Indians which may contribute to overall body fat content later

in life (Walder *et al.*, 1998). In addition, a strong genetic linkage has been found between the UCP2/UCP3 locus and resting energy expenditure (SMR) in adult humans (Bouchard *et al.*, 1997). This finding further emphasizes the possibility that the novel UCPs may be involved in regulation of energy balance and in doing so, they remain promising targets for anti-obesity drug development aimed at increasing thermogenesis.

1.5 Understanding the Role of Genetics in Obesity Using Mouse Models

Although the state of obesity in itself can be described accurately and simplistically by a defect in energy balance, the actual development of obesity is influenced by a number of factors of genetic, environmental and behavioral origins, making the search for causes very onerous. It has been shown by a number of studies that human obesity exhibits a strong familial tendancy (Bouchard, 1991; Bouchard *et al.*, 1991; Bouchard and Perusse, 1988) (Bouchard, 1997; Bouchard and Tremblay, 1997), but due to its multifactorial nature, earlier efforts to identify the genetic factors contributing to human obesity were largely unsuccessful. However, the recent development and fine tuning of a technique using highly polymorphic markers and new statistical procedures has made it possible to analyze polygenic quantitative traits for obesity in animal models (Lander and Botstein, 1989; Warden and Fisler, 1994).

Using mouse models which mimic human obesity has been and continues to be a very helpful approach to better understand and characterize the role of genetics in the etiology of obesity (Chagnon and Bouchard, 1996; York, 1996). Several chromosomal regions have been linked to the control of body fat in the mouse through quantitative trait locus (QTL) mapping. To date, at least 22 QTLs that affect murine body fatness have been

identified in mouse crosses (Chagnon *et al.*, 1998), a number of which are located on chromosome 7 (Moody *et al.*, 1997; Taylor and Phillips, 1997; Warden *et al.*, 1995; West *et al.*, 1995; York *et al.*, 1996). One of these QTLs, the more distal obesity QTL on mouse chromosome 7, maps over the chromosomal locations for the *tub* (Coleman *et al.*, 1978), *Ucp2* and *Ucp3* genes. As such, there is a possibility that allelic variants of one or more of these genes could be responsible for some of the obesity-trait loci (body fat QTL) mapped to this chromosome (York *et al.*, 1999). However, the close proximity of these genes prevents genetic linkage studies from discriminating between them.

A useful approach in isolating a certain chromosomal region from other genes possibly contributing to a specific trait, in this case obesity, is the development of congenic mouse lines. The use of such models allows researchers to achieve a finer and more specific localization of traits and to obtain an improved understanding of the interactions involved at a particular locus (York *et al.*, 1999).

1.6 UCP2/3 Congenic Mice: C57BL/6J Background with a CAST/Ei Donated UCP2/3-containing Segment on Chromosome 7

Congenic mice are mice that have been bred to be essentially isogenic with a given inbred strain of mice except for a selected differential chromosomal segment (Silver, 1995). The conceptual basis for the development of such mice was first formulated in the 1940s by a researcher at the Jackson Laboratory, named George Snell, who was later awarded a Nobel prize for his achievements. The creation of congenic mice involves a multigeneration breeding protocol based on repeated backcrossing to trap a single locus from one mouse strain (the donor) in the genetic background of another (the recipient inbred partner). The first cross is always an outcross between the recipient inbred partner

and an animal that carries the donor allele. The second and all subsequent generation crosses are backcrosses to the recipient inbred strain (see Figure 1.3). This approach causes the newly forming congenic strain to become increasingly similar to the inbred partner at each generation since only those offspring having received the donor allele at the differential locus are selected to participate in the next round of backcrossing (Silver, 1995).

The research described in this thesis involves the study of a congenic mouse model having a C57BL/6J (referred to hereafter as: B6) background and a CAST/Ei (from the *Mus Castaneous* strain; referred to hereafter as: CAST) derived donated segment on mid to distal chromosome 7. This donated segment is a 26 cM chromosomal fragment which spans the length from approximately 36 to 62 cM (see Figure 1.4). It encompasses nearly one hundred genes including three, namely *tub*, *Ucp2* and *Ucp3*, which, as mentioned previously, are co-incidental with a QTL having been linked to the control of body fat in the mouse. Accordingly, the introduction of this CAST DNA segment into the background of the B6 mouse, which is known for its susceptibility to obesity, has been shown to result in a 50% decrease in fat deposition in mice fed a high fat diet (York *et al.*, 1999) compared with B6 control mice fed the same diet.

1.6.1 Overall Objectives of this Research Project

The ultimate goal of the research presented herein is to determine the metabolic basis for the differential susceptibility to obesity observed between the B6-CAST congenic and B6 control mice when fed a high fat diet. In an attempt to elucidate the mechanisms of action of the gene or genes responsible for the observed phenotypical differences, several

Figure 1.3 Breeding scheme describing the creation of a congenic mouse strain. In this representation, the relative contributions of donor and recipient alleles at sequential generations of backcrossing are shown in white and green respectively. The checkerboard pattern of the offspring indicates heterozygous loci. By the tenth generation of backcrossing, the differential segment around the selected locus will represent the major contribution from the donor genome. (Adapted from *Mouse Genetics* [Silver, 1995 #2875] with permission from Oxford University Press Inc.)

Breeding Scheme Used in the Creation of a Congenic Strain

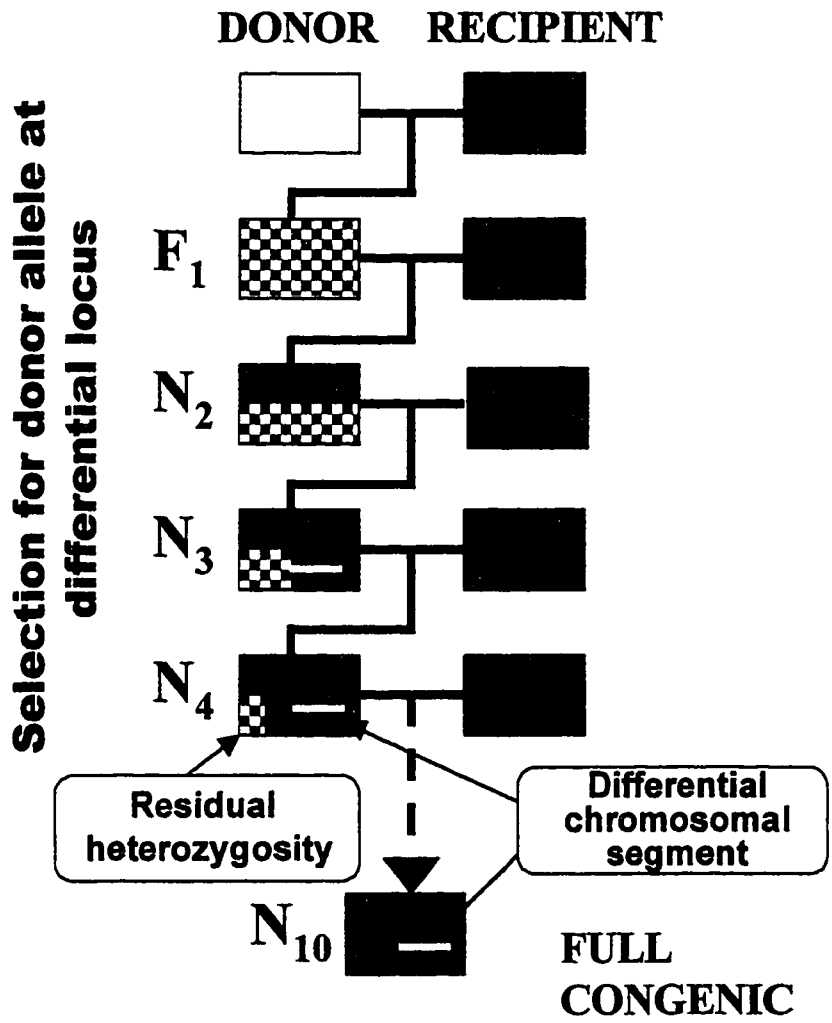

Figure 1.4 Map of distal chromosome 7 showing the extent of the CAST/Ei donor segment in our congenic mouse line. The distances in cM along the segment, which is illustrated in pink, were taken from the Jackson Laboratories database. Candidate genes and QTL positions are indicated in bolded italics. (This map was obtained from Barbara York at the Pennington Biomedical Research Centre.)

Mouse Chromosome 7

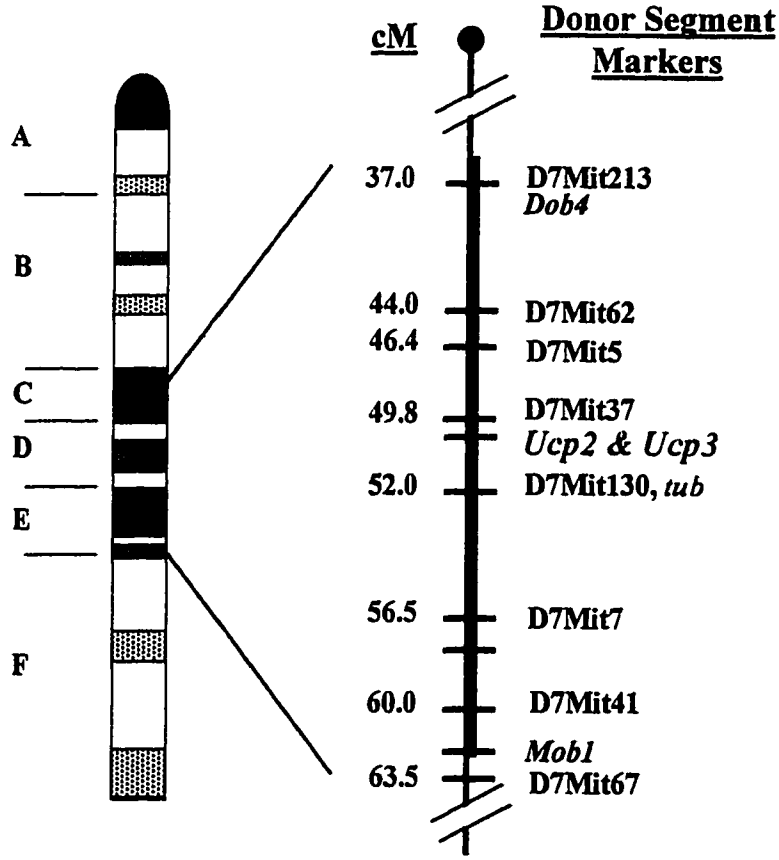

experiments were conducted which examine both the energy intake and energy expenditure aspects of energy balance. The rationale for these experiments stems from the fact that the resulting decrease in fat deposition in high fat fed B6-CAST congenics as compared to B6 controls, must be associated with a disregulation in energy balance, be it a decrease in energy intake or an increase in energy expenditure.

In the initial series of experiments I set out to examine the first of these two possibilities, which was to investigate if B6-CAST congenics did in fact eat less than the B6 control mice, which theoretically could in itself explain the observed decrease in fat deposition evidenced by fat pad weights. This was done by monitoring both food intake and body weights of the two groups of mice fed either a normal chow diet or a high fat diet over an extended period of time. I also explored the other alternative, a possible increase in energy expenditure in B6-CAST congenics as compared to B6 controls, by comparing the resting metabolic rates as well as their total 24 hour energy expenditure and their total 24 hour fasting energy expenditure. Finally, in what represents the main focus of this research, I analyzed the characteristics of the proton leak kinetics in the context of oxidative phosphorylation in mitochondria isolated from skeletal muscle of both groups of mice fed one of the two administered regimes: normal chow or high fat chow. These last experiments stem from the hypothesis that perhaps the resistance to fat deposition seen in B6-CAST congenics is based on their ability to dispose of excess energy by uncoupling respiration. Indeed, increases in mitochondrial proton leak due to functional differences in UCP2 and/or UCP3 could have a significant effect on energy expenditure and thus on fat mass. The kinetics of the leak (refer to section 1.7 for details) were specifically examined in skeletal muscle mitochondria because of the rather

selective expression of UCP3 and also the presence of UCP2 in skeletal muscle, and their potential role in mediating adaptive thermogenesis or perhaps more specifically diet-induced thermogenesis therein. Mitochondria were isolated from both hind and forelimb skeletal muscle tissues of B6-CAST congenics and B6 control mice. Since these muscles comprise a wide range of fibre types (*i.e.*, fast and slow twitch, glycolytic and oxidative), they fairly represent the bulk of the murine skeletal muscle mass.

Because of the rapidly accumulating data and evolving research in this field, I feel compelled to mention that when this project was first undertaken, much less was known about the novel uncoupling proteins and their role in energy expenditure. In fact, when we first started planning the experiments to be conducted with these B6-CAST congenic and B6 control mice, UCP3 had not yet been characterized. UCP2 was the only novel uncoupling protein homologue at the time, which explains the rationale behind a few of the experiments done on the first set of subjects (see Experimental Procedures: Section 2.2). In retrospect, different tissue types would have been collected for certain analyses which would have allowed for further interesting comparisons with those collected during the second and third studies, when the existence of UCP3 was known. The discovery of UCP3 and its hypothesized implications in adaptive thermogenesis, effectively steered this research in a slightly different direction.

1.6 Assessment of Proton Leak Kinetics via Top-Down Metabolic Control Analysis

The approach used to assess the kinetics of the proton leak in this research is that of metabolic control analysis (MCA). The aim of this approach is to derive quantitative information about the importance of reactions in the control of both, flux (or rate of the

reactions) through a metabolic pathway, and concentration of metabolites within that pathway. The theory behind the original approach to metabolic control analysis was first developed in 1973 by Kascer and Burns (Kacser and Burns, 1973), and Heinrich and Rapoport (Heinrich and Rapoport, 1973), and has since been the subject of numerous reviews (Brand and Murphy, 1987; Fell, 1992; Kacser and Burns, 1995; Kacser and Porteous, 1987). Although it is of great theoretical importance, this original approach, which involves the study of flux control coefficients for every single enzymatic step within a metabolic pathway, has limited practicality due its requirement for specific inhibitors of every individual enzyme acting within the pathway under study, and their limited availability.

In light of this, metabolic control analysis was later reevaluated and extended into what is now known as the top-down approach to metabolic control analysis (Brown *et al.*, 1990a). The enhanced applicability of this approach resides in that the control structure of a metabolic system is determined for blocks of enzymatic reactions rather than for individual reactions. This further emphasizes the idea that control may be distributed throughout a system rather than being located at one particular site such as in a "rate-limiting step". The top-down approach involves conceptually dividing a metabolic system into two or three blocks of reactions that are centered around a common intermediate chosen in that it is a component of the system which is produced by one or more blocks of reactions, and consumed by subsequent blocks. A requirement which needs to be met before the top-down approach can be applied is that the blocks of reactions must affect each other solely through the concentration of the intermediate.

One advantage that the top-down approach has over the original approach to MCA, is that it can be used to identify the sites of regulation within a system by hormones or other effectors. In this respect, the method can be valuable in assessing the metabolic effects of certain drugs and even those of a transgene insertion, gene knockout, or, as in this study, the presence of the CAST/Ei derived segment in the B6 background. The data generated in a top-down elasticity analysis provides all the information needed to mathematically calculate flux control and concentration control coefficients for blocks of enzyme reactions in a metabolic pathway allowing a full control analysis to be completed. This, however, was not the goal of the present study, which was mainly to examine the kinetics of the proton leak and look for differences between that in B6-CAST congenic and B6 control mice. The overall kinetics of a block of reaction such as the proton leak reactions are often referred to as, or described in terms of elasticity. The latter is defined as the fractional change in the flux through the block of reactions that is caused by an infinitesimal fractional change in the concentration of the intermediate (Harper and Brand, 1995).

For the purposes of this research, the metabolic system of choice is obviously the oxidative phosphorylation system. As might be expected in view of the complexity of the whole system, control of oxidative phosphorylation does not occur by simple feedback inhibition or by simple allosteric mechanisms. The rate of oxidative phosphorylation depends on substrate availability and cellular energy demand. As mentioned in a previous section, the control of cellular respiration and oxidative phosphorylation has been the subject of intensive study (Brown, 1992a; Groen *et al.*, 1982; Hafner *et al.*, 1990; Letellier *et al.*, 1993; Rolfe and Brown, 1997). The advent of

top-down metabolic control analysis and its extension, elasticity analysis, has shed some light on the matter by helping to determine how oxidative phosphorylation is controlled and regulated.

In order to study the oxidative phosphorylation pathway, it was first conceptually divided into a tripartite system comprising the substrate oxidation, the phosphorylation and the proton leak blocks of reactions which are all centered around the common intermediate that is mitochondrial protonmotive force or Δp (see Figure 1.5). Here, Δp is an appropriate intermediate since it is a component of the system that is produced by one pathway (the substrate oxidation reactions: substrate transport, the citric acid cycle and the electron transport chain) and consumed by subsequent pathways (the proton leak reactions and the phosphorylating or ATP turnover reactions). By manipulating the concentration of the intermediate (the value of Δp) by titrating with various inhibitors and uncouplers of the blocks of reactions, and simultaneously measuring the flux rate through the pathway (oxygen consumption), distribution of control, or in this case, sites of regulation within the system can be determined. In the top-down elasticity analyses conducted herein, the overall kinetic response of the proton leak pathway to the concentration of the intermediate was measured in the presence and absence of the effector, which in this case is the CAST/Ei derived segment in the B6 background. If this block of reactions has a changed kinetic response to the intermediate, it must then contain sites of effector action, which are significant in changing the flux through the intermediate. Thus, in general, the top-down approach allows the identification of blocks of reactions whose overall kinetic response to a common intermediate (Δp) has been significantly altered by the effector (Harper and Brand, 1995).

Figure 1.5 Schematic representation of the branched oxidative phosphorylation system under consideration. Mitochondrial protonmotive force (Δp; the intermediate) is produced by the "substrate oxidation reactions" and consumed by both the "phosphorylation reactions" and the "proton leak reactions". The substrate oxidation subsystem consists of all the steps involved from added and endogenous substrates to the production of Δp, including substrate transport, TCA cycle, mitochondrial oxidative reactions (fatty acid β-oxidation), and the respiratory electron transport chain. The phosphorylation subsystem includes mitochondrial ATP synthesis reactions (phosphate carrier, adenine nucleotide translocator and the ATP synthase) as well as all cellular ATP-consuming reactions. The proton leak subsystem includes the leak of protons and any cation cycles across the mitochondrial inner membrane.

Oxidative Phosphorylation:
A Conceptual Tripartite Representaion

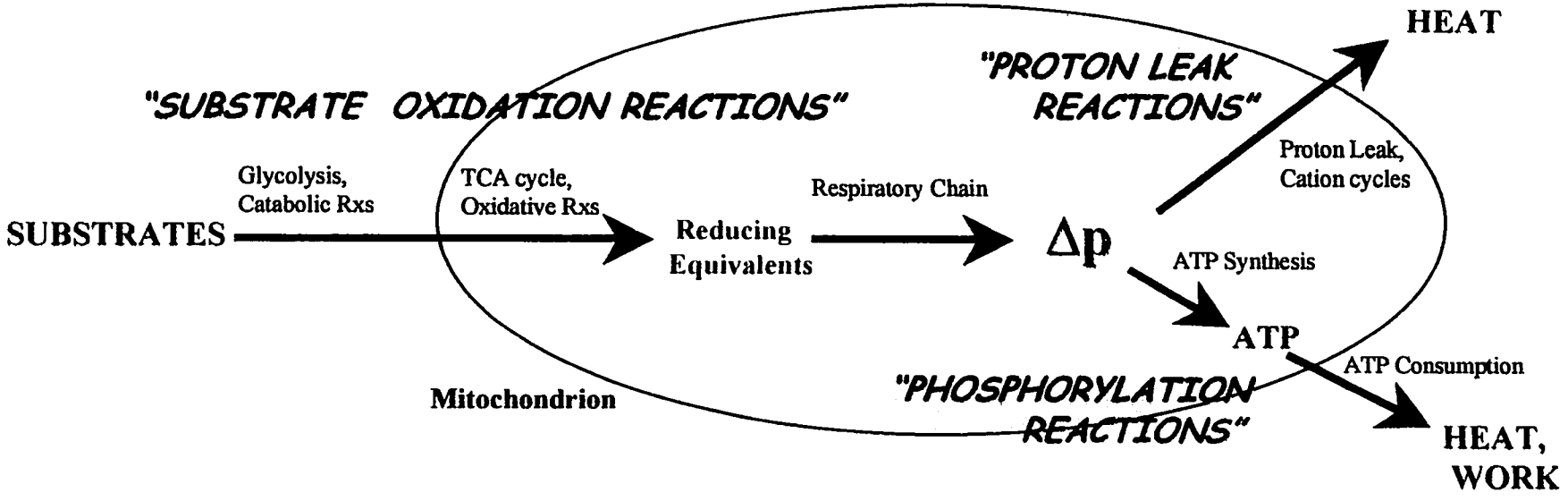

Since the objective was to specifically look at the kinetics of the mitochondrial proton leak, this branch of reactions had to be isolated from the other consumers of protonmotive force (Δp) in the system (*i.e.*, the phosphorylation branch). This was done by adding oligomycin, an antibiotic that specifically inhibits ATP synthase and prevents any protons from returning into the matrix via this route (see Figure 1.6). Any oxygen consumption that remains in these isolated mitochondria under these conditions, is that which is used to support the proton leak reactions. It is often referred to as State 4 respiration or maximal non-phosphorylating respiration. By causing variations in Δp using sequential additions of malonate (an inhibitor of complex II in the electron transport chain), the causative effects on oxygen consumption (measured as the flux through the pathway) can then be monitored. A graphical representation of Δp against oxygen consumption assessed at every point of malonate addition produces a curve, which corresponds to the kinetics of the proton leak. When two curves, say one for each strain of mice, are plotted on the same graph, comparisons of proton leak kinetics can be made and any effects of the differential chromosomal segment between the two strains of mice can be evaluated.

Figure 1.6 Isolation of the proton leak subsystem for kinetic analyses. In this simplified diagram of the oxidative phosphorylation tripartite system, the reactions of the proton leak are isolated from the other consumer of mitochondrial protonmotive force, namely the ATP turnover or phosphorylating reactions, by the addition of oligomycin. The latter compound specifically inhibits the ATP synthase by binding to the F_o subunit of the protein thus preventing any protons from returning to the matrix via this route. Once ATP synthesis is inhibited the kinetics of the leak are assessed via titrations with sequential additions of malonate which inhibits the electron transport chain at the level of complex II thereby causing decreases in both oxygen consumption and protonmotive force.

Isolation of the Proton Leak Branch of Reactions

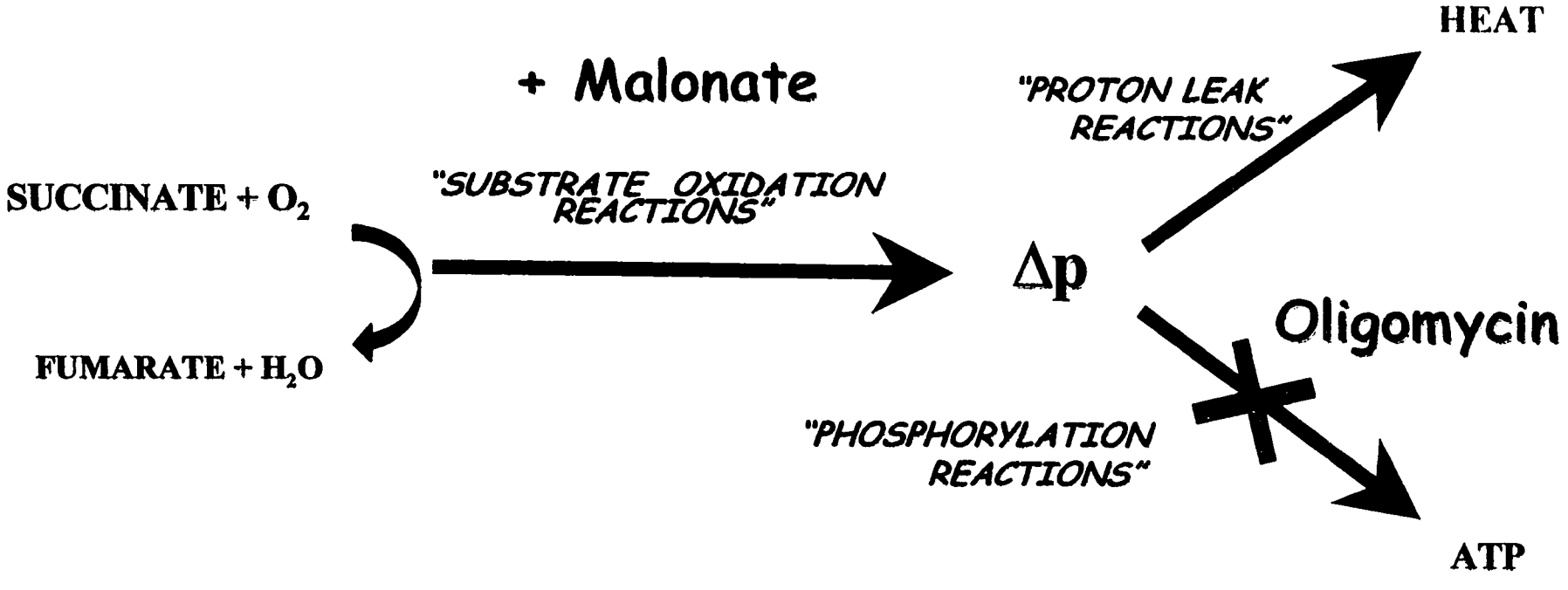

2. EXPERIMENTAL PROCEDURES

2.1 Treatment of Animals

Over the course of this project, three separate series of B6-CAST congenic and control C57BL/6J mice were studied. B6-CAST congenics were received from the Pennington Biomedical Research Center (PBRC) at Louisiana State University in Baton Rouge, LA. All control C57BL/6J mice were obtained from The Jackson Laboratory in Bar Harbor, ME. Upon arrival, the animals were individually housed in polycarbonate cages lined with wood chips and equipped with a nestlet and an open-ended hollow tube, and kept under an ambient temperature of 23 ± 2°C. They were given free access to food and tap water, and subjected to a 12:00 hour:12:00 hour light-dark cycle (lights on between 07:00-19:00). Before starting any experimental manipulations, the animals were allowed to adapt to room and cage environments for at least one week. All mice were cared for and handled according to the guidelines of the Canadian Council of Animal Care. The procedures and methods specific to this research were also approved by the University of Ottawa's Animal Care Committee Protocol Review Group.

2.1.1 Creation of the B6-CAST Congenic Mice

The congenic animals used in these studies, originated from a cross between C57BL/6J (B6) and CAST/Ei mice, followed by 10 generations of backcrosses of the progeny to B6 mice, using D7Mit41 and D7Mit297, or D7Mit213 and D7Mit67 as selection markers. The resulting mice were then bred to homozygosity at the selection markers D7Mit7 and D7Mit62, and later D7Mit37 and D7Mit130 using sib x sib breeding

(York *et al.*, 1999). All procedures outlined above were carried out by qualified technicians at the PBRC. The control mice used in each of the three described series of experiments were C57BL/6 mice that were age-matched with the B6-CAST congenics as well as possible (limited by their availability from the Jackson Laboratory).

2.2 Study Design

2.2.1 First Set of Mice (1st Study)

For the first series of experiments, male B6-CAST congenics (N=8, BWt: 24.8-29.5g, age: 16 wks) and male B6 controls (N=8, BWt: 22.4-26.0g, age: 14 wks) were fed *ad libitum* with a commercial pelleted laboratory chow diet (Charles River Rodent Animal Diet, distributed by Ralston Products, Woodstock, Ontario, Canada) with a gross energy content of 4.1kcal/g, a physiological fuel value (PFV) of 3.4kcal/g and a metabolizable energy content of 3.13kcal/g, for a period of eight weeks, during which time body weights and food intake were closely monitored. At the end of the feeding study, the mice were killed by decapitation after which epididymal white adipose tissue (EpiWAT) depots and major skeletal muscles (see below for specifics) were collected. Skeletal muscles were processed for the isolation of mitochondria (BSA containing protocol – described below), and used in analyses of proton leak kinetics, which comprise simultaneous measurements of oxygen consumption and titrations of membrane potential. A portion of the isolated mitochondria was also used in experiments leading to the measurement of mitochondrial matrix volume and $TPMP^+$ binding correction factors, needed for calculations of mitochondrial membrane potential ($\Delta\Psi m$) from $TPMP^+$ differential distribution data.

2.2.2 Second Set of Mice (2nd Study)

In the second series of experiments, male B6-CAST congenics (N=8, BWt: 23.2-26.3g, age: 5 wks) and male B6 controls (N=8, BWt: 22.2-25.5g, age: 8 wks) were given *ad libitum* access to a high fat condensed milk pelleted rodent diet available from Research Diets, Inc., New Brunswick, NJ (Product #C11024). This high fat diet has a physiological fuel value of 4.5kcal/g and a metabolizable energy content of 4.15kcal/g. The mice were fed for a period of six weeks, during which time body weights and food intake were closely monitored. At several time points before and during the high fat feeding, resting metabolic rates (RMR) and respiratory exchange ratios (RER) were assessed by indirect calorimetry. After the mice were sacrificed, blood was collected and several adipose tissue depots were removed, weighed, flash frozen in liquid nitrogen and stored. The latter depots included interscapular brown adipose tissue (IBAT), inguinal adipose tissue (IngWAT), and EpiWAT. Skeletal muscles were also removed, and again mitochondria were isolated (using the same BSA containing protocol) and used to assess mitochondrial proton leak kinetics. Blood serum samples as well as any remaining mitochondria were also flash frozen in liquid nitrogen and stored at -80°C for future use in serum and Western blot analyses, respectively.

2.2.3 Third Set of Mice (3rd study)

During the initial phase of this last set of experiments, male (N=4) and female (N=3) B6-CAST congenics (BWt: 17.2-22.7g, age: 7 wks), and male B6 controls (N=8, BWt: 19.0-22.7g, age: 7 wks) were maintained for seven weeks on the above described Charles River Rodent chow diet. While on this regime, twenty-four hour energy expenditure, as well as twenty-four hour fasting energy expenditure determinations were conducted via

indirect calorimetry. Both groups of mice were then subjected to the same six week high fat diet given during the 2nd study. At the end of this period, the mice were killed by decapitation, tissues (IBAT, EpiWAT, IngWAT, skeletal muscle) were dissected out, and once again, skeletal muscle mitochondria were isolated for proton leak titrations. This time however, a BSA free protocol (described below) was employed for the incubation of the mitochondria. The other tissues collected were weighed and stored in Formalin™ for use in histological analyses (described below).

2.3 Whole Body Experiments

2.3.1 Body Weight (BWt) and Food Intake Data Collection

Assessments of BWt and food intake were done every two to four days between 11:00-13:00 h. Both body weights and food intake were recorded to the nearest 0.1g on a Sartorius rodent balance (Model #BP2100, Sartorius Corporation, Edgewood, NY). Daily food intake was calculated as the difference between the weight of chow given to each mouse on a particular day and that of remaining chow on assessment day, divided by the number of days within this period. During food intake assessments, spillage was carefully monitored, and intake was corrected accordingly.

2.3.1.1 Energy Intake Determination

Daily energy intake was calculated by multiplying the average weight of food consumed each day per mouse, by the metabolizable energy content of the specific diet being fed (3.13kcal/g for the regular chow and 4.15kcal/g for the high-fat chow).

2.3.1.2 Metabolic Efficiency Determination

Estimates of metabolic efficiency, defined here as grams of body weight gained per kcal of dietary energy (g BWt /kcal), were derived using the BWt and food intake data collected during the high fat feeding study conducted with the second set of mice. Body weight gained over the entire six week study period was divided by the total amount of metabolizable dietary energy consumed over that same time.

2.3.2 Resting Metabolic Rates (RMR) and Respiratory Exchange Ratio (RER) Determinations

At several time points before and during the high-fat feeding regimen (0, 2, 4 and 6 weeks), resting metabolic rate (RMR) and respiratory exchange ratio (RER; or respiratory quotient, RQ) of all eight mice in each of the two groups were assessed by indirect calorimetry. The mice were individually placed in the metabolic chambers of a temperature controlled Oxymax open circuit indirect calorimeter system manufactured by Columbus Instruments International Corporation, Columbus, Ohio. The system includes four metabolic chambers, O_2 and CO_2 sensors, electronic flow regulators and an automated switching system to sample from each metabolic chamber in turn. For mice. the volume of each chamber is approximately 2.5 liters. Compressed air from a tank supplies the chambers at a rate of 0.5 liters/min, and the air that is being sampled from the chambers is dried in a Drierite (anhydrous $CaSO_4$) column and then passed through the system's oxygen and carbon dioxide analysers. Air from each chamber is sampled sequentially for 2 minutes. The gas fractions and flow measurements are then used to calculate oxygen consumption (VO_2 - ml O_2/min/mouse), carbon dioxide production (VCO_2 – ml CO_2/min/mouse), RER (VCO_2/VO_2) and heat production (kcal/min/mouse).

The control, measurement, display and storage of the accumulated data is performed automatically by a personal computer loaded with an Oxymax specialized software package.

For RMR and RER determinations, non-fasted mice were placed in metabolic chambers contained within the temperature-controlled unit set at 28°C. Each metabolic chamber has a floor area of 210cm^2 and a height of 12cm, allowing free movement of the mice. A grid was placed about 1 inch over the floor of the chamber to draw excrements away from the mice. While in the chambers, the mice did not have access to any food or water. Individual assessments typically ran for approximately 3 hours, during which time the mice were monitored for activity at frequent intervals. For each mouse, the three lowest rates of oxygen consumption corresponding to periods of inactivity were averaged as estimates of resting metabolic rate. It was at these same time points that RER values were taken for the mean resting RER determinations.

2.3.3 24 Hour Energy Expenditure Assessments

These assessments were conducted using the same Oxymax system described above. In this case however, the mice had *ad libitum* access to food and tap water while in the metabolic chambers, and the temperature-controlled unit was set at 31°C, a temperature approximating murine thermoneutrality. The mice were left in the chambers for 24 hours and were exposed to a 12:00 hour:12:00 hour light-dark cycle (lights on from 7:00 to 19:00 h).

2.3.4 24 Hour Fasting Energy Expenditure Assessments

Here again, measurements were taken using the Oxymax system described in section 2.3.2. For these assessments, the mice were placed in the metabolic chambers at an ambient temperature of 31°C, and had free access to water only. The study period began at 07:00h with the lights on and continued for 24 hours with the lights being automatically shut off at 19:00h. After 24 hours, the mice were transiently taken out of the chambers in order to measure their rectal temperature using a Physitemp Thermalert rectal probe (model TH-8; Physitemp Instruments Inc., Clifton, NJ) coated with glycerine. The mice were then returned to the metabolic chambers and given pelleted chow. Data collection continued for six hours post-refeeding after which time the mice were taken out of the calorimeter.

2.4 Tissue Analyses

2.4.1 Tissue Collection

All the mice used in these experiments were sacrificed by decapitation. At the time of killing, blood was collected in conical centrifuge tubes placed on ice, left to clot for 2-4 hours and centrifuged at 7000rpm for approximately 15 minutes using a Clini-Cool™ Refrigerated Centrifuge (Damon / OEC Division, Needham Heights, MA). The blood serum was then transferred into Eppendorf™ microfuge tubes with a Pasteur pipette, flash frozen in liquid nitrogen, and stored until use at -80°C. Interscapular BAT (IBAT) and epididymal and inguinal white adipose tissues (Epi/IngWAT) were rapidly dissected out immediately after blood collection and cleaned of tissue debris including connective tissue, WAT (in the case of IBAT), adherent muscle and vasculatures. After careful

weighing, these tissues were either immediately frozen in liquid nitrogen and stored at -80°C, or placed in 10 times the volume of 10% (w/v) buffered Formalin™ (4% formaldehyde solution) in glass scintillation vials kept at room temperature.

2.4.2 Serum Assays

2.4.2.1 Serum Free Fatty-Acid Determination

Quantitative determination of non-esterified (or free) fatty acids (NEFA) in serum was performed as stated in the instruction manual of the *Wako NEFA-C test kit* manufactured by Wako Chemicals Gmbh (Germany) and distributed by Wako Chemicals USA, Inc., Richmond, VA. This test kit utilizes an *in vitro* enzymatic colorimetric method. Briefly, it relies upon the acylation of coenzyme A by the serum free fatty acids in the presence of added acyl-CoA synthetase. The acyl-CoA produced is oxidized by added acyl-CoA oxidase with generation of hydrogen peroxide. When peroxidase is added, this hydrogen peroxide leads to the oxidative condensation of two external reagents resulting in a purple coloured adduct with an absorption maximum at 550 nm. The concentration of NEFA in the sample was obtained through Beer's law and the absorbance of a standard of known concentration. It was verified for accuracy using Normal Accutrol™ Chemistry Controls from Sigma Diagnostics (St-Louis, MO).

2.4.2.2 Serum Glucose Determination

The level of glucose in the serum samples was quantitatively determined using the Glucose (Trinder) reagent (Procedure No.315) from Sigma Diagnostics (St-Louis, MO). This assay involves first the glucose oxidase catalysed conversion of glucose to gluconic acid and hydrogen peroxide. The hydrogen peroxide formed reacts in the presence of

peroxidase with two external reagents to form a quinoneimine dye, which absorbs maximally at 505nm. The intensity of the resulting colour is directly proportional to the glucose concentration in the sample, which is obtained through Beer's law and the absorbance of a standard of known concentration. It is verified for accuracy using Normal Accutrol™ Chemistry Controls also form Sigma Diagnostics.

2.4.2.3 Serum Triglyceride Determination

An enzymatic assay from Sigma Diagnostics (Procedure No.339) was used to determine quantitatively the level of triglycerides in the serum samples. The Triglyceride (GPO-Trinder) reagent's actions are based on the same principles as stated above for glucose determination. Here, serum triglycerides (TG) are split into FFA and glycerol, which is phosphorylated and subsequently oxidized leading to the generation of hydrogen peroxide. In this case, the quinoneimine dye produced has an absorption maximum at 540nm. Sample TG concentration is calculated and verified for accuracy as above.

2.4.3 Histological Analyses: Light Microscopy of Thin Sections

As mentionned in section 2.4.1, certain tissues (IBAT, IngWAT and EpiWAT) were placed in Formalin™ immediately after being dissected out and weighed. These tissues were left to fix in the Formalin™ solution for a minimum of three days before being processed. All subsequent processing steps including embedding, preparation of slides, staining and photographs were done by Linda Jui, a skilled technician in Dr. Jean Himms-Hagen's laboratory.

2.4.3.1 Paraffin Embedding of Tissue Sections

The tissue pieces were placed in plastic cassettes (HISTOSETTE® I, Simport Plastics). The tissue was then processed in an automatic machine in the following manner. First the tissue was dehydrated using incremental proportions of ethanol in ddH_2O (60%, 70%, 80%, 90%, 100%). The tissue was then cleared with xylene twice and finally with paraffin. The tissue was embedded in paraffin by hand. The blocks were then sliced into 4μm thick sections using a microtome (Tissue-Tek® "820" microtome, Spencer) and placed onto Superfrost Plus slides.

2.4.3.2 Staining of Thin Sections

The paraffin embedded sections were then deparaffinized and rehydrated according to the following scheme. The sections were left in xylene for 5 minutes (twice), then washed twice in 100% ethanol for 3 minutes, once in 95% ethanol for 3 minutes, once in 70% ethanol for 3 minutes, and once in water for 5 minutes. For hematoxylin and eosin (H&E) staining, the sections were first incubated in filtered Delafield's Haematoxylin solution (Sigma Cat# GHS-2-16) for 6 minutes, and then rinsed in water and differentiated in acid-alcohol (30% alcohol + 1% HCl) for 3 seconds. They were then washed in lithium carbonate (1g/100mL distilled water) until the section was blue. After a 10 minute wash in running tap water, the sections were placed in alcoholic eosin solution (Sigma Cat# HT110-1-16) for 2 minutes. They were then dehydrated once in 95% alcohol for 2 minutes, twice in 100% alcohol for 2 mintues, and once in xylol for 5 minutes. Finally, the sections were mounted on slides with Permount (Bancroft, 1975; Lillie and Fulmer, 1976).

2.4.3.3 Viewing and Photographic Development of Slides

The sections were viewed using a light microscope (Zeiss Axioskop 20, West Germany) under 400x magnification (objective 40X OPTvar 1.25X objective of camera 16) and were photographed using an attached camera. The film used was Kodak Ektachrome 64T (tungsten) Professional, Colour Reversal Film (EPY 135-36) and was taken to a photographic shop for processing.

2.4.4 Protein Content Determination in Interscapular BAT

Frozen IBAT samples were taken out of the -80°C freezer and left to thaw on ice. The samples were then homogenised in ice-cold isolation medium (0.25M sucrose, 1mM *N*-2-hydroxyethylpiperazine-*N'*-ethanesulfonic acid, 0.2mM potassium EDTA, adjusted to pH 7.2 with 1.0M KOH) using a Potter-Elvehjem homogeniser (Talboys Engineering Corporation, Emerson, NJ) equipped with an ice-cold teflon pestle. The ratio of the volume of isolation medium to the weight of each sample was approximately four.

The protein content of the IBAT homogenate was measured using a Lowry assay (Lowry *et al.*, 1951) as modified by Schacterle and Pollack (Schacterle and Pollack, 1973). Bovine serum albumin (BSA) was used as a standard. A six point calibration curve using BSA standards (0, 15, 30, 60, 90 and 120μg protein) was used to calculate protein concentration in the samples. Both standards and samples were treated identically. The homogenate to be assayed and the protein standards were aliquoted in triplicate into conical plastic tubes to which 5mL of 12.5% TCA was added. The tubes were then mixed, covered with parafilm, and left to incubate overnight at 4°C to allow the protein to precipitate. The next morning the tubes were centrifuged at 4,000rpm for

30 minutes in a Beckman J-6B refrigerated centrifuge equipped with dark green adapters. The resulting infranatant was then aspirated along with any fat that could interfere with the assay. Following this procedure, 1.15mL of 0.5N NaOH was added to each tube and the contents were mixed. All of the precipitated protein was redissolved by placing the tubes in a water bath maintained at 55°C for 10 minutes, and then by mixing. After allowing the tubes to cool to room temperature, a volume of copper reagent (10% w/v sodium carbonate, 0.1% w/v potassium tartrate, 0.05% w/v cupric sulphate) was added to the tubes which were then mixed and left to incubate for 10 minutes at room temperature. Next, a volume of Folin reagent (2N phenol reagent -Folin & Ciocalteu- diluted 1:16 with water immediately before use) was added to the tubes, which were then vortexed and incubated at 55°C for 5 minutes. The tubes were then placed on ice for 5-10 minutes to stop the reaction. Within 30 minutes, the absorbance of the samples at 650nm was read on a Beckman DU-50 spectrophotometer equipped with a linear software data pack. Values of triplicates that were within 10% of each other were retained and their protein concentration determined using the calibration curve.

2.5 Mitochondrial Analyses

2.5.1 Isolation and Incubation of Skeletal Muscle Mitochondria in the Presence of 0.5% (w/v) Defatted BSA

Immediately following the extraction of IBAT and Epi/IngWAT, several skeletal muscle groups were quickly and carefully removed and placed in ice-cold isolation medium (100mM sucrose, 10mM EDTA, 100mM Tris-HCl, 46mM KCl; pH 7.4). These muscle groups included those from the hindlimb, including most major leg muscles

(gluteus maximus, gluteus medius, gluteus minimus, vastus lateralis, rectus femoris, biceps femoris, adductor magnus, adductor brevis, semimembranosus, gastrocnemius, tibialis anterior) and a small amount of back muscles. Forelimb muscles including those of the shoulder (subscapularis, supraspinatus, spinodeltoideus) and brachial (triceps longus, triceps medius, biceps brevis, biceps longus) musculatures, were also used.

Mitochondria were isolated from these skeletal muscle groups by the method of Bhattacharya *et al.* (Bhattacharya *et al.*, 1991) with a few slight modifications. The cold muscle tissue was quickly cleaned of any visible bone, connective tissue and fat, and was finely chopped on a pre-chilled watchglass using two safety razor blades. The minced tissue was then added to 25mL of cold isolation medium containing 0.5% (w/v) defatted bovine serum albumin (BSA) (*see section 2.5.1.1*) and 5mg Nagarse (Type XXVII; 7.8 units/mg), and incubated at room temperature for 5 minutes with gentle swirling. Further disruption of the tissue was achieved through homogenisation. Avoiding suction and/or bubble formation, the tissue was homogenized by making 3-5 long strokes followed by several small strokes of the rotating pestle down the homogenization tube using a Potter-Elvehjem homogeniser (Talboys Engineering Corporation, Emerson, NJ) equipped with an ice-cold teflon pestle. The homogenate was then left to incubate on ice with occasional stirring for approximately 5 minutes, and centrifuged at 3,000rpm (700g) for 10 minutes in a Sorvall superspeed RC2-B automatic refrigerated centrifuge (SS-34 rotor, 4°C). The supernatant was then poured through a 253μm Nitex filter and centrifuged at 10,000rpm (16,000g) for another 10 minutes. At this point, any white fluffy material surrounding the pellet was gently removed by gentle swirling and dabbing with a long cotton swab. This pellet was then resuspended in 5mL of isolation medium containing

0.5% (w/v) defatted BSA, using the blunt end of a pre-chilled glass stirring rod, and was centrifuged at 10,000rpm (16,000g) for 10 minutes. The mitochondrial pellet was then resuspended in ice-cold suspension medium (120mM KCl, 20mM sucrose, 20mM glucose, 10mM KH_2PO_4, 5mM HEPES, 2mM $MgCl_2$, 1mM EGTA, 0.5% (w/v) BSA; pH 7.2) and stored on ice until use. The protein concentration of this mitochondrial preparation was assayed using the Biuret method of protein determination (*see section 2.5.1.2*), and corrected for BSA present in the suspension.

2.5.1.1 Defatting of Bovine Serum Albumin (BSA)

Stock BSA was defatted according to the protocol outlined by Chen (Chen, 1967). First, 50g of BSA (Fraction V, Sigma A7906) were added to 250ml of ddH_2O and stirred on a magnetic plate until dissolved. A suspension of activated charcoal (25g of acid washed (BDH 33033) in 100mL ddH_2O) was then added to the BSA solution and any resulting froth removed with a tissue. The mixture was slowly brought to a pH of 3 with HCl and stirred on ice for 1 hour. It was then centrifuged at 11,300rpm (20,000g) using a Beckman J2-21M centrifuge (JA14 rotor) for 20 minutes at 4°C. The resulting supernatant was slowly decanted into a 500mL beaker, and 10M NaOH was added dropwise to bring the pH to 7. The same spin was repeated and the supernatant decanted and left to sit for a few hours before being vacuum-filtered sequentially through 0.45μm (Millipore HA type) and 0.22μm (Millipore GS type) filters. The resulting filtrate was dialysed three times (through 24/32 dialysis tubing having been boiled first for 5min in 50-100mM Na_2EDTA and then in ddH_2O for 5min) against 153mM NaCl and 11mM KCl; twice for 1 hour and once overnight at 4°C. The protein concentration of this defatted BSA preparation was determined using the Biuret method (see below). After

being diluted to 9% (w/v) with dialysis medium, 10mL aliquots of the defatted BSA stock were stored at -20°C.

2.5.1.2 Biuret Determination of Protein Concentration

The protein concentration of all mitochondrial preparations were determined using the Biuret method (Gornall *et al.*, 1949) which is based on the formation of a coloured complex between peptide bonds and copper in alkaline solutions. To perform this test, 25μL of the mitochondrial preparations were added to 200μL of suspension medium (see section 2.5.1) and 25μL of sodium deoxycholate (0.1% w/v). A reference or blank test tube was also prepared which contained 225μL of suspension medium and 25μL of sodium deoxycholate. Next, 1mL of the Biuret reagent (1.5g $CuSO_4 \cdot 5H_2O$ dissolved in 500mL ddH_2O, 6g $K_2C_4H_4O_6$, 300mL 10% NaOH, 1g KI, diluted to 1L) was added to each tube. The tubes were then incubated for 10 minutes in a hot water bath maintained at 37°C. Once allowed to cool to room temperature, the absorbances of both the sample and the blank were read at 540nm using a Beckman DU-50 spectrophotometer. A six point calibration curve using BSA as a standard (0, 2, 4, 6, 8, 10mg/mL) was used to calculate the protein concentration of the mitochondrial preparation from its measured absorbance corrected for that of the blank.

2.5.2 Isolation and Incubation of Skeletal Muscle Mitochondria in the Absence of 0.5% (w/v) Defatted BSA

As detailed in section 2.5.1, after sacrificing the mice and removing tissues of interest, various skeletal muscle groups were dissected out and used to isolate mitochondria. The mitochondrial isolation protocol described here and used for proton

leak analyses of the third set of mice, has also been adapted from that of Bhattacharya *et al.*(Bhattacharya *et al.*, 1991). It is essentially the same as the protocol outlined above in section 2.5.1, except that 0.5% (w/v) defatted BSA was not added to the 25mL of Nagarse containing isolation medium in which were placed the minced skeletal muscle tissue pieces, nor was it added to the 300μL of suspension medium used to resuspend the final mitochondrial pellet.

2.5.3 Assessment of Overall Mitochondrial Proton Leak Kinetics in Skeletal Muscle

Measurements of mitochondrial oxygen consumption and membrane potential were carried out simultaneously in a water jacket temperature-controlled incubation vessel.

2.5.3.1 Measurements of Mitochondrial Oxygen Consumption

Mitochondrial respiration rates were measured using a Hansatech Clark-type oxygen electrode present in the base of the incubation vessel. At the start of each new titration, 1mL of suspension medium (120mM KCl, 20mM sucrose, 20mM glucose, 10mM KH_2PO_4, 5mM HEPES, 2mM $MgCl_2$, 1mM EGTA, with (1^{st} and 2^{nd} studies) or without (3^{rd} study) 0.5% (w/v) BSA; pH 7.2), was added to the magnetically stirred chamber thermostatically maintained at 37°C by hot water circulating through its jacketed walls. To this medium, 5μM rotenone (10μL of 5mM stock) was added in order to prevent the respiration of any endogenous NAD-linked substrates. Nigericin (80ng/mL; 4μL of 24μg/mL stock in EtOH) was also added (during the 1^{st} and 2^{nd} studies only) in an attempt to bring $-z\Delta pH$ close to zero (Brand, 1995). At this point, the medium was left stirring in the open chamber in order to reach equilibrium with the oxygen in the surrounding air. Once the oxygen electrode trace reached a steady state, defined as 100%

oxygen saturation, mitochondria (0.5mg protein/ml) were added and the chamber was capped with a plunger containing two small holes; one left open for syringe additions of substrates and inhibitors, the other fitted with a $TPMP^+$-sensitive electrode used to measure membrane potential (see next section for details). Respiration of the mitochondria was initiated by adding succinate to a final concentration of 10mM (10μL of 1M stock). This resulted in the steady decline of the electrode trace as the medium was slowly being depleted of oxygen. From this point, various inhibitors were added to establish both respiratory control ratios (state 3 /state 4) and kinetics of the proton leak reactions. State 3 respiration was achieved by initially adding 100μM ADP followed by 10μL of hexokinase (0.65units/mL); 0.05μM FCCP (5-20μL of 1μM stock) was later added to stimulate maximal respiration. State 4 respiration was attained with the addition of 4μg of oligomycin (40μL of 100μg/mL stock), a specific inhibitor of ATP synthase. Complete inhibition of the enzyme was confirmed when additional oligomycin caused no further drop in oxygen consumption and no further increase in membrane potential. Titrations of the mitochondrial proton leak were carried out in the presence of saturating amounts of oligomycin (State 4), by sequential additions of 1M malonate (a competitive inhibitor of complex II of the respiratory chain), to give final concentrations of 0.33, 0.67, 1.0, 2.0, 3.0, and 5.0mM. Oxygen consumption rates were calculated from the slopes of the oxygen electrode trace (units/min) with the assumption that the oxygen concentration in the air-saturated incubation medium was 406 nmol O/mL at 37°C (Reynafarje *et al.*, 1985).

2.5.3.2 Measurements of Mitochondrial Membrane Potential ($\Delta\Psi m$)

Membrane potential was determined with the help of an amphipathic organic cation, $TPMP^+$ (triphenylmethylphosphonium) used as a probe, since it distributes itself on either side of the mitochondrial inner membrane according to its membrane potential. By using a $TPMP^+$-sensitive electrode, the accumulation of the $TPMP^+$ probe can be monitored by measuring its external concentration. Provided that there is no active transport, $TPMP^+$ eventually comes to equilibrium according to the Nernst equation:

$$\Delta\Psi = 61.5 \log ([TPMP^+]_{in} / [TPMP^+]_{out})$$

From the change in external concentration, the volume of the mitochondrial matrix (section 2.5.3.2.2) and a correction factor for non-specific binding (section 2.5.3.2.3), it is possible to calculate the intramitochondrial concentration, and thus the value of $\Delta\Psi$ (Brand, 1995).

The Kwik-Tip™ $TPMP^+$-sensitive electrodes used here were constructed according to the methods of Kamo (Kamo *et al.*, 1979). The outputs from both the $TPMP^+$ and the oxygen electrodes were transferred to two voltmeters whose reference sockets were connected together. The data collected were then fed into a data analysis software package (Duo 18™ data recording system; World Precision Instruments, Sarasota, FL) which allowed for computer assisted real-time monitoring, recording and storing of data.

2.5.3.2.1 Calibration of $TPMP^+$-sensitive Electrodes

With the mitochondria (0.5mg protein/mL) incubating in the 1 mL of suspension medium (plus 5μM rotenone and 80ng/mL nigericin) contained in the oxygen electrode chamber, the chamber was effectively sealed using a plunger fitted with the $TPMP^+$

electrode. After the electrode traces became steady, the $TPMP^+$ electrode was calibrated by sequential 10μM additions of TPMP-bromide (10μL of 1mM stock) over the range of 10-50μM. Before each addition, the trace was allowed to reach a new steady state (5-30sec). Once a total $TPMP^+$ concentration of 50uM in the incubation medium was reached, respiration of the mitochondria was initiated by adding 10mM succinate. The mitochondria were then allowed to accumulate the $TPMP^+$ for 30-60 seconds until an equilibrium distribution was achieved and the extramitochondrial $TPMP^+$ concentration (which the electrode measures) was stable (Brand, 1995). Additions of various inhibitors and uncouplers were then made, with the new steady state value of $\Delta\Psi$ being obtained within 30-60 seconds of each addition. The intramitochondrial amount of $TPMP^+$ could then be calculated from the amount of $TPMP^+$ added by subtracting the amount remaining externally (see below for details).

2.5.3.2.2 Calculation of ΔΨm from $TPMP^+$ Electrode Data

The relationship between $\Delta\Psi m$ and $TPMP^+$ distribution at 37ºC is defined by:

$$\Delta\Psi m = 61.5 \log \left\{ \frac{[TPMP^+]_{matrix} \times \text{TPMP binding correction factor (or } a_m)}{[TPMP^+]_{external}} \right\}$$

where:

$$[TPMP^+]_{matrix} = \frac{\{ [TPMP]_{added} - [TPMP]_{external} \}}{\{0.001 \times \text{matrix volume (MV in } \mu L/mg \text{ protein)} \times \text{mg protein/mL}\}}$$

Using the latter equation, the intramitochondrial amount of $TPMP^+$ can be calculated from the amount of $TPMP^+$ added, the amount of $TPMP^+$ in the external medium and the volume of the mitochondrial matrix. The measurement of this last variable is described in the following section.

In order to obtain actual values of extramitochondrial $TPMP^+$ from the electrode data, a calibration graph was produced by plotting the deflection caused by each 10 μM

$TPMP^+$ addition in chart units from the baseline, against the logarithm of the final $TPMP^+$ concentration. To measure the external $TPMP^+$ concentration for any given electrode signal, the deflection from the baseline (in chart units) to the desired steady state was determined and the external $TPMP^+$ was read off the calibration graph directly.

Both $[TPMP^+]_{matrix}$ and $[TPMP^+]_{external}$ were determined for state 3 and state 4 as well as for each point within the mitochondrial proton leak titration and used to calculate $\Delta\Psi m$ from the equation stated above. The measurement of non-specific TPMP binding (a_m correction factor) appearing in this equation is described in section 2.5.3.2.4.

2.5.3.2.3 Assessment of Mitochondrial Matrix Volume (MV)

By incubating mitochondria with a radiolabelled probe such as ^3H_2O and then sedimenting them through centrifugation, the accessible volume of the pellet (that of the mitochondria) can be derived from the specific activity of the probe in the supernatant and the total radioactivity in the pellet. The difference in accessible volume ('pellet space') for permeant probes like ^3H_2O and probes like [^{14}C]-sucrose that can not permeate the inner membrane, is equal to the volume of the mitochondrial matrix (Brand, 1995). To do this, mitochondria (2mg protein; 40-80μL depending on the preparation) were incubated for 2 minutes at 37°C in 1mL of incubation medium (120mM KCl, 5mM HEPES, 1mM EGTA, 5 μM rotenone; pH 7.2; 37°C) containing 10μL of ^3H_2O (100μCi/mL stock; f.c. 1μCi) and 10μL of [C^{14}]-sucrose (10μCi/mL stock; f.c. 0.1μCi), in 1.5mL Eppendorf™ minitubes. The mitochondria were then sedimented at 7,000rpm (12,000g) in a Fisher minicentrifuge for 30sec. Next, 500μL aliquots of the supernatant were pipetted into scintillation vials and immediately mixed with 7.5mL of scintillation

cocktail (Amersham ACSII, Arlington, IL). The residual supernatant was slowly decanted so as not to disturb the pellet, and twisted tissue swabs were used to carefully wipe the sides and cap of each tube dry. Addition of 40μL of 20% (w/v) Triton X-100 to the pellet allowed for its resuspension upon vigorous vortex mixing. The tip of the minitube containing the whole pellet suspension was then clipped into a scintillation vial using dog nail clippers and immediately covered with 7.5mL of scintillant. After sufficient vortex mixing of the scintillation vials, radioactivity in the supernatant and pellet was determined by dual-channel liquid scintillation counting for ^{3}H and ^{14}C using the appropriate background, quench and crossover corrections. The mitochondrial matrix volume, given as μL/mg protein, was then calculated as:

$$MV = \frac{(^{3}H_2O \text{ space} - [^{14}C]\text{-sucrose space})}{\text{mg mitochondrial protein}}$$

where:

$$^{3}H_2O \text{ space or } [^{14}C]\text{-sucrose space} = \frac{(\text{dpm of pellet x volume of supernatant})}{\text{dpm of supernatant}}$$

Average mitochondrial matrix volumes were found to be 0.46 μL/mg protein (± 0.05) in B6-CAST congenic mice and 0.39 μL/mg protein (± 0.03) in B6 controls. These values were based on duplicate determinations completed on skeletal muscle mitochondria isolated from each of 5 congenic and 8 control mice.

2.5.3.2.4 Assessment of Non-specific $TPMP^+$ Binding Correction Factor (a_m)

Due to its hydrophobic character, which allows it to cross lipid membranes, a probe such as $TPMP^+$ is also prone to considerable non-specific binding within the mitochondrial matrix. This effect needs to be accounted for and corrected for accordingly in order to obtain quantitative measurements of membrane potential. To do so, an empirical rather than theoretical correction is made which involves calibrating the

$TPMP^+$ signal against a probe such as the radioisotope congener of K^+, $^{86}Rb^+$ that does not bind (Brand, 1995). The correction protocol used here adjusts the accumulation ratio for $TPMP^+$ to that for $^{86}Rb^+$ measured over a range of membrane potentials as described by Nobes *et al.* (Nobes *et al.*, 1990). This was done by comparing [^{3}H]-$TPMP^+$ and $^{86}Rb^+$ accumulation ratios, defined as $[TPMP^+]_{tot}/[TPMP^+]_{external}$ and $[Rb^+]_{tot}/[Rb^+]_{external}$ respectively, at different values of mitochondrial membrane potential. Membrane potential was set using valinomycin and three different extramitochondrial concentrations of KCl (0.2, 1.0 and 5.0mM). For each concentration of KCl, two duplicate sets of minitubes were prepared. Each set contained approximately 2mg protein (80 µl of mitochondrial preparation), 1.0 mL of incubation medium (200mM sucrose, 5mM HEPES, 5mM LiCl, 1mM EGTA, 5µM rotenone, 1µM TPMP-Br; pH 7.2), and 0.2 µg/mL valinomycin. To one set of minitubes, 0.035 µCi ^{86}RbCl/mL and 0.15 µCi [^{3}H]-$TPMP^+$/mL were added. To the other set, additions of 1.5 µCi ^3H_2O/mL and 0.15 µCi [^{14}C]-sucrose/mL were made. Subsequently, 5mM succinate/mL (10µL of 500 mM stock brought to pH 7.0 with LiOH) was added to all minitubes, which were then mixed by inversion. After 2 minutes at room temperature the mitochondria were sedimented in a Fisher minicentrifuge at 7000 rpm (12,000*g*) for 2 minutes. Next, 500µL aliquots of the supernatant were pipetted into scintillation vials containing 7.5mL of scintillation cocktail (Amersham ACSII, Arlington, IL). The residual supernatant was slowly decanted, tissue swabs were used to carefully dry the sides and cap of each tube, and 40µL of 20% (w/v) Triton X-100 were added to resuspended the pellet. After vigorous vortex mixing, the tip of the minitube containing the resuspended pellet was clipped into a scintillation vial and immediately mixed with 7.5mL of scintillant and 150µL of

ddH_2O. After shaking to mix the contents of the scintillation vials, radioactivity in the supernatant and pellet was determined by dual-channel liquid scintillation counting for ^3H and ^{14}C using the appropriate background, quench and crossover corrections.

The [^{3}H]-TPMP$^+$ and $^{86}Rb^+$ accumulation ratios (a/r) were then calculated as:

$$[^3H]TPMP^+ \text{ a/r} = \frac{[^3H]TPMP^+ \text{ space} - [^{14}C]\text{sucrose space}}{^3H_2O \text{ space} - [^{14}C]\text{sucrose space}}$$

and

$$^{86}RbCl \text{ a/r} = \frac{^{86}Rb^+ \text{ space} - [^{14}C]\text{sucrose space}}{^3H_2O \text{ space} - [^{14}C]\text{sucrose space}}$$

where the apparent volume of space available to each isotope (in µl) was calculated as dpm in total pellet divided by dpm/µl of supernatant sample. A plot of [^{3}H]TPMP$^+$ a/r against $^{86}Rb^+$ a/r gives a linear relationship, the inverse slope of which is defined as a_m, which represents the fraction of TPMP$^+$ which is actually free inside the matrix.

For B6-CAST congenic and B6 control mice, values of a_m were determined to be 0.29 and 0.21 respectively. In each case, these values were based on data from skeletal muscle mitochondria and represent the inverse slope of a three point graph with each point being an average of 6 replicates from 3 mice for congenics, and 18 replicates from 6 mice for controls.

2.5.4 Western Blot Analyses

Western blot analyses were performed on isolated skeletal muscle mitochondria from both B6-CAST congenic and B6 control mice, in an attempt to examine and compare differences (if any) in the level of uncoupling proteins, specifically UCP2 and (especially) UCP3. The mitochondria used in these analyses were isolated and prepared as described in section 2.5.1. Any mitochondria left over from experiments of proton

leak kinetic assessments were transferred to minitubes and immediately flash frozen in liquid nitrogen and stored at -80°C until needed.

2.5.4.1 Preparation of Samples

Uncoupling proteins were detected in these mitochondria by SDS-polyacrylamide gel electrophoresis (PAGE) and Western blotting. On the day of the assay, a volume of mitochondria containing 20μg of protein was combined with an equal volume of sample loading buffer (2% SDS, 0.1M Tris-HCl, 4mM PMSF in isopropanol, 2mM EDTA with bromophenol, 20% (w/v) glycerol and 10% (v/v) β-mercaptoethanol). Before being loaded on the gel, the samples were boiled for approximately 5 minutes. Along with the samples, Amersham Rainbow™ coloured protein molecular weight markers, Bio-Rad biotinylated molecular weight markers, and a standard of purified rat uncoupling protein (0.25-0.5μg), were also loaded. The Rainbow™ markers were prepared by combining them 2:3:5 with PBS (phosphate buffered saline; 1.1mM K_2HPO_4, 0.3mM KH_2PO_4. 28mM NaCl, 0.6mM KCl; pH 7.4) and sample loading buffer, and boiling them for 1 minute before loading. Similarily, the biotinylated markers, were prepared by combining them 1:1:2 with PBS and sample loading buffer and boiling them for 5 minutes prior to loading. The purified rat UCP standard used in these experiments was prepared in Dr. Jean Himms-Hagen's laboratory by past and present graduate students, namely Dr. Anna-Lisa Kates and Dr. Anna Melnyk. UCP was isolated from BAT mitochondria of 12 Sprague-Dawley rats which had been cold exposed at 4°C for 4 weeks. Mitochondria were isolated according to Slinde et al. (Slinde *et al.*, 1975), and UCP was purified using the method of Lin and Klingenberg (Lin and Klingenberg, 1982).

This standard was also combined (1:1) with sample loading buffer and boiled for 5 minutes prior to loading.

2.5.4.2 Resolution of Mitochondrial Protein Samples by SDS-PAGE

The PROTEAN®II Mini Electrophoresis Cell (Bio-Rad) was used for casting and running of the gels. A separation gel (16% acrylamide/bisacrylamide, 9% Tris-base, 0.1% SDS, 0.1% ammonium persulfate) was poured the day before the experiment, overlaid with water, covered with plastic wrap, and left to polymerize at 4°C overnight. The next morning, the water was removed by inverting the apparatus and dabbing the remaining water with filter paper. After pouring the stacking gel (4% acrylamide/ biacrylamide, 0.8% Tris base, 0.1% SDS, 0.1% ammonium persulfate), the combs were inserted and 60 minutes were allowed for polymerization. The combs were then removed and the gels placed in a running buffer (0.3% Tris-base, 1.42% glycine, 0.1% SDS, 0.01% PMSF) filled electrophoresis cell tank. The samples were loaded in the wells with a Hamilton microsyringe and the gels were run at 180V for 2 hours and 50 minutes.

After this time, the gels were placed in transfer buffer (0.72% glycine, 0.15% Tris-base, 20% (v/v) methanol, 0.1% PMSF), and left to equilibrate for 30 minutes with gentle shaking at room temperature. Transfer of the proteins was subsequently carried out using a Mini Trans-Blot® Electrophoretic Cell from Bio-Rad. Transfer 'sandwiches' were assembled in the following order: 2 sponge fiber pads, 2 pieces of filter paper, an equilibrated gel, a nitrocellulose membrane (NCM), 2 filter papers and 2 more sponge fiber pads, all of which had been pre-soaked in transfer buffer for 30 minutes prior to the assembly process. These sandwiches were set up in transfer cassettes, which were then placed in the Trans-blot cell with the NCM facing the anode. An ice pack and a stir bar

were added to the chamber, and the transfer was allowed to proceeded at 120V for exactly one hour. Once the transfer was completed, the nitrocellulose membrane was gently removed, wrapped in plastic wrap and stored at -20°C until further processing.

2.5.4.3 Western Blotting With Two Different UCP Antibodies

On the day of immunoblotting, the nitrocellulose membrane was removed from its plastic wrap and placed in blocking solution (PBS plus 0.1% (v/v) Tween-20 and 5% w/v skim milk powder) for 1 hour at room temperature with gentle shaking on a Belly Dancer® Shaker (Stovall Life Science Inc.). The blot was then washed several times (2 quick rinses, 2 five min washes, 1 fifteen min wash) with fresh washing solution (PBS plus 0.1% (v/v) Tween-20) and vigorous shaking on the Belly Dancer®. The biotinylated MW marker lane was cut off the blot at this stage and placed in 0.1% (v/v) Tween-20 until the incubation with the secondary antibody. The remainder of the blot was then incubated with a primary antibody. For this project, two different primary antibodies were used and compared for their abilities to specifically bind UCPs in the skeletal muscle mitochondrial preparations. One of these primary antibodies was an antibody against an 18 amino acid peptide between the 3rd and 4th transmembrane domains of rat UCP3 purchased from Alpha-Diagnostics International, Inc., San Antonio, TX; the other was a rabbit anti-hamster UCP antibody (prepared once again by former members of Dr. Jean Himms-Hagen's laboratory, Dr. Anna-Lisa Kates and Christine Villemeure, who immunized rabbits with purifed hamster UCP from cold- acclimated hamsters according to Fernandez et al. (Fernandez *et al.*, 1987)). The blots were incubated with either one of these primary antibodies diluted 1:1,000 (rUCP3$_L$ Ab) or 1:16,000 (hamster UCP Ab) in PBS and 0.05% (v/v) Tween-20 for 1 hour. The washes

were then repeated, but this time with an additional 15 min wash at the end. The blot was then incubated at room temperature with gentle shaking for 1 hour in the secondary antibody solution containing goat anti-rabbit IgG horseradish peroxidase (HRPO) conjugate (Cedarlane Laboratories Ltd., Hornby, Ont.), diluted 1:10,000 in PBS plus 5% (w/v) skim milk powder. The biotinylated MW markers were simultaneously incubated with Avidin HRPO conjugate (Bio-Rad, Hercules, CA), diluted 1:3,000 in PBS plus 5% (w/v) skim milk powder. Both blots and biotinylated MW markers were then washed as above, but with an extra 15 minute wash. Finally, the blots and markers were subjected to 2 quick rinses and 2 five minute washes in PBS alone to remove the Tween-20, and were left in PBS until processed for detection.

2.5.4.4 Detection of the Blots Using Enhanced Chemiluminescence Methods

Detection of the antibody-bound uncoupling proteins was done using a commercially available enhanced chemiluminescence (ECL™) Western blotting kit from Amersham (Cat#: RPN 2109). This is a light emitting non-radioactive method of detecting immobilized specific antigens, conjugated with horseradish peroxidase-labeled antibodies. In this case, the mitochondrial proteins were immobilized on the nitrocellulose membrane, the primary anti-hamster UCP antibody was bound directly to the uncoupling proteins present on the membrane, and the secondary goat anti-rabbit IgG HRPO conjugate was bound to the primary antibody and therefore indirectly to UCP which is being detected.

Enhanced chemiluminescence is achieved when an added luminol susbstrate is oxidized, in the presence of phenol chemical enhancers, by the horseradish peroxidase conjugated to the secondary antibody.

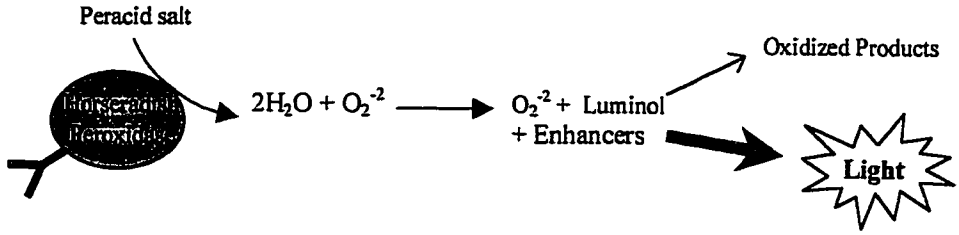

Light is produced by this reaction and is detected upon exposure of the membrane to photographic polaroid film (3¼"x 4¼") contained within the Polaroid® ECL Mini-Camera (RPN 2069; CB-103 film holder and processing back; Amersham Life Science) used for detection.

After taking the blot out of the PBS solution, it was laid flat in a large weigh boat, and its entire surface was gently covered with 2mL of the ECL™ kit mixed reagents (1mL of Reagent #1 plus 1mL of Reagent #2 mixed immediately before pouring). This "developing" solution was left undisturbed on the blot for exactly 1 minute, after which the weigh boat was tipped and the excess solution was removed by blotting the edge of the membrane on a tissue paper. The blot was then placed face down in the camera dish and any air pockets were smoothed out. The lid of the camera was put back in place and the blot was exposed to the film for varying lengths of time (2-30 minutes depending on the desired intensity of the picture). The shutter was then closed and the picture revealed by peeling the cover after 30 seconds.

2.6 Materials

Oligomycin, rotenone, nigericin, succinate, valinomycin, FCCP, malonate, NaEDTA, Tris-HCl, KH_2PO_4, HEPES, EGTA, ATP, ADP, GDP, TPMP bromide, 20% (w/v) Triton X-100, BSA (fraction V), Nagarse (Type XXVII, 7.8units/mg), Hexokinase (Type III), haematoxylin, eosin, TCA, TBS, TCT, DAB and cupric sulfate were purchased from

Sigma (St. Louis, MO). Dimethyl sulfoxide (Sigma) was also used to dissolve water insoluble compounds. Sucrose, glucose, KCl, K_2HPO_4, $MgCl_2$, NaOH, NaCl, LiOH, Folin reagent and glycine were obtained from BDH Chemicals (Toronto, Ontario). Sodium dodecyl sulfate (SDS), Tween-20, PMSF, β-mercaptoethanol, bromophenol, acrylamide/bisacrylamide and ammonium persulfate all came from Bio-Rad Laboratories (Hercules, CA). Tris-base, Permount, xylene, xylol and 10% (w/v) Formalin™ were from Fisher Scientific (Fair Lawn, NJ). Radioactive compounds such as ^3H_2O, [^{14}C]-sucrose, ^{86}RbCl, and [^{3}H]-TPMP$^+$ bromide were all from Mandel-Dupont-NEN (Guelph, Ontario).

2.7 Statistical Analyses

Unless otherwise stated, results are expressed as means ± SEM. Differences between two individual means were examined by the two-tailed unpaired Student's t-test. Analyses of variance (One-way ANOVA & Tukey's post-hoc tests, Repeated Measures ANOVA, and Two-way ANOVA) were used to determine significant differences between more than two groups. Statistics were performed using GraphPad Prism2 for Windows as well as the Data Analysis Tool Pak in Microsoft Excel 97. A p-value of less than 0.05 was considered statistically significant. Unless otherwise stated, the level of significance between means as shown in bar graphs is indicated using the following systematic labelling: * is used for $p < 0.05$, ** is used for $p < 0.01$, and *** is used for $p < 0.001$.

3. RESULTS

3.1 Evidence of phenotypic differences between B6-CAST congenic and B6 control mice

3.1.1 Adiposity

As shown in Figure 3.1, results from the first study in which the mice were fed a normal chow diet for a period of four and a half weeks, show that there were no differences in the weight of epididymal fat pads from B6-CAST congenic (0.33g(±0.04)) and B6 control mice (0.31g(±0.02)). After six weeks on the high fat condensed milk diet however, results from both the 2nd and the 3rd studies during which both epididymal and inguinal white adipose tissue depots were collected, show that the weight of these depots were much lower in B6-CAST congenic mice as compared to those of B6 controls. Weights of the epididymal white fat pads from B6 control mice nearly doubled (2nd study: 0.83g(±0.03) vs 0.43g(±0.02); $p<0.05$) and even tripled (3rd study: 1.3g(±0.1) vs 0.33g(±0.08); $p<0.001$) those from B6-CAST congenic mice. B6 control mice also had greater inguinal WAT depot weights than B6-CAST congenic mice fed the high fat diet, 0.55g(±0.04) vs 0.37g(±0.03) (2nd study; $p<0.05$) and 0.92g(±0.13) vs 0.33g(±0.07) (3rd study; $p<0.001$).

Interscapular brown adipose tissue (BAT) weights (shown in Figure 3.2A) were found to be similar between both groups of mice fed the high fat diet in the 2nd study (congenics: 0.086g(±0.003); controls: 0.091g(±0.004); $p=0.35$), but greater in B6 control mice as compared to B6-CAST congenic mice during the high fat feeding of the 3rd study (0.09g(±0.01) vs 0.054g(±0.006); $p=0.0082$). As mentioned in the Introduction, because of the limited extent of knowledge in this area at the onset of our research, our focus was

Figure 3.1 Average white fat pad wet weights from B6-CAST congenic and B6 control mice fed a normal chow diet for four and a half weeks (1st study), or a high fat diet for a minimum of six weeks (2nd and 3rd studies). Results shown are expressed as means ± SEM for the eight mice studied in each group during each of the three studies conducted. Statistical significance is indicated such that * denotes statistically significant differences between each of the paired columns at the level of $p<0.05$, ** at the level of $p<0.01$ and *** at the level of $p<0.001$, as shown by ANOVA and Tukey's post-hoc tests. Abbreviations: Epi – epididymal, Ing – inguinal, HFD – high fat diet, WAT – white adipose tissue.

White Fat Pad Weights

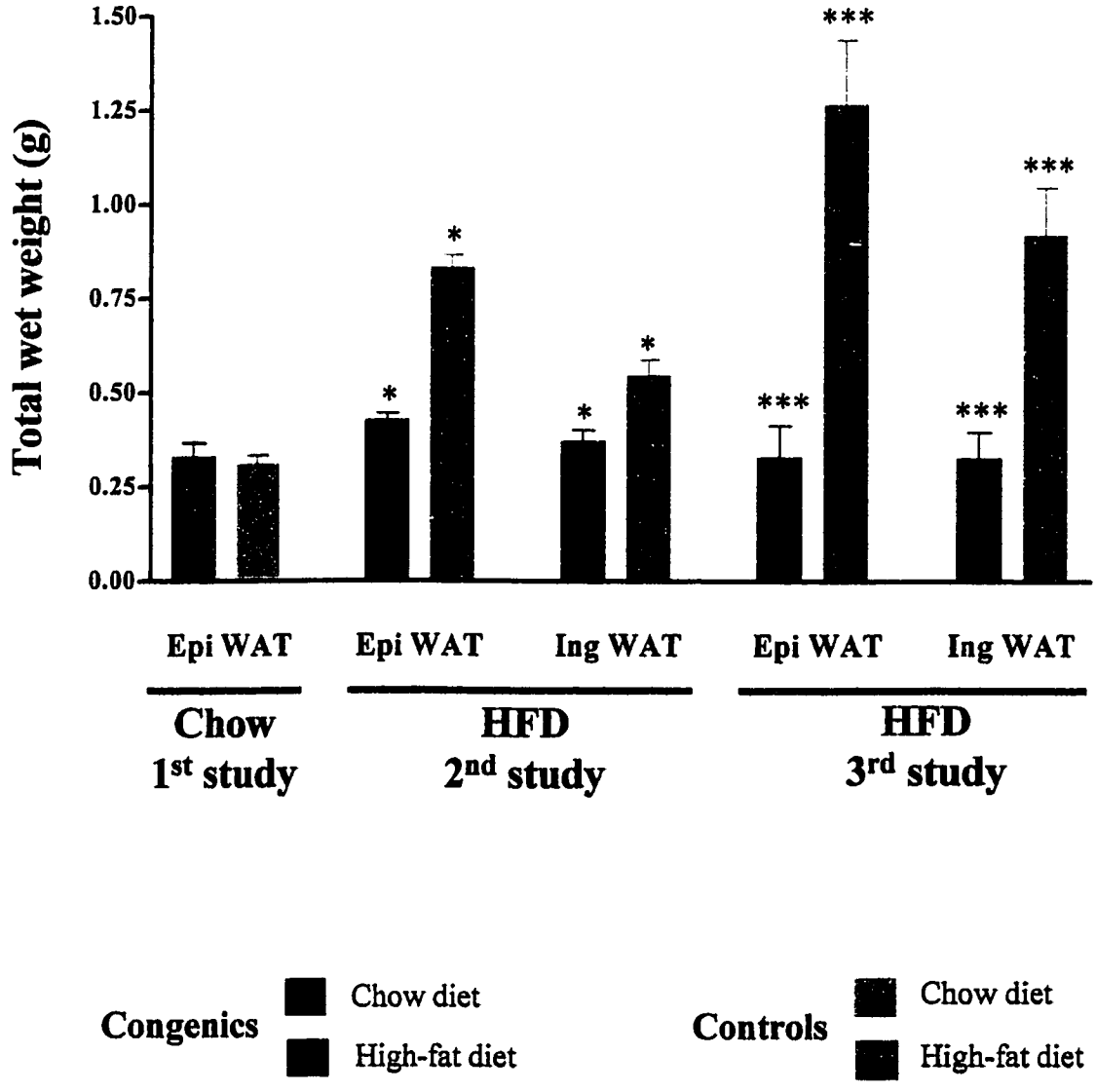

Figure 3.2 Average interscapular brown fat pad weights (A) and total IBAT protein per depot (B) of B6-CAST congenic and B6 control mice fed a high fat diet for a minimum of six weeks . Results shown in A are means ± SEM for the eight mice studied in each group during the second and third studies. In B, results shown are means ± SEM for six control and five congenic mice used during the second study and for four control and three congenic mice used in the third study. ** indicates statistically significant differences between the paired columns at the level of $p<0.01$ as determined by Student's unpaired t-tests. Abbreviations: HFD – high fat diet.

A

Interscapular Brown Fat Pad Weight

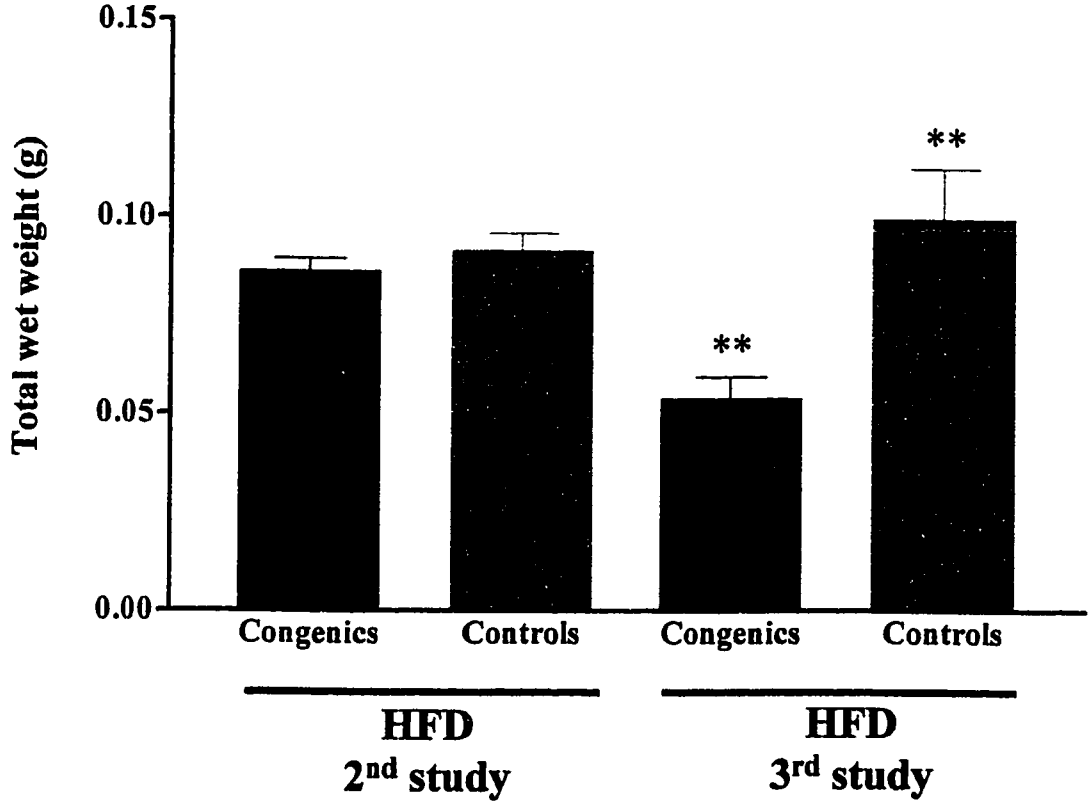

B

Total IBAT Protein

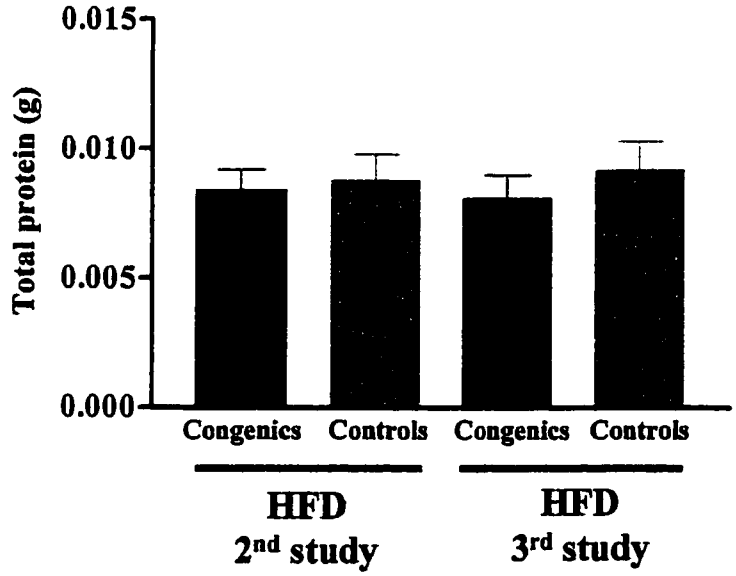

slightly different then, which explains why certain important tissues, such as IBAT were unfortunately not collected during the 1st study. Due to the discrepancies between the IBAT weights obtained in the two high fat diet studies, total IBAT protein per depot was assayed for both groups of mice to get an idea of the total thermogenic potential of the IBAT depots in each group. From Figure 3.2B we see that no significant differences were found as the total amount of protein per IBAT depot for B6-CAST congenic mice and for B6 control mice were similar during the two studies (2nd study: 0.0084g(±0.0008) and 0.0088g(±0.0010); 3rd study: 0.0081g(±0.0009) and 0.0092g(±0.0011), respectively). This indicates that the bulk of the extra weight of the IBAT depots of B6 control mice in the 3rd study was fat.

3.1.2 Histological studies of adipose tissue depots

Figures 3.3 and 3.4 show histology of epididymal and inguinal white adipose tissues magnified 200 times. Stained in dark purple are the nuclei of the cells and in a lighter shade, the cellular membranes. These figures clearly demonstrate unilocular cells with much smaller lipid droplets in the tissues from B6-CAST congenic mice (top panels) as compared to those from B6 control mice (bottom panels).

Histology of IBAT in Figure 3.5 reveals multilocular cells with darkly stained nuclei. As is the case in the white adipose tissues, the lipid droplets within the brown adipocytes of B6-CAST congenic mice (top panel) are remarkably smaller than those in B6 control mice (bottom panel).

Figure 3.3 Histology of epididymal white adipose tissue. Hematoxylin and eosin stained 4μm sections of EpiWAT from B6-CAST congenic (top) and B6 control (bottom) mice fed a high fat diet for a minimum of six weeks. Magnification x 200. Note the increased size of the lipid droplets in the unilocular cells of the tissue from control mice as compared to those from congenic mice.

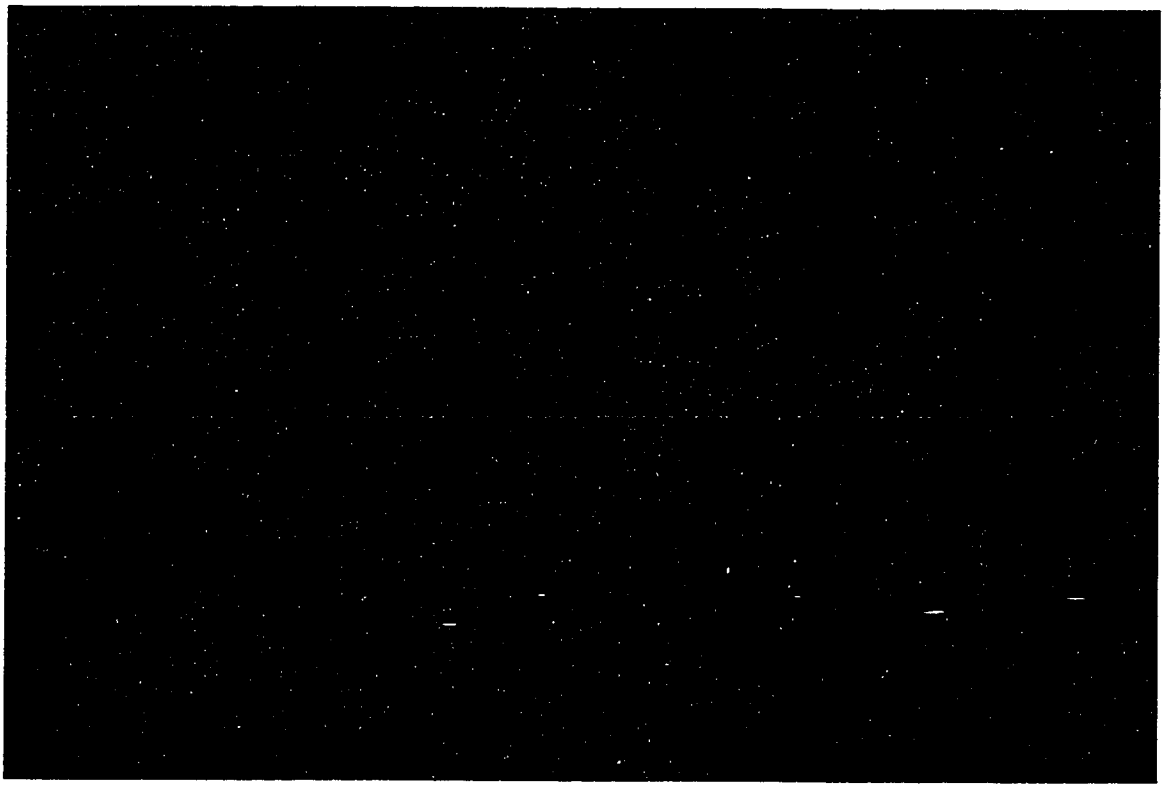

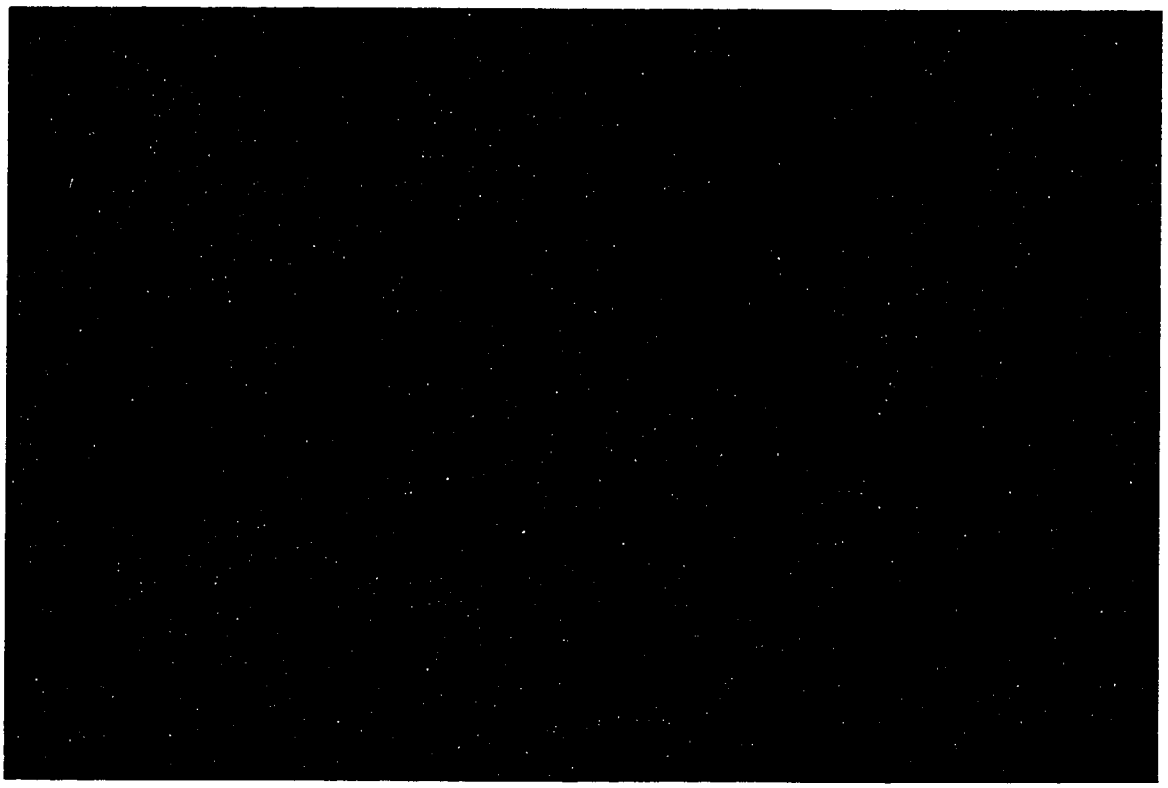

Figure 3.4 Histology of inguinal white adipose tissue. Hematoxylin and eosin stained 4μm sections of IngWAT from B6-CAST congenic (top) and B6 control (bottom) mice fed a high fat diet for a minimum of six weeks. Magnification x 200. Note the increased size of the lipid droplets in the unilocular cells of the tissue from control mice as compared to those from congenic mice.

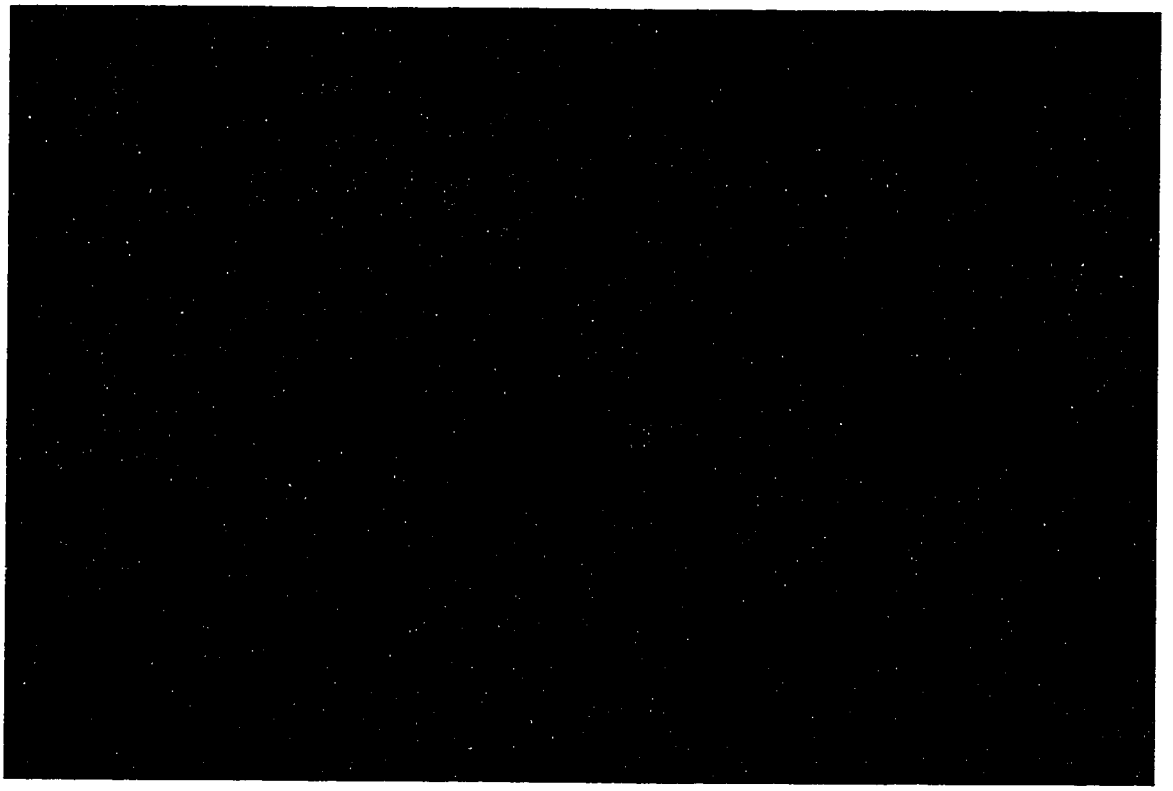

Figure 3.5 Histology of interscapular brown adipose tissue. Hematoxylin and eosin stained 4μm sections of IBAT from B6-CAST congenic (top) and B6 control (bottom) mice fed a high fat diet for a minimum of six weeks. Magnification x 400. Note the increased size of the lipid droplets in the multilocular cells of the tissue from control mice as compared to those from congenic mice.

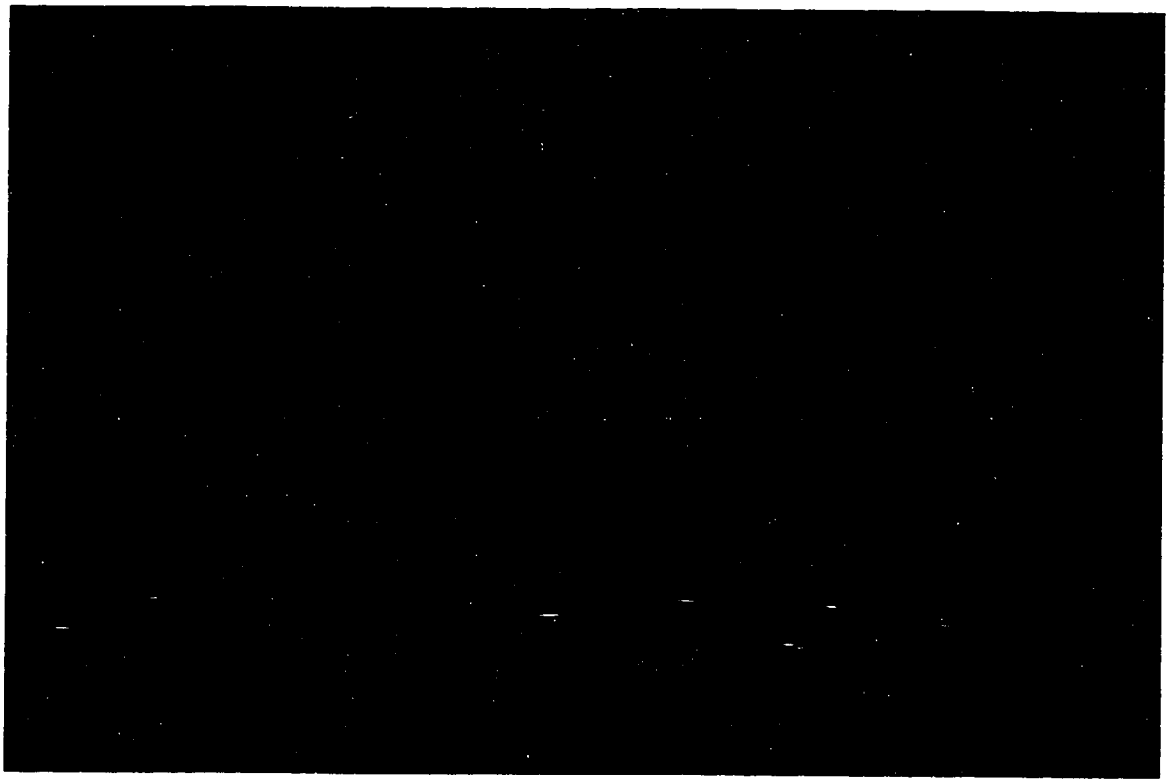

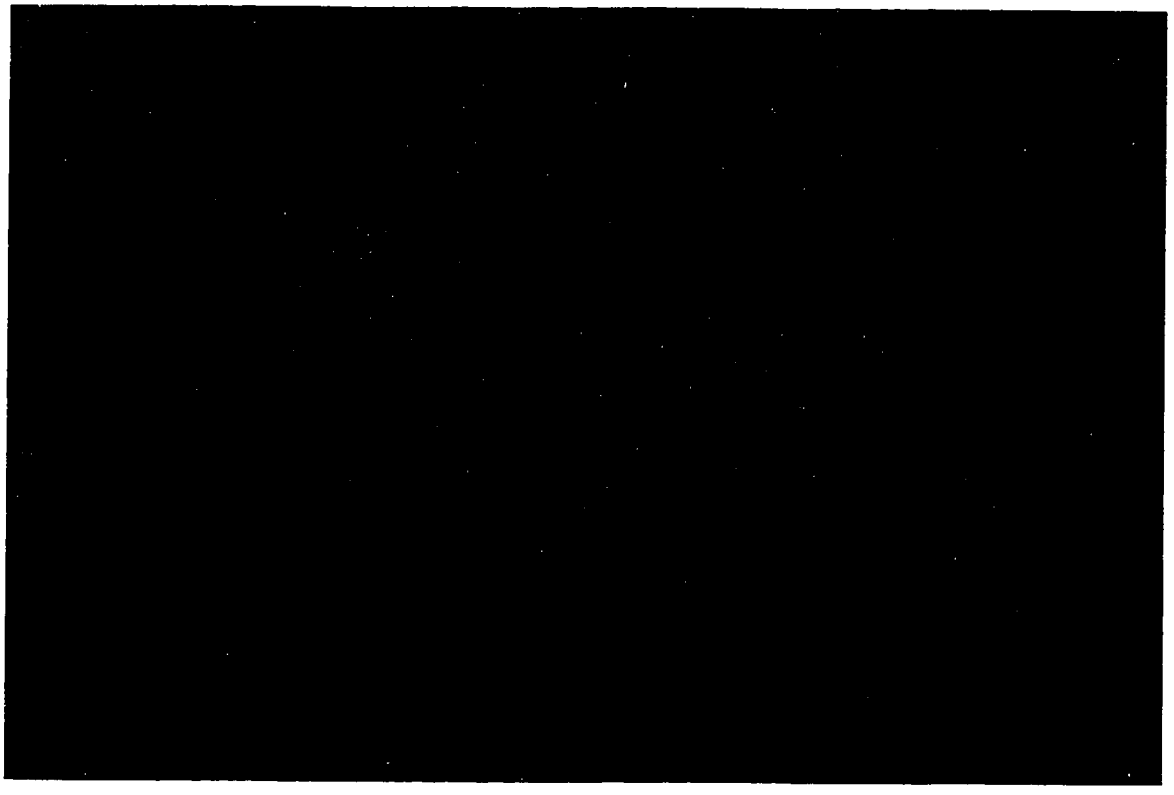

3.2 Serological analyses of high fat fed B6-CAST congenic and B6 control mice

In an attempt to further identify any possible metabolic differences between the two groups of mice fed the high fat diet, serological analyses of non-esterified fatty acid (NEFA), triglyceride and glucose were performed using commercially available kits. No significant differences were found in the levels of serum non-esterified fatty acids (Figure 3.6A) between the two groups (congenics: 0.60 mM (±0.06); controls: 0.55 mM (±0.02); $p>0.05$), who both demonstrated physiologically normal levels of NEFA (~600μM) (Susulic *et al.*, 1995). The levels of serum triglycerides (Figure 3.6B) were significantly greater in B6-CAST congenic mice than those in B6 control mice (138.1 mg/dL (±18.3) vs 85.6 mg/dL (±5.6); $p=0.0088$). Finally, as shown in Figure 3.6C, the serum glucose levels of B6-CAST congenic mice were slightly, but significantly, lower than those of B6 controls (209.8 mg/dL (±7.1) vs 239.2 mg/dL (±6.7), respectively; $p=0.0052$).

3.3 Body weight, food intake and metabolic efficiency studies

Since the B6-CAST congenic mice obviously deposited less fat than the B6 control mice when fed the high fat condensed milk diet, we aimed to ascertain whether this resistance to obesity was attributed to a decrease in energy intake or to an increase in energy expenditure or both in these animals. In order to examine the first of these two possibilities, body weight, food intake and metabolic efficiency studies were performed by closely monitoring the two groups of mice both on a normal chow diet (1st study) and on the high fat diet (2nd and 3rd studies).

Figure 3.6 Serum analyses of B6-CAST congenic and B6 control mice fed a high fat diet for a minimum of six weeks. Non-esterified fatty-acids (NEFA) (A), triglyceride (B) and glucose (C) levels were assessed in serum samples from both groups of mice using commercially available kits. Results shown represent the means ± SEM of duplicate determinations for each of the eight mice studied in each group. Unpaired t-tests showed no significant differences between the levels of NEFA in the two groups ($p>0.05$), but revealed significantly greater levels of triglycerides in congenics compared to controls, and of glucose in controls compared to congenics (** $p<0.01$).

A **Serum Non-esterified Fatty-Acid Levels**

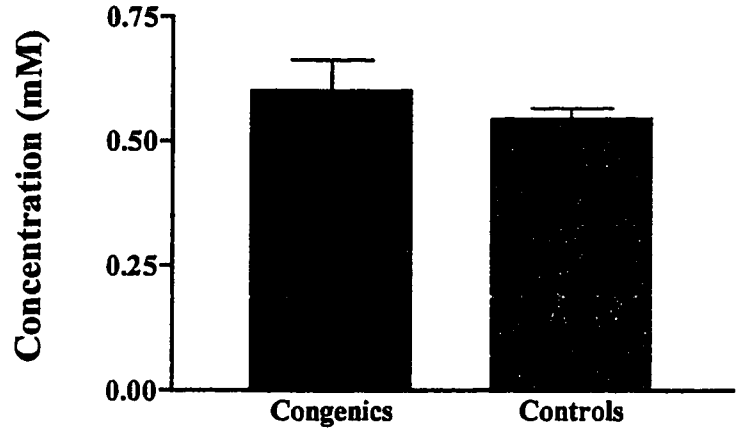

B **Serum Triglyceride Levels**

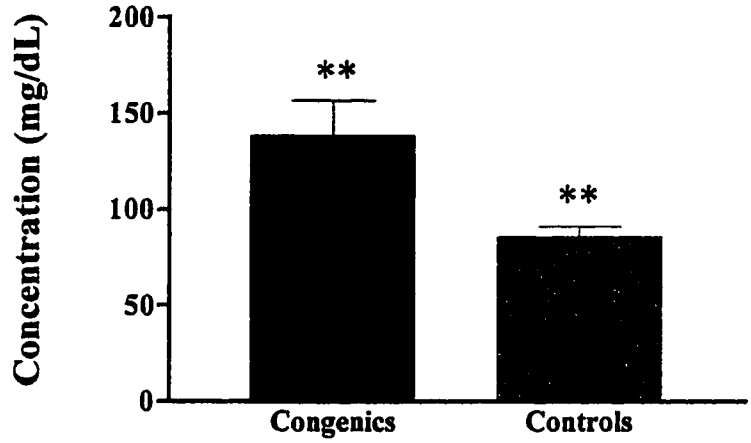

C **Serum Glucose Levels**

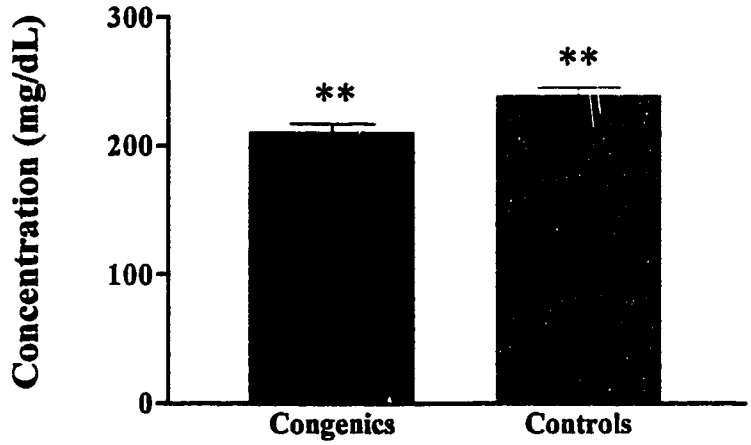

3.3.1 Body weights

When fed the normal chow diet *ad libitum* for a period of four and a half weeks, the average body weights of both the B6-CAST congenic and B6 control mice remained relatively unchanged (see Figures 3.7A- "before" and "after", and 3.8A) throughout the feeding period. There was no significant weight gain in either group. The average body weight of the congenics was however slightly but significantly higher than that of controls, which may be attributed to litter differences as the mice came from two different suppliers. Figures 3.7B and 3.7C depict the average body weights of B6-CAST congenic and B6 control mice before and after the feeding of the high fat diet. In both the 2nd and 3rd studies, the average body weight of the B6-CAST congenic mice was not significantly altered by the high fat feeding ($p>0.05$). The average body weight of B6 control mice however, was significantly greater at the end of the feeding period than it was initially (2nd study: 27.2g(±0.4) vs 23.6g(±0.4), $p<0.0001$; 3rd study: 29.9g(±1.1) vs 24.0g(±0.5), $p=0.0002$). These represent body weight gains of 3.6g(±0.4) and 5.9g(±0.8), respectively. Figure 3.8B shows the change in average body weight over time for the two groups of mice.

3.3.2 Energy Intake

The average daily energy intake of the B6-CAST congenic mice was not significantly different than that of the B6 control mice on either the normal chow (10.7 kcal/day (±0.2) vs 10.5 kcal/day (±0.2), respectively) or the high fat condensed milk diet (11.1 kcal/day (±0.3) vs 11.1 kcal/day (±0.1), respectively), though the energy intake of all animals rose slightly when fed the high-fat diet (Figures 3.9 and 3.10). Note that in Figure 3.10B there was a significant drop in the energy intake of both groups of mice

Figure 3.7 Average body weights of B6-CAST congenic and B6 control mice before and after the administration of either a normal chow diet for four and a half weeks (A) or a high fat diet for six weeks (B and C). During each study, the mice were given *ad libitum* access to the respective diets. Results are expressed as means ± SEM for the eight mice in each group during the first and second study, and for seven B6-CAST congenic and eight B6 control mice during the third study. *** denotes a statistically significant difference between the means of the paired columns at the level of $p<0.001$, as determined by Student's paired t-test.

Body Weight Results

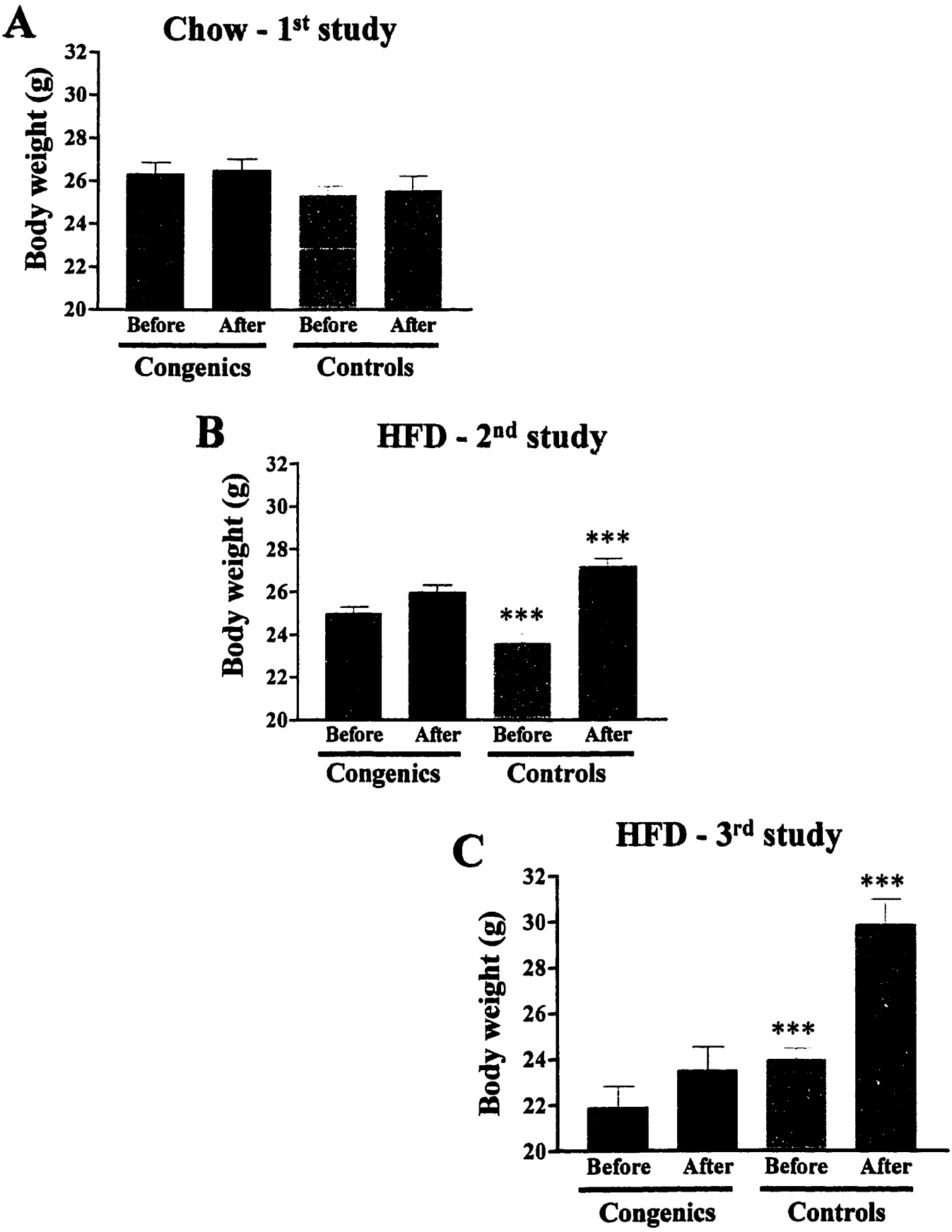

Figure 3.8 Time course monitoring of body weights (g) for B6-CAST congenic and B6 control mice fed a normal chow diet (A) or a high fat diet (B). In A, the data were collected twice weekly over a four and a half week period during which the mice had *ad libitum* access to a normal chow diet which had a metabolizable energy content of 3.13kcal/g. In B, the data were collected three times a week over six weeks while the mice had *ad libitum* access to a high fat diet with a metabolizable energy content of 4.15kcal/g. Each data point represents the mean ± SEM of eight mice studied in each group at each time point. A repeated measures ANOVA showed no significant effect of time ($p>0.05$) on the body weights of both groups of mice fed the chow diet. There was however a significant effect of time on the body weights of controls on the high fat diet ($p=0.0012$).

Body Weights Monitored over Time

A

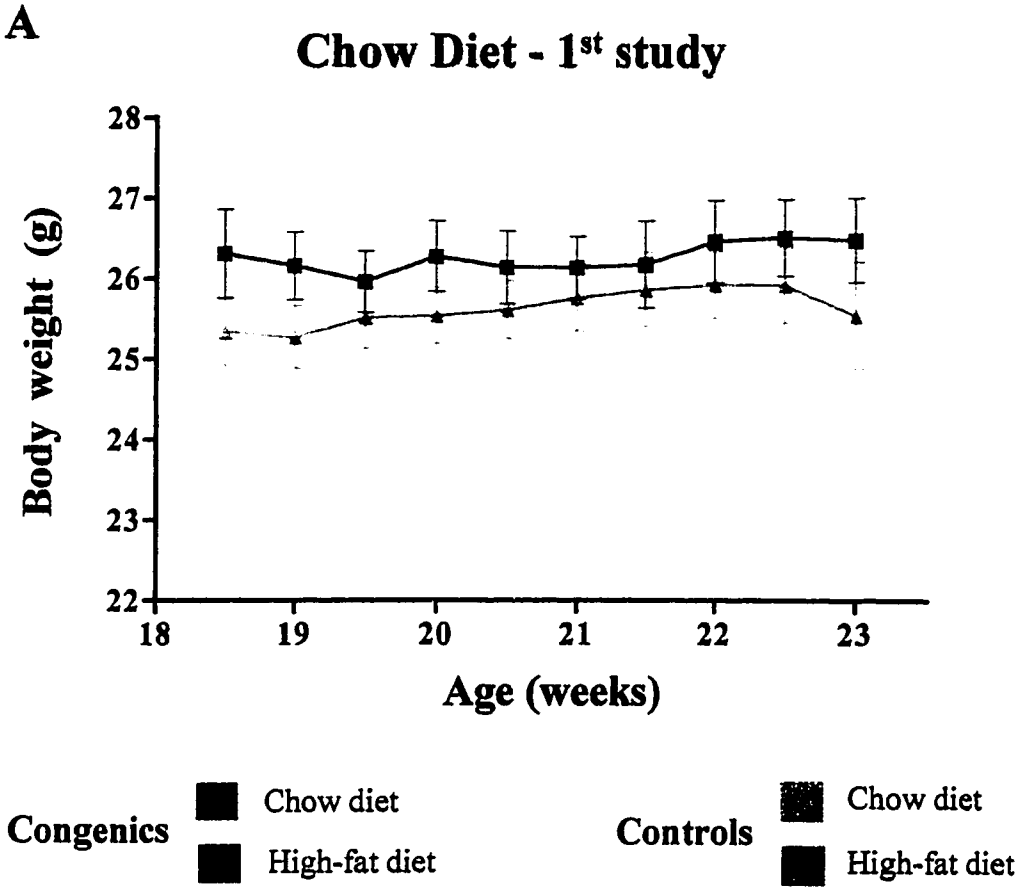

B

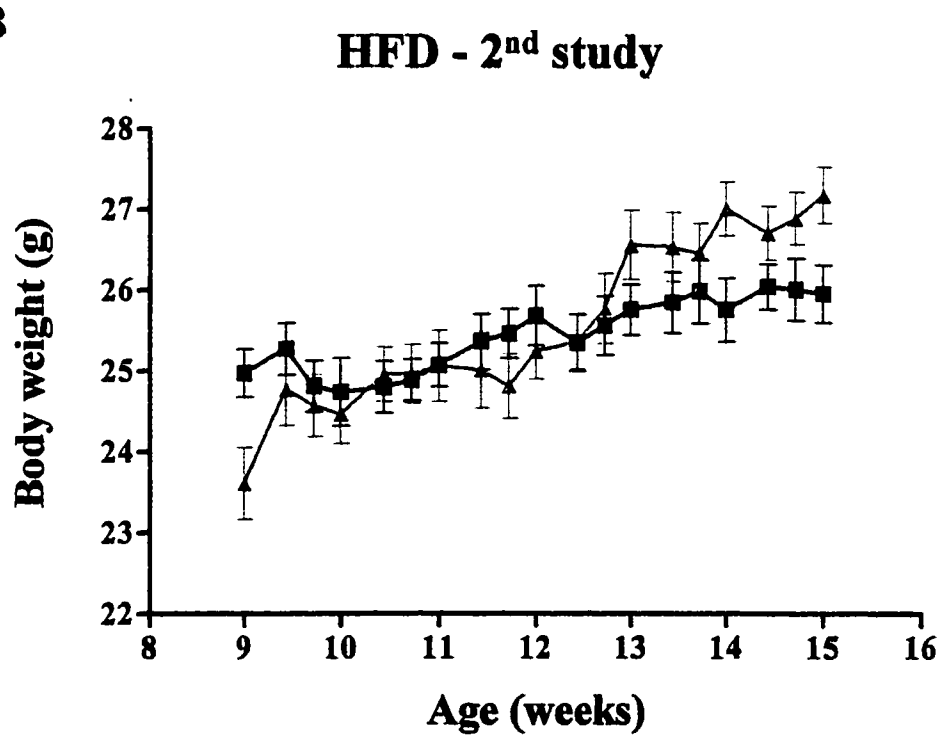

Figure 3.9 Average daily energy intake of B6-CAST congenic and B6 control mice fed either a normal chow diet for four and a half weeks or a high fat diet for six weeks. During each study, the mice were given *ad libitum* access to the diets, which had metabolizable energy contents of 3.13kcal/g and 4.15kcal/g, respectively. Results are expressed as means ± SEM of eight mice in each group, and were obtained by multiplying the average weight (g) of food consumed daily per mouse by the metabolizable energy content of the respective diets. Statistical analyses using Student's unpaired t-tests showed no significant differences in energy intake between the two groups on either of the diets. Abbreviations: HFD = high fat diet.

Daily Energy Intake Results

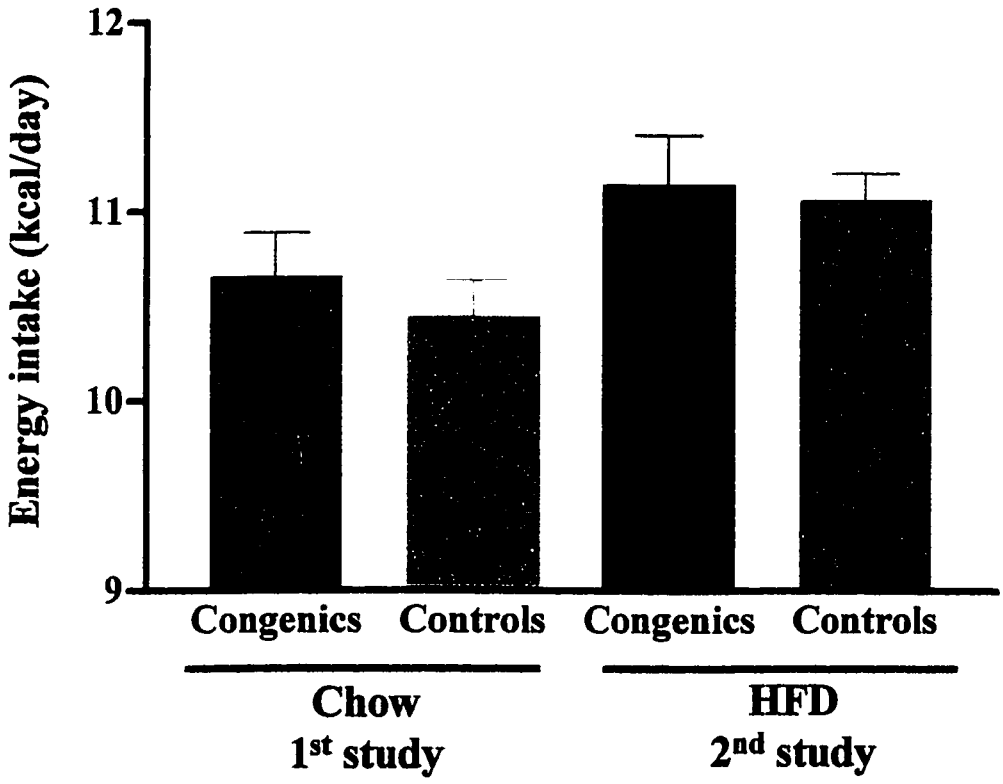

Congenics
Chow diet
High-fat diet

Controls
Chow diet
High-fat diet

Figure 3.10 Time course monitoring of daily energy intake (kcal/day) for B6-CAST congenic and B6 control mice fed a normal chow diet (A) or a high fat diet (B). In A, the data was collected twice weekly over a four and a half week period during which the mice had *ad libitum* access to a normal chow diet with a metabolizable energy content of 3.13kcal/g. In B, the data was collected three times a week over six weeks while the mice had *ad libitum* access to a high fat diet with a metabolizable energy content of 4.15kcal/g. Each data point represents the mean ± SEM of eight mice studied in each group at each time point. Results shown were obtained by multiplying the average weight (g) of food consumed daily per mouse by the metabolizable energy content of the respective diets. Repeated measures ANOVA and two-way ANOVA showed no significant effect of time nor of group (congenics vs controls) ($p>0.05$) on daily energy intake of mice fed the high fat diet. In the case of the normal chow diet, these same analyses revealed an effect of group with the energy intake of congenics being greater than that of controls; however, there was no effect of time. Abbreviations: HFD = high fat diet.

Daily Energy Intake Monitored over Time

A

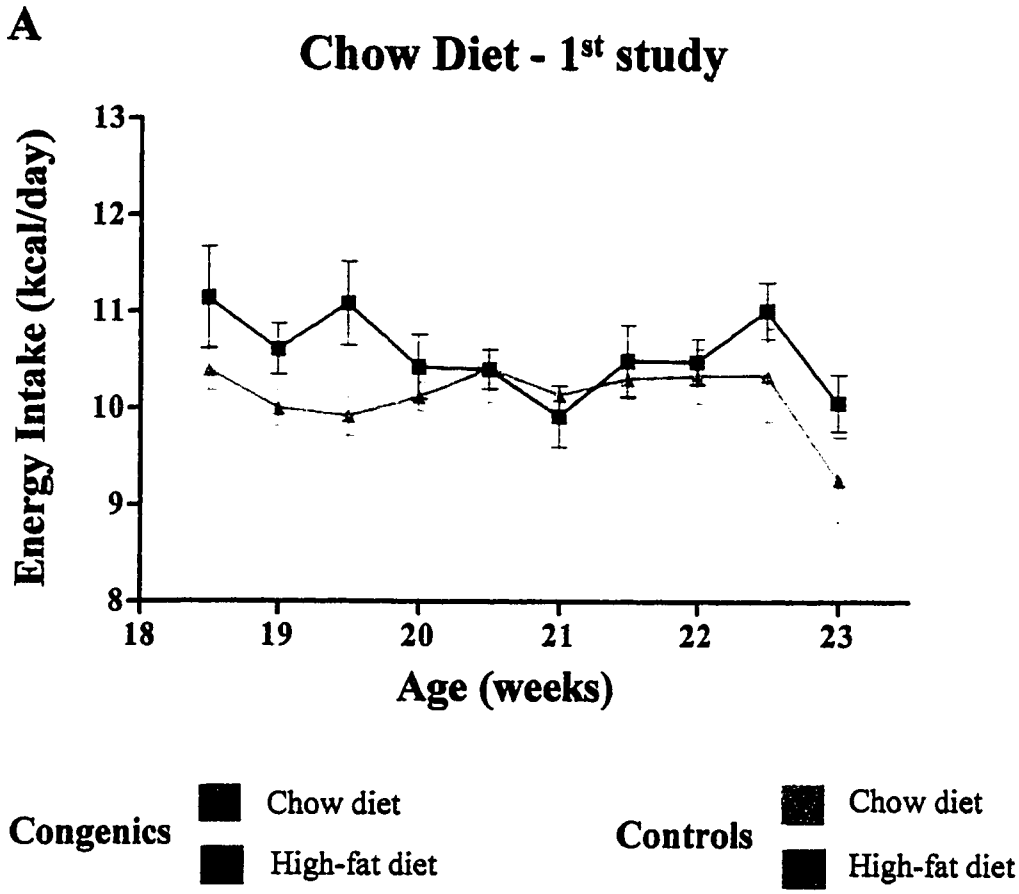

B

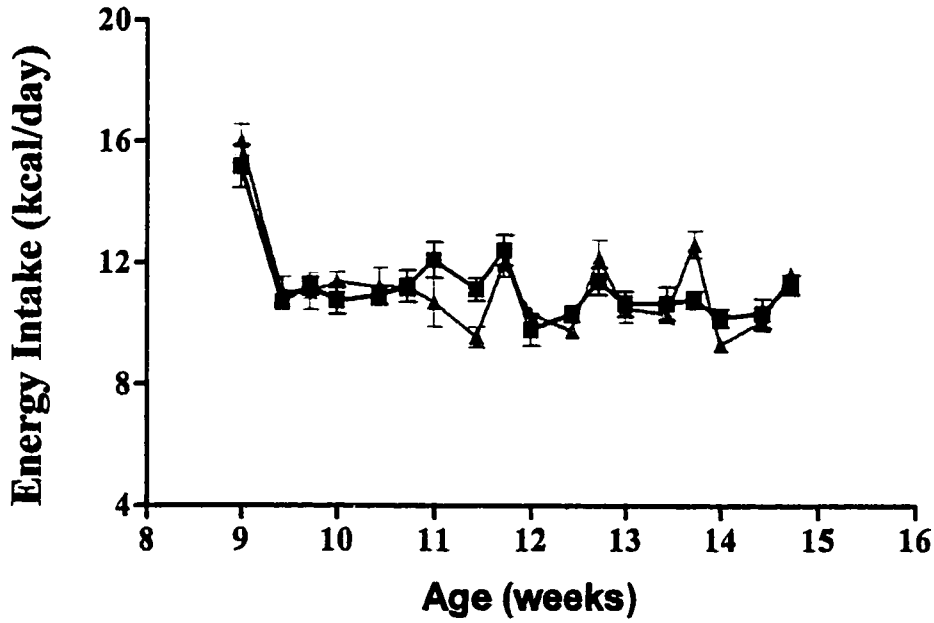

after the first point. This can arguably be attributed to the ability of the mice to sense the higher energy content of the diet and to adapt rather quickly by eating smaller amounts of the diet ensuring that their overall energy intake does not rise substantially. The energy intake results presented here were calculated by multiplying the average daily weight of consumed food by the metabolizable energy content of the respective diets. Metabolizable energy content was used rather than the total energy content of the diets in order to allow for more accurate comparisons of energy intake with energy expenditure later on.

3.3.3 Metabolic efficiency

Estimates of metabolic efficiency (body weight gained (g) divided by metabolizable energy intake (kcal)) were calculated using the total amount of weight gained over the feeding period and the total energy intake over the same feeding period. The results are presented in Figure 3.11. As there was no apparent body weight gained by either of the two groups of mice fed the regular chow diet, an estimate of metabolic efficiency could not be conducted. However, following the six weeks of high fat feeding the metabolic efficiency of the B6-CAST congenic mice was significantly lower than that of the B6 control mice (2.1g BWt gained/kcal consumed (±0.4) vs 7.7g BWt gained/kcal consumed (±0.8); $p<0.0001$). In fact, the control mice had a metabolic efficiency nearly four fold greater than that of the congenic mice, which reflects an enhanced ability to metabolize the energy substrates consumed with a lower amount of energy being wasted. This is consistent with the increased adiposity observed in control compared to congenic mice.

Figure 3.11 Metabolic efficiencies of B6-CAST congenic and B6 control mice fed a high fat diet for six weeks. These data are expressed as the average total body weight gained divided by the average total metabolizable energy (kcal) consumed during the duration of the second study. Results shown are means ± SEM for the eight mice studied in each group. An unpaired t-test showed that the metabolic efficiency of controls is significantly greater than that of congenics at the level of $p<0.001$ (denoted by ***).

Metabolic Efficiencies

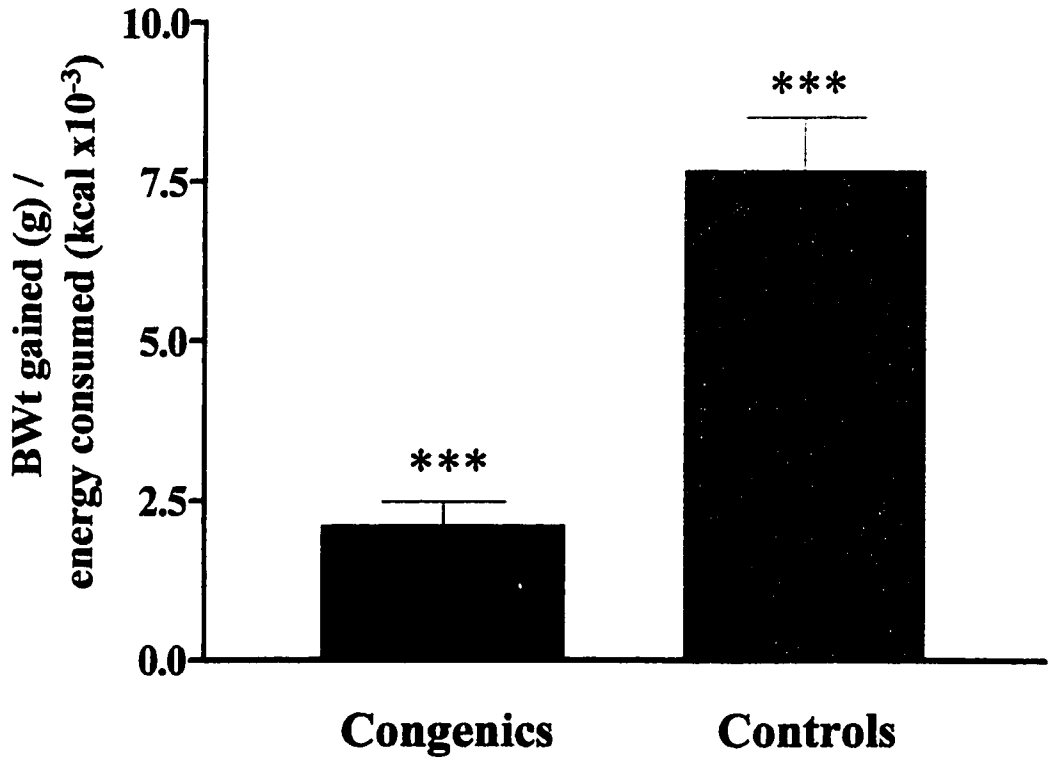

3.4 Indirect calorimetry assessments of energy expenditure

The above described findings indicated that the phenotypic resistance to obesity in B6-CAST congenic mice challenged with a high fat diet, could not be attributed to a lower energy intake when compared to B6 control mice. We thus aimed to examine the characteristics of energy expenditure, to investigate whether B6-CAST congenic mice have a higher energy expenditure than B6 control mice. Indirect calorimetry was used to assess resting metabolic rates, respiratory exchange ratios, and total 24 hour fed and fasted energy expenditure of the two groups of mice.

3.4.1 Resting metabolic rates and respiratory exchange ratios

As shown in Figure 3.12 resting metabolic rates (RMR; ml O_2/min/mouse) and respiratory exchange ratios (RER: VCO_2/VO_2) of B6-CAST congenic and B6 control mice remained fairly constant throughout the entire six weeks of high fat feeding ($p>0.05$: Repeated measures ANOVA). No effect of diet was observed; RMR and RER values assessed prior to the start of the high fat feeding resemble those assessed later on at different time points during the study. Each individual assessment of RMR and RER was calculated as the mean of the three lowest data points on the readouts during periods of inactivity for each mouse.

3.4.2 24 hour energy expenditure – Assessments of VO_2, RER and heat production

As there were no apparent differences in resting metabolic rates between the two groups of mice on either of the diets, total 24 hour energy expenditure assessments were conducted to investigate the possibility that perhaps these longer term continuous assessments of energy expenditure would reveal differences that may not be apparent

Figure 3.12 Resting metabolic rates (RMR) and respiratory exchange ratios (RER) for B6-CAST congenic and B6 control mice fed a regular chow diet (marked "Before HFD") and a high fat diet (HFD-2nd Study). RMR is expressed as the amount of oxygen consumed (in mL) per minute per mouse, whereas RER represents the ratio of the volume of CO_2 produced to the volume of O_2 consumed by each mouse. These assessments were obtained by indirect calorimetry at 28°C. Results shown represent means ± SEM of the 8 mice studied in each group at each time point. Each individual assessment was taken as the mean of the three lowest points on the readouts when the mice were inactive. Repeated measures ANOVA indicated that both RMR and RER were not significantly different between the two groups at each time point ($p>0.05$) and that these did not vary significantly over time. Abbreviations: HFD = high fat diet.

Resting Metabolic Rate (RMR)

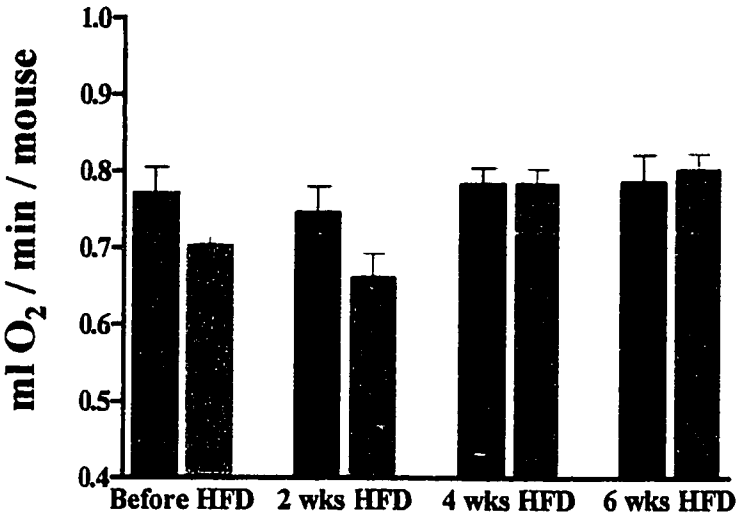

Congenics
Chow diet
High-fat diet

Controls
Chow diet
High-fat diet

Respiratory Exchange Ratio (RER)

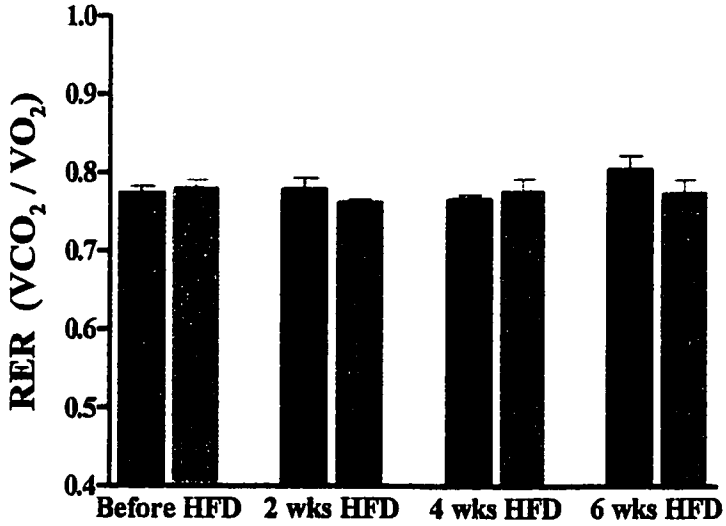

simply by looking at the energy expended for basal metabolism. These assessments were conducted again by indirect calorimetry at 31°C with the mice having access to a normal chow diet and water for the duration of the 24 hour study period. The mice were raised closer to thermoneutrality to eliminate thermoregulatory energy expenditure. The results of these assessments are shown in the top panels of Figures 3.13 to 3.18 and are summarized in Table 3.1. Presented are results of oxygen consumption (VO_2), respiratory exchange ratios (RER) and heat production, as well as these same results ranked in ascending order (as opposed to ranked chronologically), in a further attempt to identify any differences, and facilitate comparisons between the two groups of mice. Looking at the circadian patterns in Figure 3.13, it can be seen that oxygen consumption expectedly rose at night when the mice are most active. Similar patterns are observed for RER and heat production (Figures 3.15 and 3.17) primarily caused by the increased consumption of the high carbohydrate diet by both groups of mice during the night hours. Upon examination of Figures 3.14, 3.16 and 3.18 however, it becomes apparent (judging by the overlapping error bars of the two lines in each graph) that there are no significant measurable differences in any of the three interrelated parameters studied between B6-CAST congenic and B6 control mice when they are fed a normal chow diet. Mean total energy expenditure assessments were 7.68 kcal/24hours (±0.12) for B6-CAST congenics and 7.57 kcal/24hours (±0.14) for B6 controls ($p=0.552$). As expected, mean nocturnal energy expenditure was far greater than mean diurnal energy expenditure, but similar between both groups of mice ($p>0.05$).

Figure 3.13 Twenty-four hour continuous oxygen consumption assessments for B6-CAST congenic and B6 control mice fed a normal chow diet. Results are expressed in terms of oxygen consumed per minute per mouse (mL/min/mouse) as determined by indirect calorimetry at 31°C with a 12:00hr-12:00hr light-dark cycle (lights on between 07:00 and 19:00 as indicated by the colored boxes on top of each graph: day=yellow, night=indigo). Throughout the experiments, all mice had *ad libitum* access to drinking water and either a normal chow diet (top graph -fed state) or no chow at all (bottom graph- fasted state). The bottom graph shows results for mice that were fasting for 24 hours and were subsequently refed and monitored for an additional 6 hours. Each point represents an average of data from six mice and is expressed as the mean ± SEM.

Oxygen Consumption

Fed State

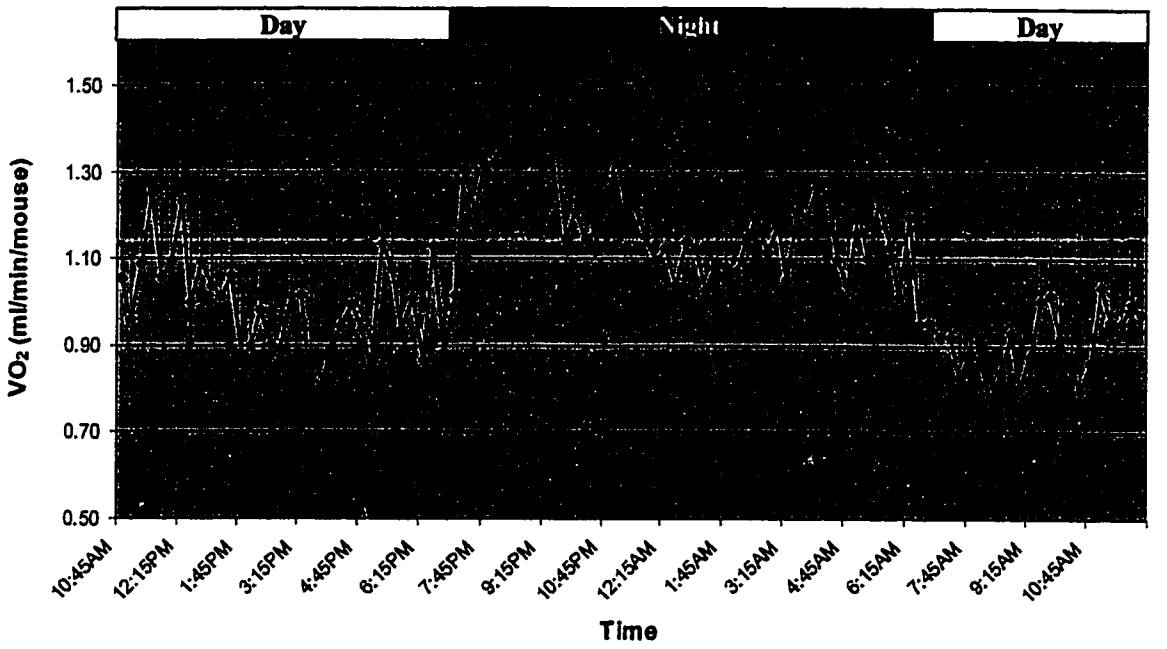

Fasted State

Refeed Period

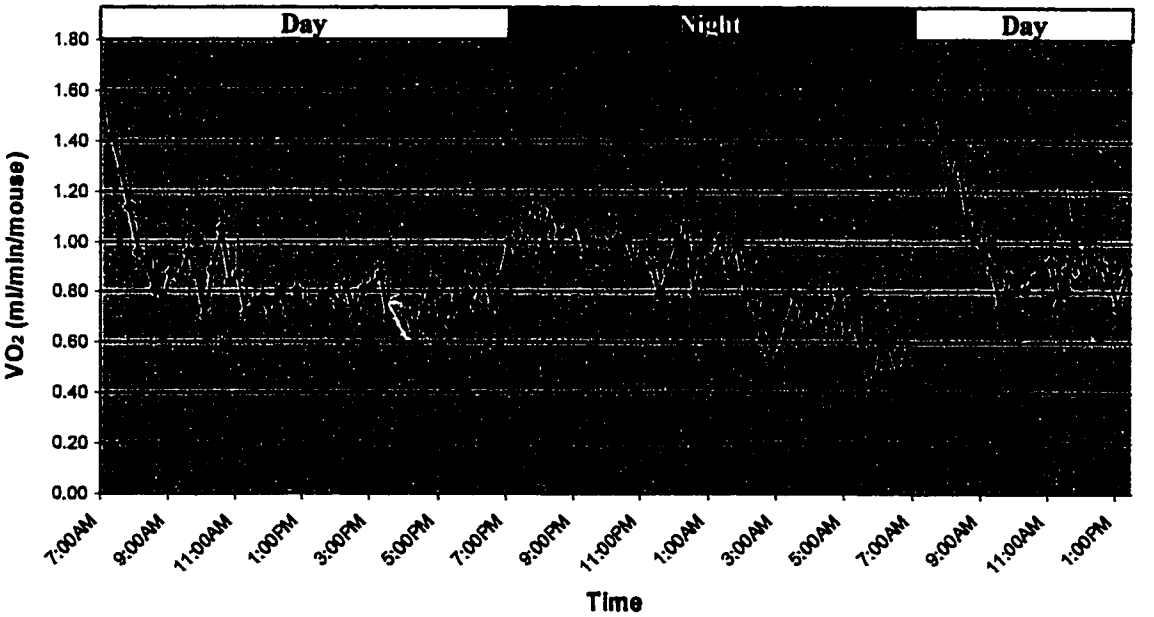

Figure 3.14 Ranked oxygen consumption assessments for B6-CAST congenic and B6 control mice fed a normal chow diet. Results are expressed in terms of oxygen consumed per minute per mouse (mL/min/mouse) as determined by indirect calorimetry at 31°C with a 12:00hr-12:00hr light-dark cycle (lights on between 07:00 and 19:00). Data points collected continuously over 24 hours were ranked in ascending order in an attempt to identify any differences, and facilitate comparisons, between the two groups of mice. Throughout the experiments, all mice had *ad libitum* access to drinking water and either a normal chow diet (top graph -fed state) or no chow at all (bottom graph- fasted state). The bottom graph shows only the data points collected during the first 24 hours when the mice were fasting; data points collected during the refeed period were not considered. Each point represents an average of data from six mice and is expressed as the mean ± SEM.

Oxygen Consumption
Ranked in Ascending Order

Fed State

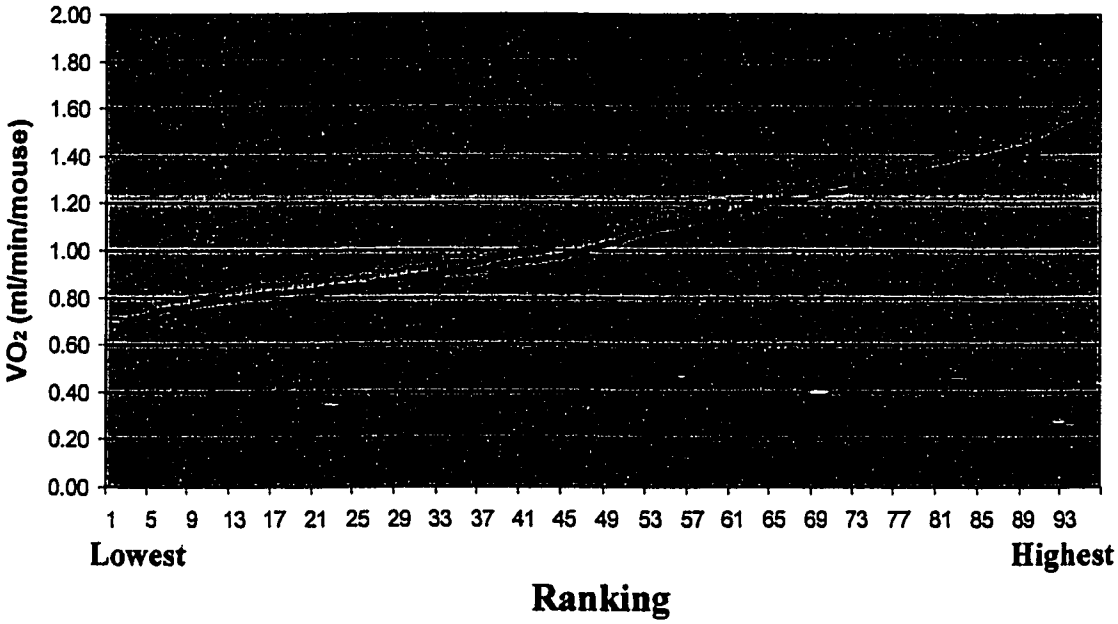

Fasted State

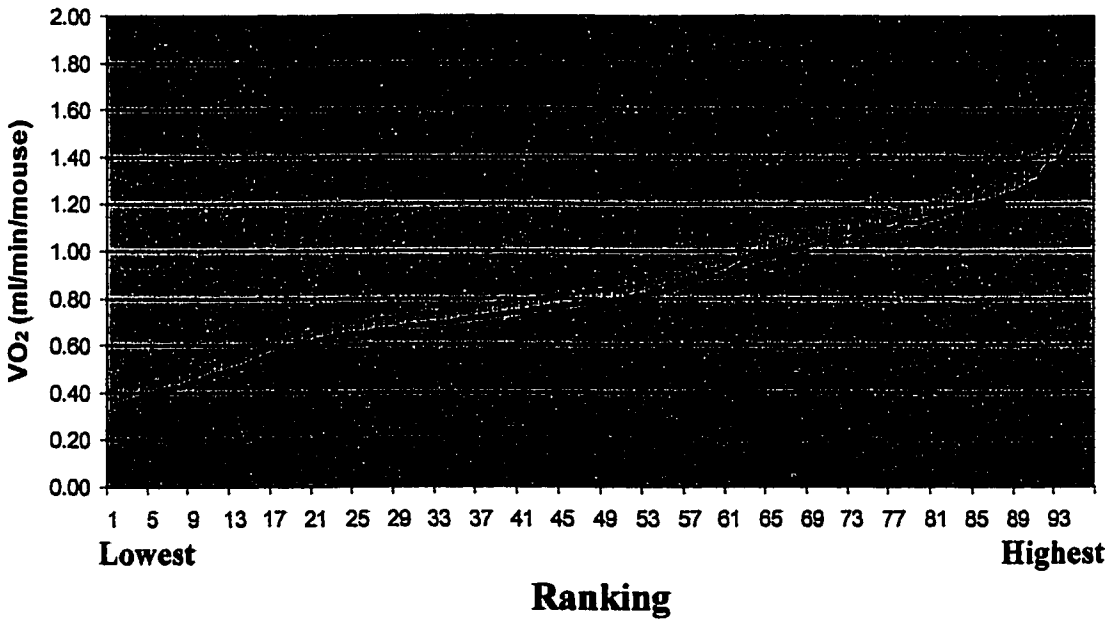

Figure 3.15 Twenty-four hour assessment of respiratory exchange ratios for B6-CAST congenic and B6 control mice fed a normal chow diet. These values represent the ratio of the volume of CO_2 produced to the volume of O_2 consumed by each mouse as determined by indirect calorimetry at 31°C with a 12:00hr-12:00hr light-dark cycle (lights on between 07:00 and 19:00 as indicated by the colored boxes on top of each graph: day=yellow, night=indigo). Throughout the experiments, all mice had *ad libitum* access to drinking water and either a normal chow diet (top graph -fed state) or no chow at all (bottom graph- fasted state). The bottom graph shows results for mice that were fasting for 24 hours and were subsequently refed and monitored for an additional 6 hours. Each point represents an average of data from six mice and is expressed as the mean ± SEM.

Respiratory Exchange Ratios

Fed State

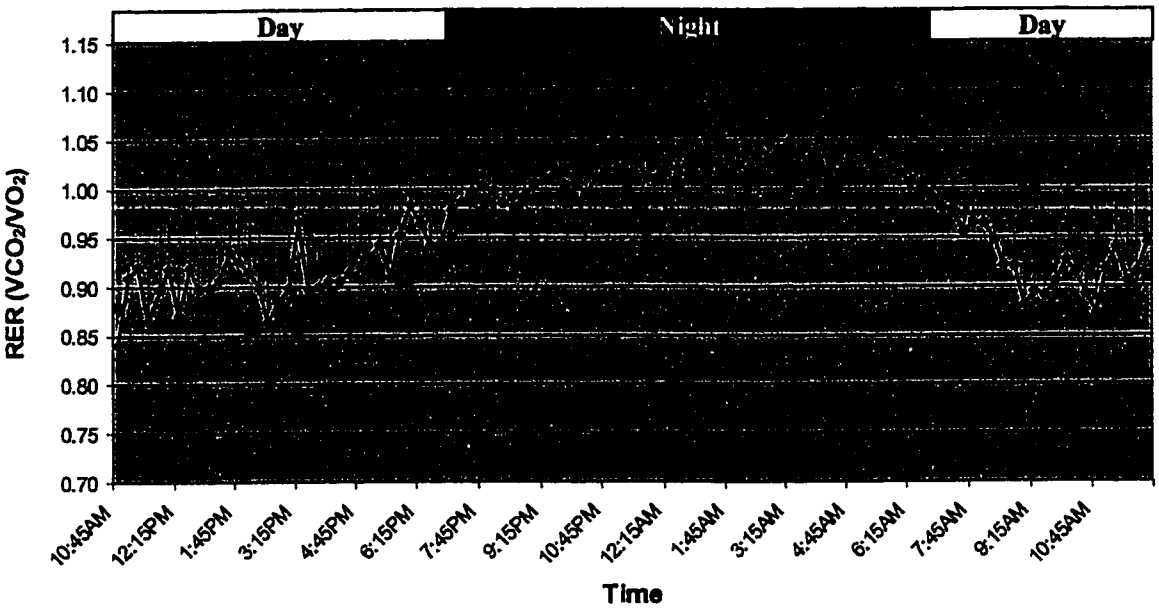

Fasted State

Refeed Period

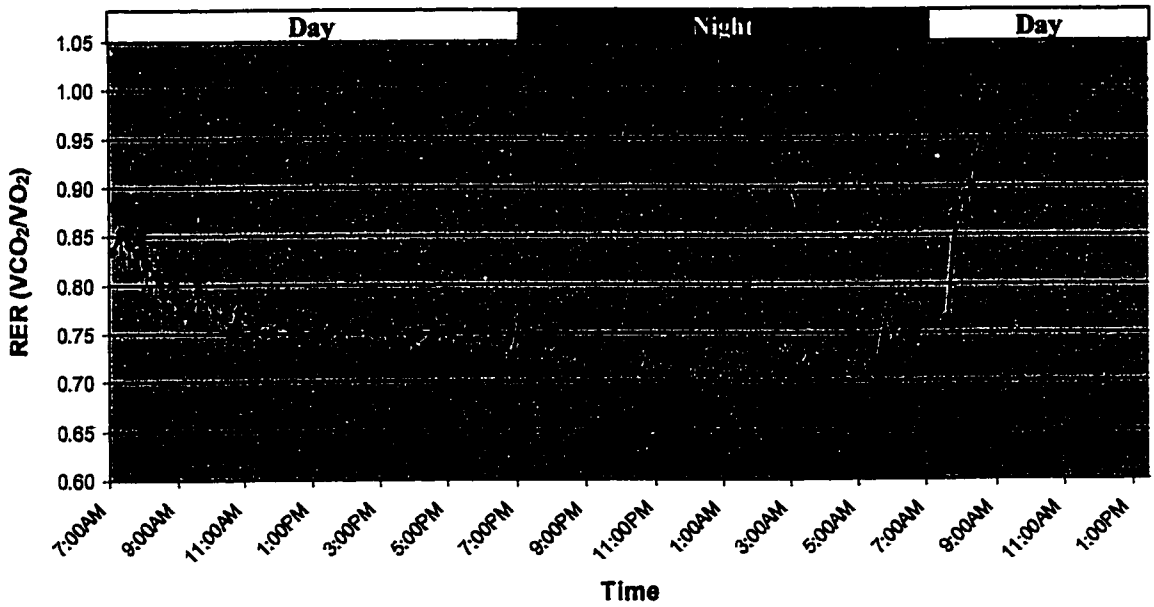

Figure 3.16 Ranked respiratory exchange ratio assessments for B6-CAST congenic and B6 control mice fed a normal chow diet. These values represent the ratio of the volume of CO_2 produced to the volume of O_2 consumed by each mouse as determined by indirect calorimetry at 31°C with a 12:00hr-12:00hr light-dark cycle (lights on between 07:00 and 19:00). Data points collected continuously over 24 hours were ranked in ascending order in an attempt to identify any differences, and facilitate comparisons, between the two groups of mice. Throughout the experiments, all mice had *ad libitum* access to drinking water and either a normal chow diet (top graph -fed state) or no chow at all (bottom graph- fasted state). The bottom graph shows only the data points collected during the first 24 hours when the mice were fasting; data points collected during the refeed period were not considered. Each point represents an average of data from six mice and is expressed as the mean ± SEM.

RER
Ranked in Ascending Order

Fed State

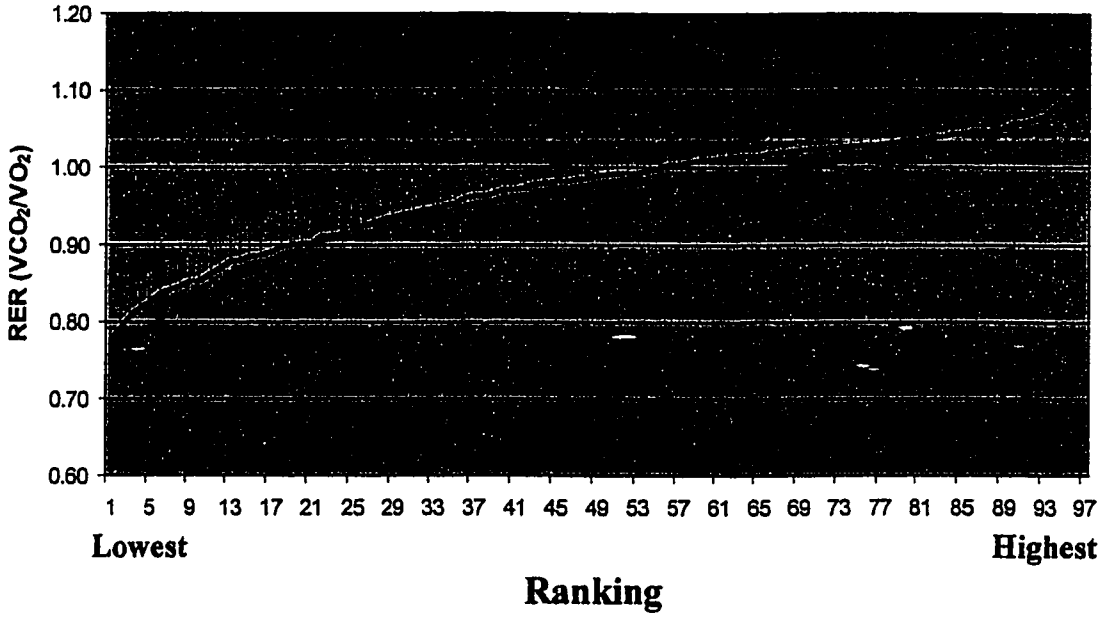

Fasted State

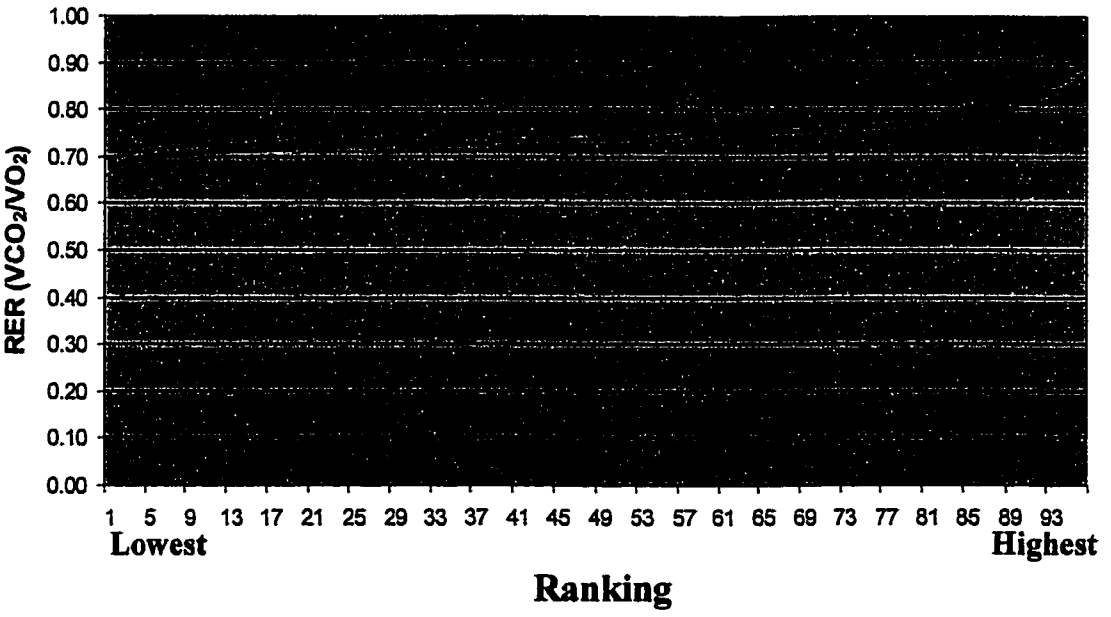

Figure 3.17 Twenty-four hour assessment of heat production for B6-CAST congenic and B6 control mice fed a normal chow diet. These values were calculated using the equation: HEAT = CV x VO_2, where CV = 3.815 + (1.232 x RER), and the VO_2 and RER data obtained from indirect calorimetric determinations at 31°C with a 12:00hr-12:00hr light-dark cycle (lights on between 07:00 and 19:00 as indicated by the colored boxes on top of each graph: day=yellow, night=indigo). Throughout the experiments, all mice had *ad libitum* access to drinking water and either a normal chow diet (top graph - fed state) or no chow at all (bottom graph- fasted state). The bottom graph shows results for mice that were fasting for 24 hours and were subsequently refed and monitored for an additional 6 hours. Each point represents an average of data from six mice and is expressed as the mean ± SEM. Abbreviations: CV = calorific value (in kcal), RER= respiratory exchange ratio. The equations used to calculate heat production were taken from the Oxymax Software Instruction Manual (p.12) provided with the indirect calorimeter manufactured by Columbus Instruments Inc. (Columbus, Ohio).

Heat Production

Fed State

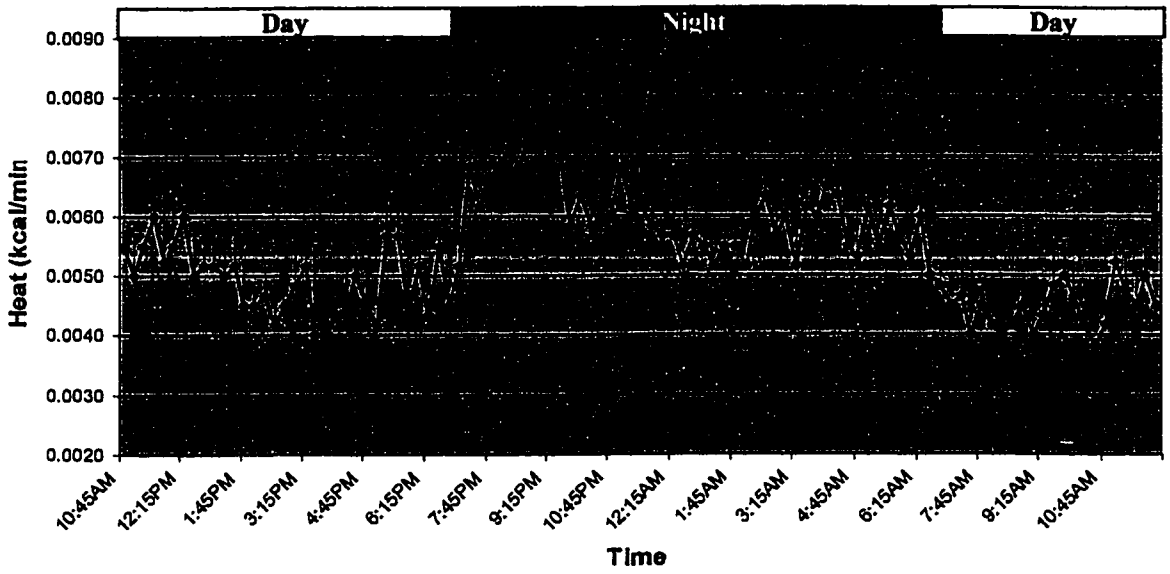

Fasted State

Refeed Period

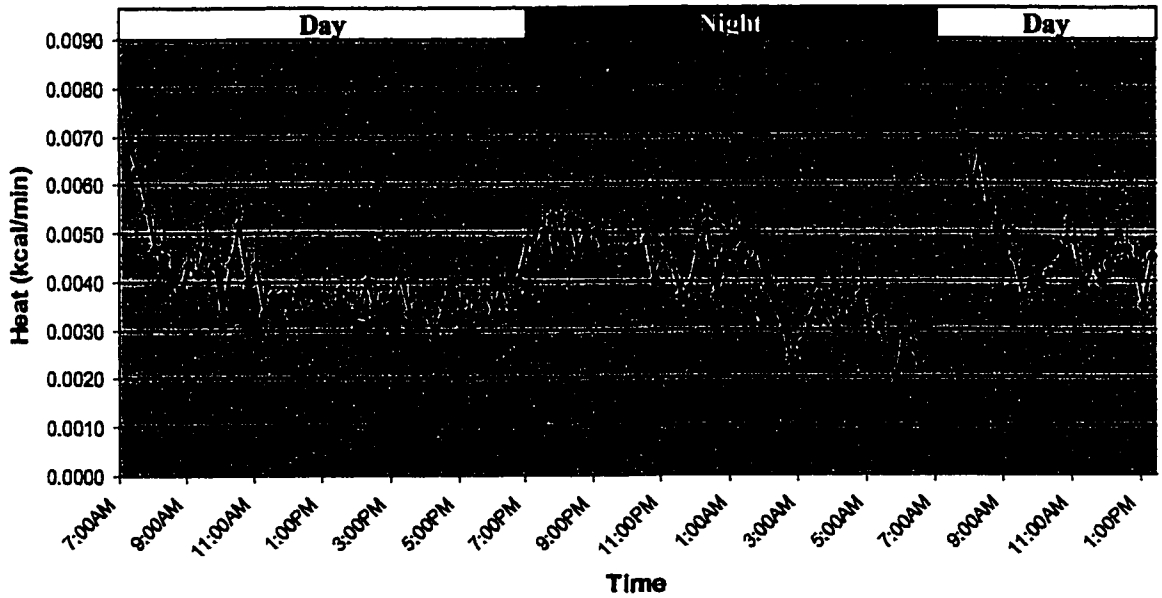

Figure 3.18 Ranked heat production assessments for B6-CAST congenic and B6 control mice fed a normal chow diet. These values were calculated using the equation: HEAT = CV x VO_2, where CV = 3.815 + (1.232 x RER), and the VO_2 and RER data obtained from indirect calorimetric determinations at 31°C with a 12:00hr-12:00hr light-dark cycle (lights on between 07:00 and 19:00). Data points collected continuously over 24 hours were ranked in ascending order in an attempt to identify any differences, and facilitate comparisons, between the two groups of mice. Throughout the experiments, all mice had *ad libitum* access to drinking water and either a normal chow diet (top graph -fed state) or no chow at all (bottom graph- fasted state). The bottom graph shows only the data points collected during the first 24 hours when the mice were fasting; data points collected during the refeed period were not considered. Each point represents an average of data from six mice and is expressed as the mean ± SEM. Abbreviations: CV = calorific value (in kcal), RER= respiratory exchange ratio. The equations used to calculate heat production were taken from the Oxymax Software Instruction Manual (p.12) provided with the indirect calorimeter manufactured by Columbus Instruments Inc. (Columbus, Ohio).

Heat Production

Ranked in Ascending Order

Fed State

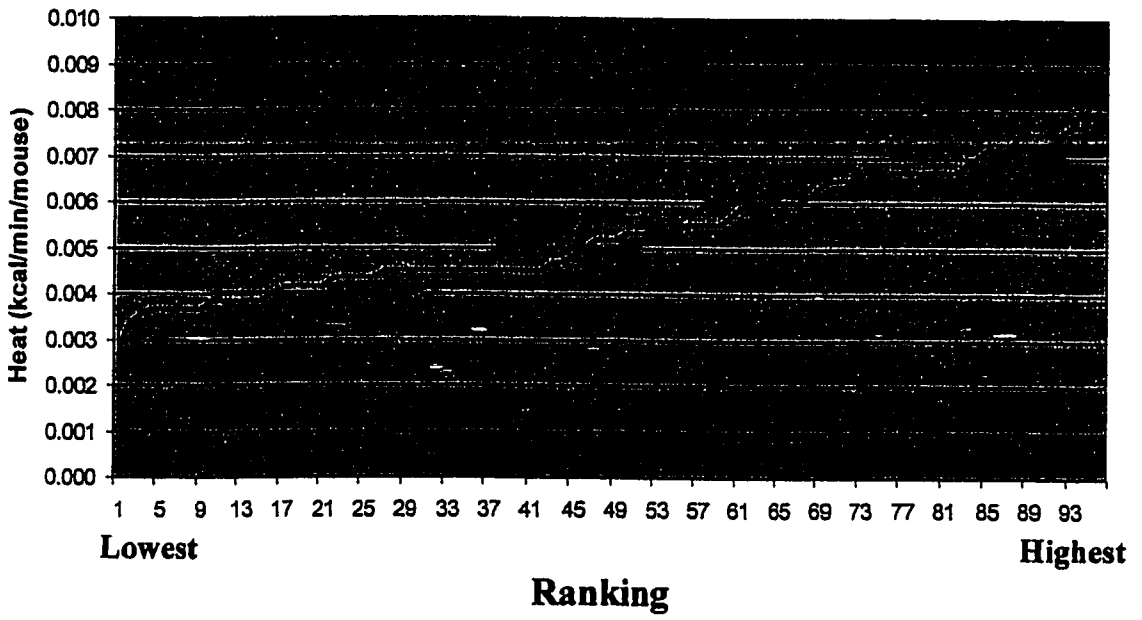

Fasted State

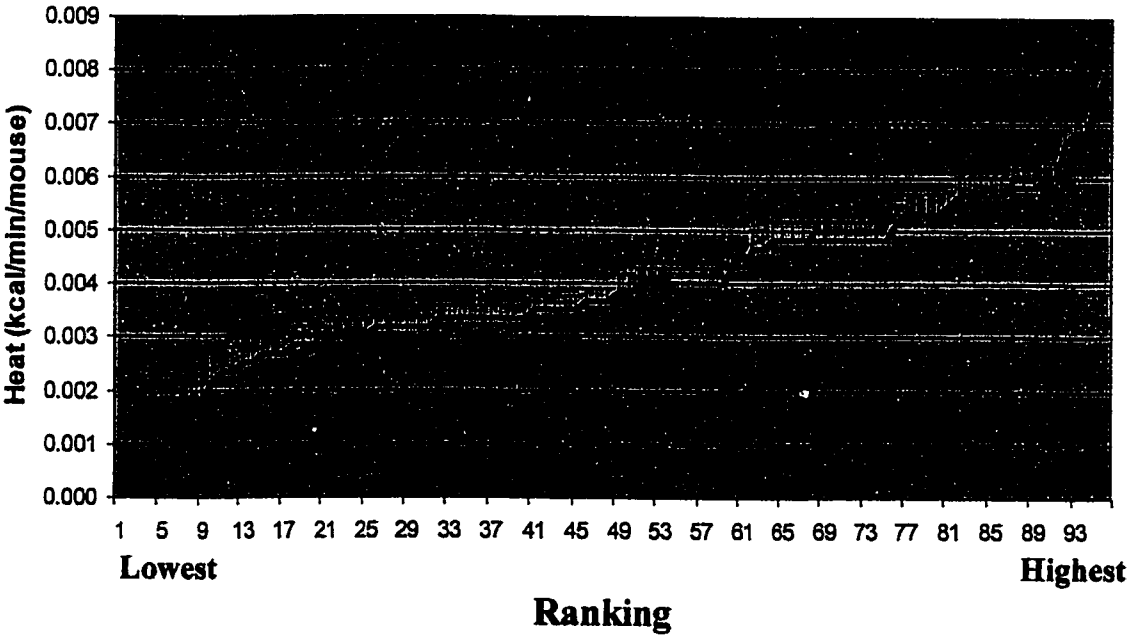

Table 3.1 Summary of total 24 hour energy expenditure and respiratory exchange ratios (RER) for B6-CAST congenic and B6 control mice in fed and fasted states. Assessments were conducted by indirect calorimetry over continuous 24 hour periods at 31°C with a 12:00hr-12:00hr light-dark cycle (lights on between 07:00 and 19:00). Throughout the experiments, all mice had access to drinking water and either a normal chow diet (fed state) or no chow at all (fasted state). For mean energy expenditure and mean RER determinations, results are expressed as the mean ± SEM of 96 total time point assessments for each of 6 control and 6 congenic mice. For daytime and nighttime determinations, results represent mean ± SEM of 48 time point assessments for each mouse in a group. All p values were obtained using Student's unpaired t-tests, and reveal statistically insignificant differences for each assessed parameter between the two groups, except for that of nocturnal RER in the fed state which is significantly greater in congenic mice as compared to control mice ($p<0.0001$).

Total 24 Hour Energy Expenditure and Respiratory Exchange Ratios

FED STATE			
	B6-CAST congenics	B6 controls	p values
Diurnal energy expenditure (kcal/24hrs)	6.83 ± 0.14	6.47 ± 0.12	0.054
Nocturnal energy expenditure (kcal/24hrs)	8.65 ± 0.14	8.80 ±0.12	0.418
Mean energy expenditure (kcal/24hrs)	7.68 ± 0.12	7.57 ± 0.14	0.552
Diurnal RER	0.918 ± 0.004	0.913 ± 0.010	0.590
Nocturnal RER	1.018 ± 0.003	0.990 ± 0.003	<0.0001*
Mean RER	0.966 ± 0.006	0.949 ± 0.007	0.058

FASTED STATE			
	B6-CAST congenics	B6 controls	p values
Diurnal energy expenditure (kcal/24hrs)	5.81 ± 0.20	5.41 ± 0.17	0.131
Nocturnal energy expenditure (kcal/24hrs)	5.65 ± 0.20	6.08 ± 0.17	0.105
Mean energy expenditure (kcal/24hrs)	5.73 ± 0.14	5.74 ± 0.12	0.957
Diurnal RER	0.766 ± 0.004	0.775 ± 0.005	0.170
Nocturnal RER	0.726 ± 0.002	0.729 ± 0.002	0.162
Mean RER	0.746 ± 0.003	0.752 ± 0.004	0.179

3.4.3 24 hour energy expenditure – Effects of fasting on VO_2, RER and heat production

With the mice still being fed a normal chow diet on an ongoing daily basis, similar assessments of energy expenditure as those described above were conducted, but this time with the mice having access to drinking water only. No food was placed in the sealed oxygen chambers, in order to examine the effect of fasting on the total 24 hour energy expenditure of both B6-CAST congenics and B6 controls and identify any possible differences between both groups of mice. The results of these assessments are shown in the bottom panels of Figures 3.13 to 3.18 and are summarized in Table 3.1. Although once again all expected trends were clearly present, such as a lessened variability between diurnal and nocturnal oxygen consumption and heat production, low and steady RER values, and subsequent returns of each parameter to its normal state upon refeeding (Figures 3.13, 3.15 and 3.17), no significant differences were observed between B6-CAST congenic and B6 control mice (Figures 3.14, 3.16 and 3.18). Mean total energy expenditure was 5.73 kcal/24hours (±0.14) for B6-CAST congenics and 5.74 kcal/24hours (±0.12) for B6 controls ($p=0.957$).

3.5 Comparison of mitochondrial proton leak kinetics in skeletal muscle of B6-CAST congenic and B6 control mice

Whilst the indirect calorimetry energy expenditure analyses failed to reveal any differences between the two groups of mice at the whole animal level, it must be kept in mind, that the observed differences in adiposity and metabolic efficiency between the two groups of mice could be explained by a very small percentage difference in energy expenditure (*i.e.*, less than 5%) that is undetectable by indirect calorimetry. Such a small

percentage difference could easily account for the phenotypic differences between congenics and controls.

We hypothesized that perhaps the resistance to fat deposition is based on the ability of the B6-CAST congenic mice to dispose of excess energy by uncoupling oxidative phosphorylation. Indeed, increases in mitochondrial proton leak due to functional differences in UCP2 or UCP3 could significantly increase energy expenditure and thus mitigate fat deposition. To verify this hypothesis, we assessed the kinetics of the proton leak in skeletal muscle mitochondria from the two groups of mice. We chose to study the kinetics of the leak in skeletal muscle mitochondria primarily because of the overall importance of skeletal muscle in overall energy expenditure, but also because of the tissue specific pattern of expression of UCP3 and the presence of UCP2, and their potential role in mediating adaptive thermogenesis, more specifically diet-induced thermogenesis.

As described in the last section of the Introduction, the approach used to study metabolic differences in the isolated skeletal muscle mitochondria is an extension of metabolic control analysis, referred to as top-down elasticity analysis. The data collected during these types of experiments are used to generate kinetic curves with the mitochondrial protonmotive force (Δp; -mV) on the y-axis, and oxygen consumption (nmol O/min/mg protein) on the x-axis. Figures 3.19 to 3.21 show the overall responsiveness, or 'elasticity' of leak-dependent oxygen consumption to changes in Δp. Table 3.2 summarizes the obtained values of State 3 (respiration under maximal phosphorylating conditions), State 4 (respiration under non-phosphorylating conditions) and respiratory control ratios (RCR - State 3 / State 4 respiration rates).

Figure 3.19 Relationship between mitochondrial protonmotive force (Δp) and leak-dependent respiration rate in skeletal muscle mitochondria from chow fed B6-CAST congenic and B6 control mice (1st study). The kinetic response of the proton leak-dependent oxygen consumption to Δp was measured with BSA present in the incubation medium by titrating the substrate oxidation reactions with increasing amounts of malonate (f.c. 0.33, 0.66, 1.0, 2.0, 3.0, 5.0 mM) in the presence of a saturating concentration of oligomycin (8mg/mg protein). State 4 respiration is defined as respiration under non-phosphorylating conditions achieved with the saturating concentration of oligomycin. Each point represents the mean ± SEM of duplicate determinations of both Δp and respiration rate with mitochondria from 7 control mice, and from 5 to 8 (from left to right: 5, 5, 6, 6, 7, 8, 8) congenic mice.

Skeletal Muscle
Mitochondrial Proton Leak Kinetic Curves

1st Study: Chow Diet
with BSA in incubation medium

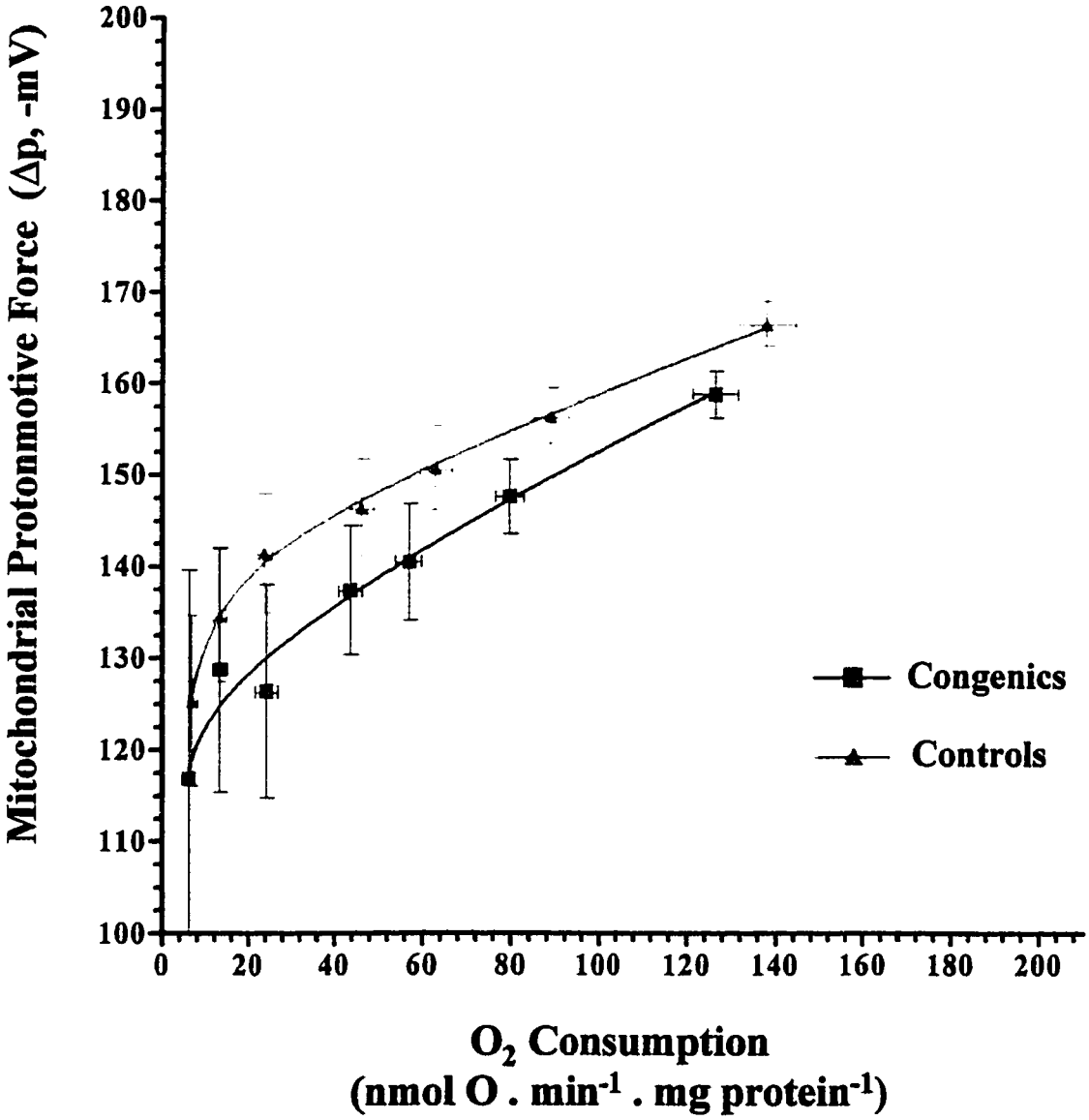

Figure 3.20 Relationship between mitochondrial protonmotive force (Δp) and leak-dependent respiration rate in skeletal muscle mitochondria from high fat fed B6-CAST congenic and B6 control mice (2^{nd} study). The kinetic response of the proton leak-dependent oxygen consumption to Δp was measured with BSA present in the incubation medium by titrating the substrate oxidation reactions with increasing amounts of malonate (f.c. 0.33, 0.66, 1.0, 2.0, 3.0, 5.0 mM) in the presence of a saturating concentration of oligomycin (8mg/mg protein). State 4 respiration is defined as respiration under non-phosphorylating conditions achieved with the saturating concentration of oligomycin. Each point represents the mean ± SEM of duplicate determinations of both Δp and respiration rate with mitochondria from 8 control and 8 congenic mice.

Skeletal Muscle
Mitochondrial Proton Leak Kinetic Curves

2nd Study: High Fat Diet
with BSA in incubation medium

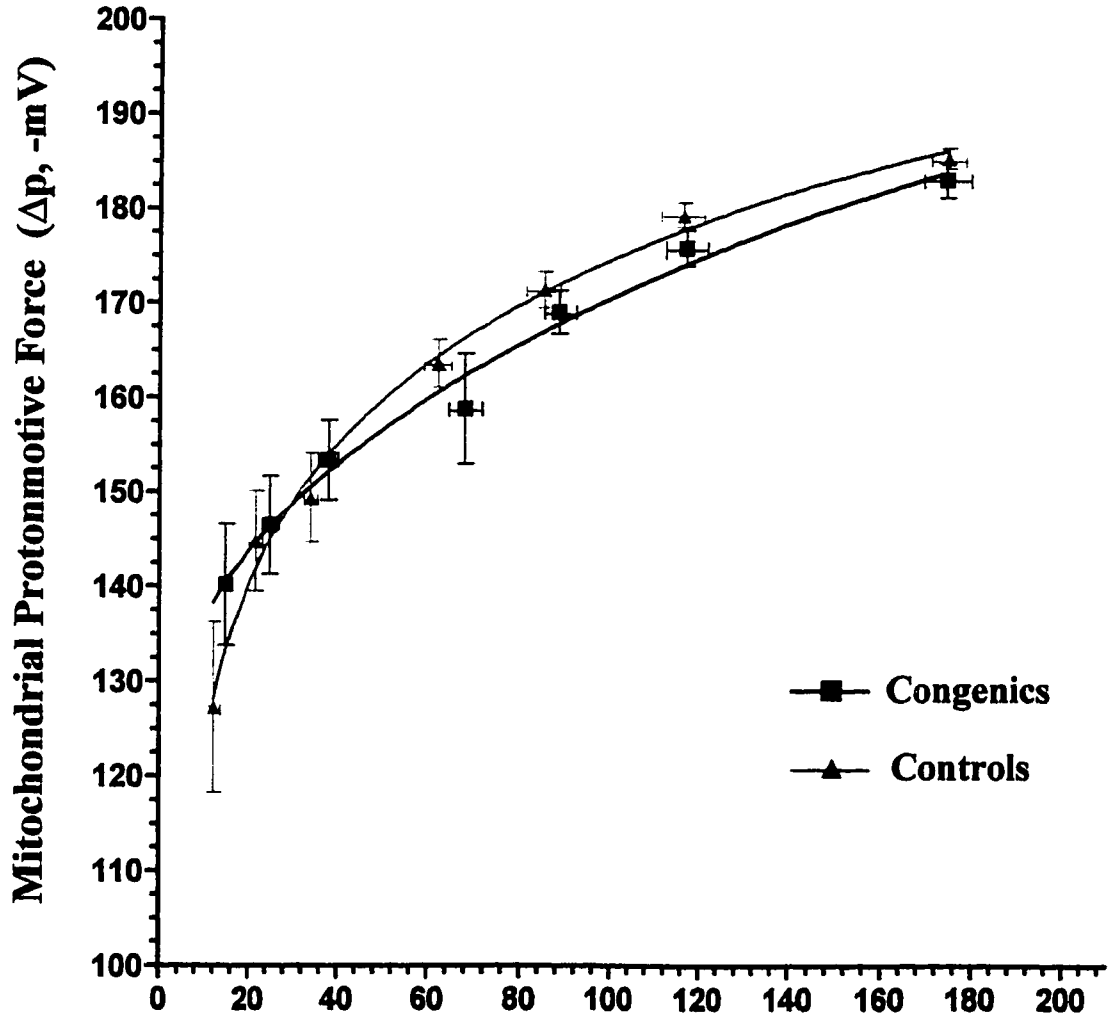

Figure 3.21 Relationship between mitochondrial protonmotive force (Δp) and leak-dependent respiration rate in skeletal muscle mitochondria from high fat fed B6-CAST congenic and B6 control mice (3rd study). The kinetic response of the proton leak-dependent oxygen consumption to Δp was measured without BSA in the incubation medium by titrating the substrate oxidation reactions with increasing amounts of malonate (f.c. 0.33, 0.66, 1.0, 2.0, 3.0, 5.0 mM) in the presence of a saturating concentration of oligomycin (8mg/mg protein). State 4 respiration is defined as respiration under non-phosphorylating conditions achieved with the saturating concentration of oligomycin. Each point represents the mean ± SEM of duplicate determinations of both Δp and respiration rate with mitochondria from 8 control and 7 congenic mice.

Skeletal Muscle
Mitochondrial Proton Leak Kinetic Curves

3rd Study: High Fat Diet
without BSA in incubation medium

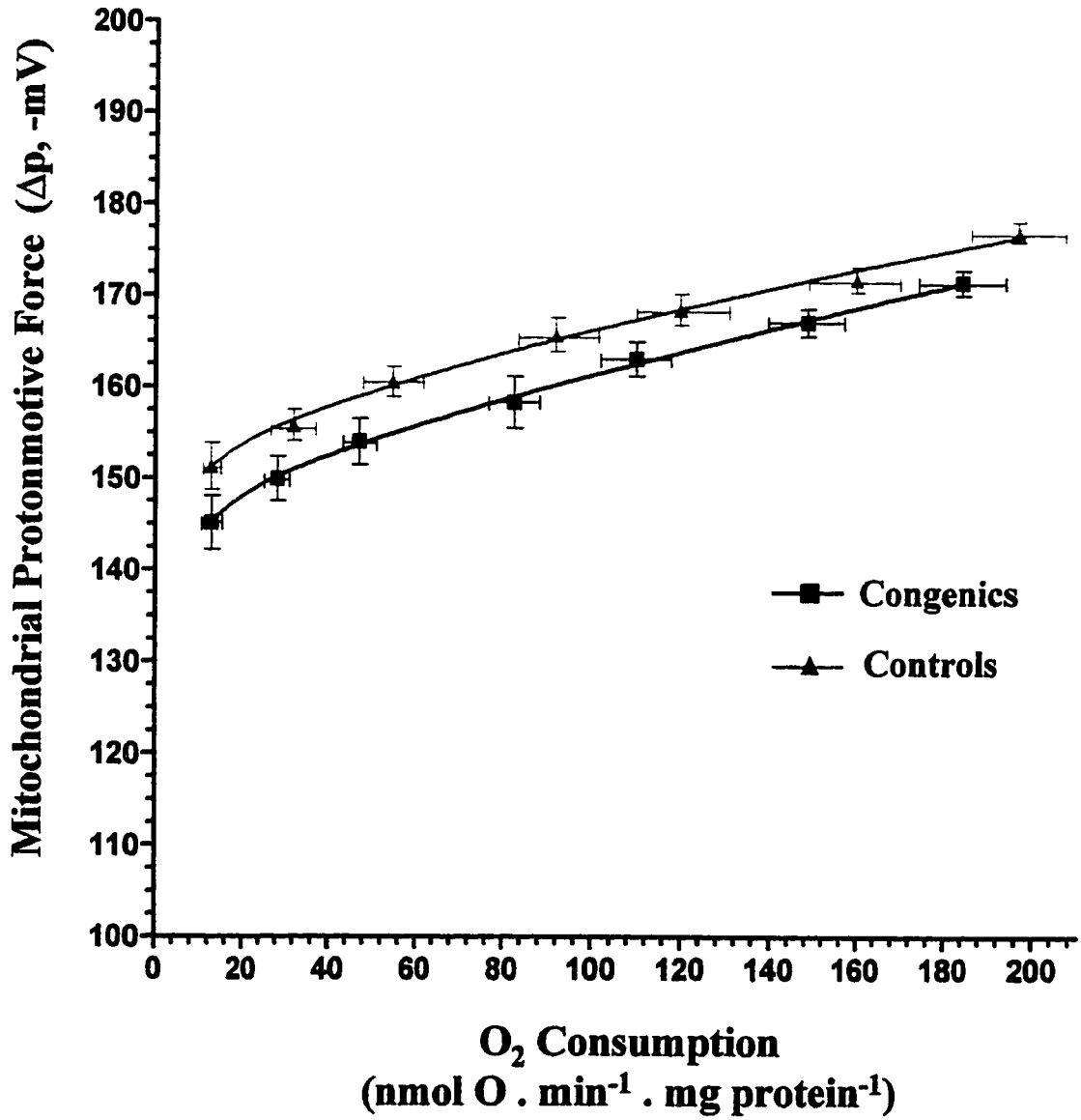

Table 3.2 Summary of results obtained from mitochondrial proton leak analyses performed during each of the three studies with B6-CAST congenic and B6 control mice. State 4 oxygen consumption represents maximal respiration under non-phosphorylating conditions and is achieved with a saturating oligomycin concentration. State 3 oxygen consumption represents respiration under maximal phosphorylating conditions achieved with ADP, hexokinase, and followed by FCCP. Respiratory control ratios (RCR) are calculated as State 3/State 4 and reflect the general health and quality of the mitochondrial preparation. The values for a_m (non-specific $TPMP^+$ binding correction factor) and matrix volume listed are those which were used in the equations for the calculation of membrane potential during all three studies. Both these values were determined using mitochondria isolated from congenic and control mice of the first study. Abbreviations: HFD = high fat diet.

Mitochondrial Proton Leak Analyses: Summary Table

	B6-CAST Congenics	B6 Controls
1st Study: Leak = Chow with BSA		
State 3 (nmol O/min/mg protein)	159 ± 10 (N=6)	163 ± 7 (N=6)
State 4 (nmol O/min/mg protein)	127 ± 5 (N=6)	138 ± 7 (N=6)
RCR	1.25	1.18
2nd Study: Leak = HFD with BSA		
State 3 (nmol O/min/mg protein)	219 ± 7 (N=7)	279 ± 13 (N=8)
State 4 (nmol O/min/mg protein)	175 ± 6 (N=8)	175 ± 4 (N=8)
RCR	1.25	1.59
3rd Study: Leak = HFD w/o BSA		
State 3 (nmol O/min/mg protein)	272 ± 19 (N=7)	250 ± 11 (N=8)
State 4 (nmol O/min/mg protein)	184 ± 10 (N=7)	197 ± 11 (N=8)
RCR	1.48	1.27
Membrane Potential Parameters		
a_m	0.29	0.21
Matrix Volume (μL/mg protein)	0.46 ± 0.05 (N=5)	0.39 ± 0.03 (N=8)

3.5.1 Skeletal muscle mitochondrial proton leak kinetics of chow fed B6-CAST congenic and B6 control mice analyzed in the presence of BSA

Figure 3.19 shows the overall kinetics of the proton leak from skeletal muscle mitochondria of B6-CAST congenic and B6 control mice fed a normal chow diet. In these experiments, mitochondrial membrane potential and oxygen consumption were measured while the mitochondria were incubating in the presence of 0.5% defatted bovine serum albumin (BSA). The resulting kinetic curves show that over a wide range of the mitochondrial protonmotive force (Δp), the amount of oxygen used to support the mitochondrial proton leak is greater for congenic mice than for control mice. Because the kinetics of the proton leak subsystem are non-linear, an analysis of covariance could not be used to test for statistical significance. However, taken together; these results show that while there is no net increase in maximal proton leak-dependent oxygen consumption (as evidenced by the similar State 4 points at the furthermost right on each curve) in mitochondria of congenics vs controls, the overall kinetics of the mitochondrial proton leak seem to be altered in skeletal muscle cells from B6-CAST congenic mice in relation to those from B6 control mice.

3.5.2 Skeletal muscle mitochondrial proton leak kinetics of high fat fed B6-CAST congenic and B6 control mice analyzed in the presence of BSA

Similar experiments as the ones outlined above were conducted with skeletal muscle mitochondria from B6-CAST congenic and B6 control mice fed the high fat condensed milk diet. Once again, mitochondrial membrane potential and oxygen consumption were measured while the mitochondria were incubating in the presence of 0.5% defatted bovine serum albumin (BSA). The resulting overall kinetics curves for the proton leak in these mitochondria are shown in Figure 3.20. These curves also reveal

similar State 4 (*i.e.*, non-phosphorylating) values indicating similar maximal proton leak-dependent respiration in mitochondria from B6-CAST congenic and B6 control mice. There is however an effect of the high fat feeding in that State 4 oxygen consumption and membrane potential both increase in congenics and in controls when switching from the normal chow to the high fat diet (compare values in Figure 3.19 to those in Figure 3.20). This is also true of membrane potential and oxygen consumption values at every other point along these leak curves.

3.5.3 Skeletal muscle mitochondrial proton leak kinetics of high fat fed B6-CAST congenic and B6 control mice analyzed in the absence of BSA

Due to earlier observations in our lab which showed that bovine serum albumin tends to decrease proton leakage across the mitochondrial inner membrane thus masking the true physiological activity of the proton leak, we decided to repeat the same experiments as above with the mice on a high fat diet, but study the kinetics of the leak in the absence of 0.5% defatted BSA. Because BSA binds a portion of the free fatty acids present in the incubation medium, our hypothesis was that by removing the BSA, we would obtain a more physiological determination of the true state of uncoupling. Fatty acids have been shown in many different studies to activate uncoupling through UCP1 (Desautels *et al.*, 1978; Nicholls and Locke, 1984). Whether or not fatty acids actually activate uncoupling protein homologues has not yet been confirmed, however the possibility remains. The resulting overall kinetics curves for the proton leak studied in the absence of BSA are shown in Figure 3.21. These curves show that, over the entire range of Δp values, there is an increase in the oxygen used to balance the leak of protons back into the matrix. For example, at -160mV, leak-dependent oxygen consumption is 55

nmol O/min/mg protein in B6 control mice, and 93 nmol O/min/mg protein in B6-CAST congenic mice. Although once again there are no significant differences in State 4 respiration between mitochondria of B6-CAST congenic and B6 control mice (184 nmol O/min/mg protein (±10) vs 197 nmol O/min/mg protein (±11); p=0.4169 – Student's unpaired t-test), the kinetics of the leak are obviously altered. A comparison of the absolute values of State 4 from this study with those from the 2nd study, reveals that the absence of BSA resulted in slight increases in both groups of mice. However, these did not reach the level of statistical significance (p>0.05).

It seems that the presence of the congenic segment within the B6 background affects the overall kinetics of the proton leak in the skeletal muscle mitochondria, without necessarily impacting on the total maximal proton leak-dependent oxygen consumption.

3.6 Western blotting for UCPs in skeletal muscle mitochondrial preparations from high fat fed B6-CAST congenic and B6 control mice

Western blot analyses were performed on isolated skeletal muscle mitochondria from both B6-CAST congenic and B6 control mice, in an attempt to compare the levels of uncoupling proteins, specifically UCP2 and UCP3. Two different antibodies were used to probe the blots. The first of these antibodies is a commercially available antibody against an 18 amino acid peptide sequence between the 3rd and 4th transmembrane domains of rat UCP3 (Alpha Diagnostics International Inc., San Antonio, TX), and thus should recognize both the long and the short form of UCP3 which differ only in that the short form lacks the 6th transmembrane domain. This rat immunogenic peptide sequence is identical in mouse UCP3 (18/18aa) and has no significant homology with UCP1 or

UCP2. The Western blots obtained using this antibody are shown in Figure 3.22. These two blots are identical except that the top blot was exposed to the film for 10 minutes and the bottom one for 16 minutes. A rat UCP standard was used as a control. This standard was prepared by isolating uncoupling proteins from brown adipose tissue of cold exposed rats (see Methods, section 2.5.4.1), and as such should contain UCP1 as well as, UCP2 and UCP3, albeit in lesser amounts. The band for this UCP standard probed with the rat UCP3 antibody described above, appears at 33.0 kDa, which is approximates the expected molecular weight for the long form of UCP3, 34kDa. In the lanes containing the mitochondrial proteins from the B6-CAST congenic and B6 control mice, two bands of very similar intensities appear at molecular weights of approximately 39kDa for the top band and 36.9kDa for the bottom one. Although the idea of the two bands being the long and short form of UCP3 was exciting at first, this is very unlikely given that the calculated molecular weights are too high, and that mice may not express the short form of UCP3. (The latter was reported at the Uncoupling Protein Symposium held in Quebec city in November of 1998.) The estimated molecular weights of these proteins based on the number of amino acids are 34kDa and 29kDa for $UCP3_L$ and $UCP3_S$ respectively. Also, even if those bands had been UCP3, given the very similar intensities of the two bands in both congenics and controls, no important conclusions on differential expression could have been drawn from these results.

The other antibody used to probe the skeletal muscle mitochondrial proteins for uncoupling proteins, is an antibody against UCPs from brown adipose tissue of cold exposed hamsters. Technically, this antibody should be able to pick up UCP1, UCP2 and UCP3 assuming that the last two were upregulated in BAT by exposure of the hamsters

Figure 3.22 Western blots of skeletal muscle mitochondrial preparations from B6-CAST congenic and B6 control mice probed using an antibody against a purified rat UCP3 immunogenic peptide obtained from Alpha-Diagnostics. The location and size of the biotinylated molecular weight markers (in lane 2) correspond to those of the Rainbow™ molecular weight markers depicted on the left of each blot. Lanes 3 and 4 both contain mitochondrial protein from B6 control mice whereas lanes 5 and 6 contain mitochondrial protein from B6-CAST congenic mice. A UCP standard purified from brown adipose tissue of cold-acclimated rats was run in lane 8. The blots shown represent similar results from two separate experiments. They only differ in exposure time.

Western Blots

Skeletal Muscle Mitochondrial proteins probed using a rUCP3 Antibody

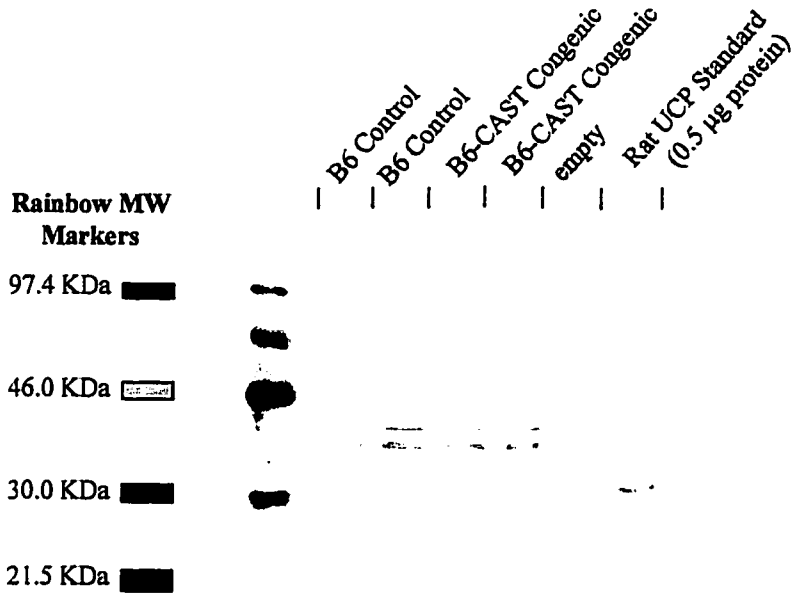

* 10 minute exposure

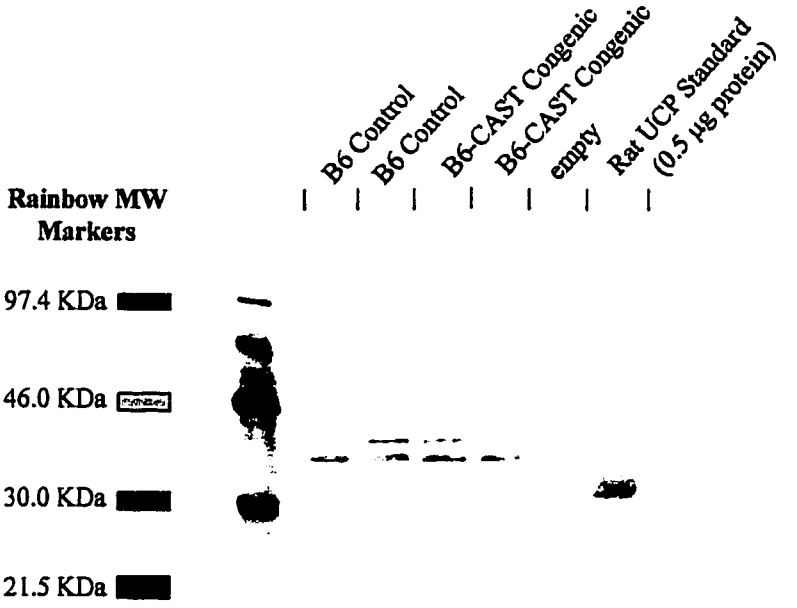

* 16 minute exposure

to cold. The Western blots probed with this antibody are displayed in Figure 3.23. In this case the two blots differ in exposure time and in that the top one contains half the amount of standard as does the bottom blot. The same standard described above was used here as a control. This lane shows a smeared multitude of bands with a large and very dark band at 35.8kDa, and a smaller and much more faint band below at 28.0kDa. Although the large band appears at a molecular weight that is slightly higher than that of the 32kDa UCP1, it is assumed here, based on a multitude of other experiments conducted by Dr. Anna Melnik in Dr. Jean Himms-Hagen's laboratory using a number of different other antibodies, that this band represents UCP1. Due to the fairly large smear of this band it is likely that the band for $UCP3_L$ and possibly that of UCP2 are overlapped and therefore not visible. The smaller band located at a calculated 28.0kDa likely represents that of $UCP3_S$, which has an estimated molecular weight of 29.0kDa. In each of the two lanes containing skeletal muscle mitochondrial proteins from B6-CAST congenic and from B6 control mice, two very clean and clear cut bands are apparent. These bands are located at calculated molecular weights of 38.8kDa and 28.9kDa for the top and bottom bands respectively. Given that it appears at the correct molecular weight, the lower band possibly represents $UCP3_S$. The upper band however, is located at a molecular weight somewhat higher than that of the estimated 34kDa of $UCP3_L$. As in the previous blots on Figure 3.23, the intensities of these bands in the lanes of congenic and control mice are practically identical. It seems then from the results of these analyses, that the level of expression of UCP3 is similar in both groups of mice.

It is important to note however, that none of the antibodies available to us commercially or otherwise have proven to be specific for any of the uncoupling proteins. Others working in this field have unfortunately encountered similar problems with the currently available antibodies for the UCPs.

Figure 3.23 Western blots of skeletal muscle mitochondrial preparations from B6-CAST congenic and B6 control mice probed using an antibody against purified hamster BAT UCP. The location and size of the biotinylated molecular weight markers (in lane 2) correspond to those of the Rainbow™ molecular weight markers depicted on the left of each blot. Lanes 3 and 4 both contain mitochondrial protein from B6 control mice whereas lanes 5 and 6 contain mitochondrial protein from B6-CAST congenic mice. A UCP standard purified from brown adipose tissue of cold-acclimated rats was run in lane 8. The blots shown represent similar results from two separate experiments. They only differ in exposure time and in the amount of standard used.

Western Blots

Skeletal muscle mitochondrial proteins probed using an Antibody against UCPs from BAT of cold exposed hamsters

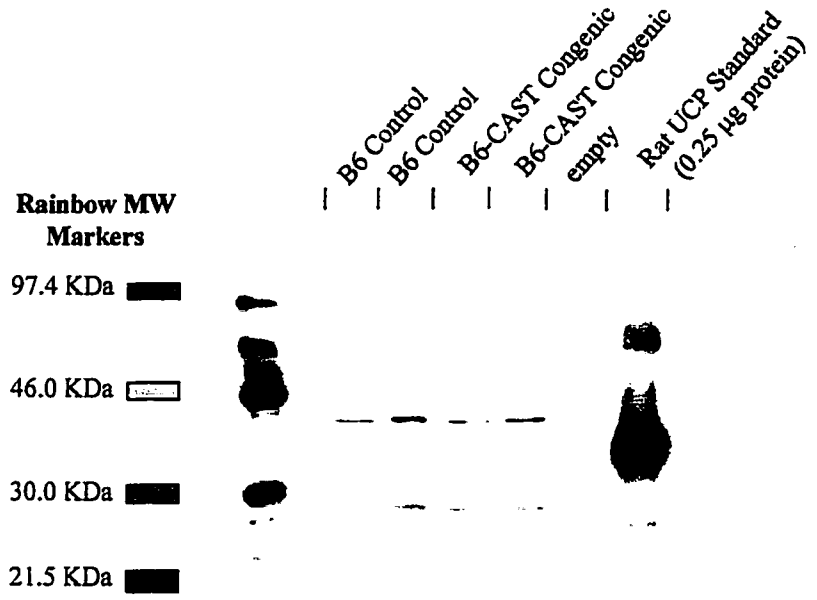

* 5 minute exposure

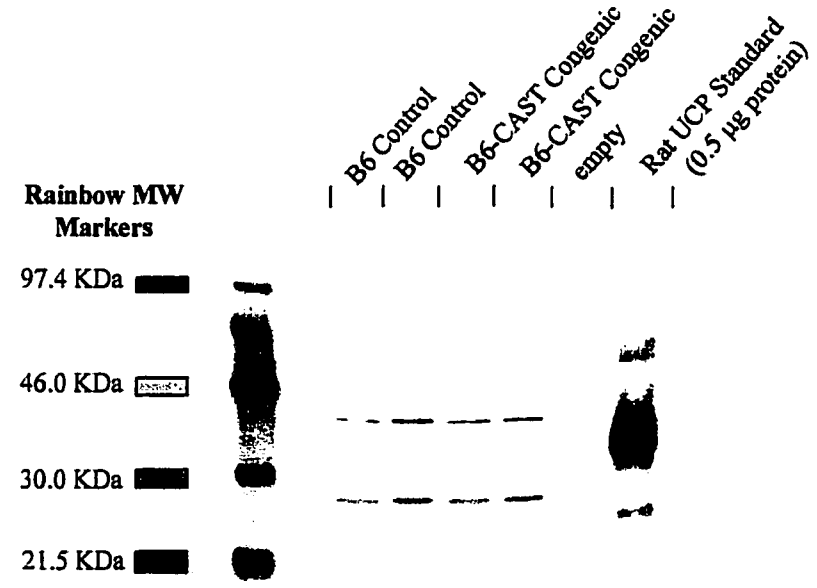

* 10 minute exposure

4. DISCUSSION

Our findings show that when challenged with a high fat diet, C57BL/6J mice bearing the CAST/Ei congenic segment on mid to distal chromosome 7 are resistant to the development of obesity. The introduction of this segment results in a 48-75% decrease in epididymal fat pad weights and a 32-64% decrease in inguinal fat pad weights, as compared to control C57BL/6J mice fed the same high fat diet. These decreases in white fat depot weights of congenics relative to controls were only apparent on the high fat condensed milk diet. No significant differences in fat pad weights were seen when the mice were fed the normal chow diet. IBAT weights were also found to be decreased (by approximately 40%) in high fat fed B6-CAST congenic mice relative to those of B6 control mice; however, this decrease was only observed in the 3rd study. The discrepencies between the IBAT weight results of the 2nd and 3rd studies prompted us to look at the total amount of IBAT protein per depot, to provide a crude estimate of the total thermogenic potential of the depots. These were found to be similar in both groups of mice in both studies, suggesting no unusual or dissimilar activity of the tissue between the two groups, regardless of the difference in wet tissue weights. This also indicates that the extra weight of the IBAT depots of B6 control mice in the 3rd study was predominantly fat.

These results corroborate those of York and colleagues who found a 50% decrease in the adiposity index (a summed weight of seven fat pads - right and left inguinal, epididymal, retroperitoneal and mesenteric - divided by the eviscerated carcass weight of each mouse) of B6-CAST congenic mice in relation to B6 control mice. They also

observed that white and brown fat depot weights of B6-CAST congenic mice were 50% lower than those of B6 control mice fed the same high fat diet (York *et al.*, 1999).

Histological analyses of white and brown adipose tissues showed dramatically smaller lipid droplets in adipocytes from B6-CAST congenic mice when compared to those from B6 control mice. It appears from these analyses that the decrease in the weights of the various adipose tissue depots of congenics is a consequence of comparably smaller amounts of lipids being stored in their adipocytes. Nonetheless, the number of adipocytes in the fat depots of congenics and controls was not empirically determined in this series of studies. In the case of IBAT however, since there were no differences in the total amount of protein per depot between congenics and controls, this strongly suggests that the increased weight of the IBAT depots of controls resulted from increased fat storage within the pre-existing adipocytes. Had there been recruitment and differentiation of supplementary preadipocytes, then one would logically expect to see differences in the total amount of protein.

Given such drastic phenotypic differences between the two groups of mice fed the high fat diet, our overall objective was to determine the metabolic basis for this observed differential susceptibility to obesity. The rationale for our experiments stemmed from the realization that the decreased fat deposition seen in B6-CAST congenic mice must be due to either a lower energy intake or a higher energy expenditure in these animals compared to B6 control mice. The first of these two possibilities was examined by monitoring the body weights and food intake of the two groups of mice both on a normal chow diet and on a high fat condensed milk diet. It was found through these studies that the average daily energy intake of both congenic and control mice was similar, be it on a normal

chow diet or on the high fat diet. Interestingly, the daily energy intake of both groups was only slightly greater on the high fat diet than it was on the chow diet. Both groups of mice sensed the more dense caloric content in the high fat chow, and adjusted their energy intake accordingly by reducing the amount of food consumed each day. Differences between the two groups of mice became apparent however when comparing their body weights before and after the feeding of the respective diets for fixed periods of time. When fed a high fat diet, B6 control mice gained significant amounts of weight compared to B6-CAST congenic mice whose average body weights were not significantly altered by the regime. On the normal chow diet however, the body weights of both groups remained fairly constant throughout the feeding period. The findings for the high fat fed mice translate into a metabolic efficiency for B6-CAST congenic mice that is 73% lower than that of B6 control mice. This indicates an inefficient use of dietary energy by B6-CAST congenic mice, which readily gets wasted as heat, rather than being stored, as is obviously the case for B6 control mice.

Since there was no evidence that the decrease in adiposity observed in the high fat fed B6-CAST congenic mice was linked to a reduced energy intake, the next logical step was to look for any indication of increased energy expenditure. This was assessed by two different means; one was by indirect calorimetry and the other by examining the total activity and the overall kinetics of skeletal muscle mitochondrial proton leak reactions using an extension of metabolic control analysis called top down elasticity analysis.

The idea of an increase in the resting metabolic rate of congenic mice as compared to control mice was originally fancied as this could in itself explain the differences in fat deposition between the two groups. Indeed, a greater steady state of heat production

occurring to maintain vital cellular metabolic processes and body temperature in congenics would result in a greater proportion of ingested energy being wasted, thereby allowing them to resist the increased fat deposition seen in control mice. Furthermore, the fact that there is a strong genetic linkage between the UCP2/UCP3 locus and resting energy expenditure in humans (Bouchard *et al.*, 1997), combined with the presence of these uncoupling protein genes in the congenic segment made the possibility all the more interesting. However, indirect calorimetry assessments of resting metabolic rates (RMR) and of respiratory exchange ratios (RER) failed to reveal any differences between B6-CAST congenic and B6 control mice. RERs were assessed since they provide valuable insights into the type of fuel substrate that is being preferentially used by an organism. A low RER (*e.g.*, 0.70) reflects increased fat oxidation, whereas an RER approaching unity indicates mostly carbohydrate utilization. Our results show that both groups of mice have an RER ranging between 0.77-0.78, which indicates that both fats and carbohydrates were used as fuel substrates in a ratio of roughly 75% fats and 25% carbohydrates (Brody, 1945).

Given the lack of any apparent differences in resting metabolic rates between the two groups of mice on either of the diets, we then moved on to examining total energy expenditure of both B6-CAST congenic and B6 control mice over 24 hour periods. The idea here was that perhaps these longer term continuous assessments of energy expenditure would reveal differences that may not be apparent by looking simply at the energy expended for basal metabolism. These assessments were conducted once again by indirect calorimetry at thermoneutrality (31°C) with the mice having been fed a normal chow diet prior to the analyses, and having access to either normal chow and

water (fed state) or water alone (fasted state) during the analyses. Under these conditions, we saw no differences in total 24 hour energy expenditure between B6-CAST congenic and B6 control mice in either the fed or fasted states. These results are in accordance with those of York and colleagues who, like us, could not detect any sign of increased energy expenditure in chow fed congenic mice as compared to controls (York *et al.*, 1999). However, because the phenotypic differences between the two groups of mice are apparent only upon the feeding of a high fat diet, it stands to reason that differences in energy expenditure may also only become apparent under those same conditions. Due to the limited availability of these specially bred mice, we were not able to complete these analyses of 24 hour total energy expenditure with the high fat fed mice on time for the writing of this thesis. Nevertheless, we have recently received a fourth set of mice, which are currently being fed the high fat condensed milk diet. They will be fed for a period of six weeks, after which time the exact same measurements of 24 hour total energy expenditure will be conducted. Similar measurements have already been conducted and published by York and colleagues who have reported no measurable difference in total 24 hour energy expenditure between congenic and control mice after one or two weeks on a high fat diet, though as expected, energy expenditure was greater and RER was lower in both groups of mice fed the high fat diet as compared to the normal chow diet (York *et al.*, 1999). From past experience however, we have noticed that the phenotypic differences between the two groups of mice become significant only after a period of at least six weeks of high fat diet feeding. It is possible that their assessments of 24 hour energy expenditure were conducted slightly too early for any differences to be apparent by indirect calorimetry.

Nonetheless, it must be kept in mind that the changes in energy intake or energy expenditure brought about by the congenic segment, could be too small to be detected by indirect calorimetry. Indeed, the observed differences in adiposity and metabolic efficiency between the two groups of mice could be explained by a very small percentage difference in energy expenditure (*i.e.*, less than 5%) that may be undetectable by indirect calorimetry, but that could easily account for the phenotypic differences between congenics and controls.

As mentioned earlier, the congenic segment under study in this research contains approximately one hundred genes located on mid-to-distal chromosome 7. Two of those genes are the genes for the uncoupling proteins UCP2 (Fleury *et al.*, 1997) and UCP3 (Boss *et al.*, 1997; Vidal-Puig *et al.*, 1997). Since these proteins uncouple respiration thereby decreasing metabolic efficiency, it is possible that allelic variations in the UCP2 and/or UCP3 genes are responsible for the decreased adiposity seen in the congenic mice carrying the CAST/Ei UCP2 and/or UCP3 alleles. In fact, four polymorphisms resulting in amino acid substitutions were reported when comparing UCP2 sequences from CAST/Ei and B6 mice (York *et al.*, 1999). These allelic variations include the replacement of an arginine with a lysine at codon 16, a threonine with an isoleucine at codon 30, a serine with a glycine at codon 47 and a tyrosine with a cysteine at codon 302 (York *et al.*, 1999). Other UCP2 polymorphisms between the two strains of mice include three that are silent (different codons; same amino acids) and one that is out of the open reading frame (York *et al.*, 1999). The UCP3 sequences are currently being determined, and as yet, no such polymorphisms have been identified. Also, recent papers by Fleury and colleagues as well as by Surwit and company, report that the degree of resistance to a

high fat diet may be associated with variations in the modulation of UCP2 expression by consumption of the diet. Their studies with A/J mice (which much like the CAST/Ei mice are resistant to diet-induced obesity), show evidence of a higher UCP2 expression in white adipose tissue than obesity prone B6 mice (Fleury *et al.*, 1997; Surwit *et al.*, 1998). Although as mentionned in the introduction, levels of mRNA do not necessarily reflect the level of actual protein expression, these findings remain quite interesting.

This led us to hypothesize that perhaps the resistance to fat deposition in B6-CAST congenic mice is based on their ability to dispose of excess energy by uncoupling oxidative phosphorylation. Indeed, increases in mitochondrial proton leak due to functional differences in UCP2 and/or UCP3 could significantly increase energy expenditure and thus mitigate fat deposition. To verify this hypothesis, top-down elasticity analysis was used to assess the kinetics of the proton leak in skeletal muscle mitochondria of the two groups of mice to identify any possible metabolic differences. We chose to study proton leak in skeletal muscle mitochondria primarily because of the overall importance of skeletal muscle in overall energy expenditure, but also because of the tissue specific pattern of expression of UCP3 and the presence of UCP2, and the potential role of these proteins in mediating adaptive thermogenesis, more specifically diet-induced thermogenesis. Proton leak kinetics were assessed in both groups of mice fed either a normal chow diet or a high fat diet, after the completion of the feeding studies. The incubation conditions of the mitochondria were modified to exclude BSA during the third study, following other recent results in our laboratory, which showed that BSA inhibited or masked the true physiological state of the proton leak. Although none of the three studies revealed a net increase in maximal proton leak-dependent oxygen

consumption (*i.e.*, State 4 respiration) of B6-CAST congenic mice as compared to B6 control mice, removing the BSA from the incubation conditions in the third study unveiled differences in the overall kinetics of the leak between the two groups. The results of this last study show that over the entire range of protonmotive force values studied, there is an increase in the oxygen used to balance the leak of protons across the mitochondrial inner membrane. These findings are consistent with the conclusion that the presence of the congenic segment within the C57BL/6J background alters the overall kinetics of the proton leak in skeletal muscle mitochondria, without necessarily affecting the total maximal leak-dependent oxygen consumption.

While these slight kinetic differences in the proton leak between the two groups of mice are significant, it is not possible at this point to state unequivocally that they are sufficient to account for the observed resistance to obesity in B6-CAST congenic mice. We must also consider that there are many other genes besides UCP2 and UCP3 within the region of the congenic donor segment, and that these could also potentially be responsible for the decrease in fat deposition. Among other candidate genes, there is the *tub* gene whose locus maps very close to those of the UCP2 and UCP3 genes (Kleyn *et al.*, 1996; Noben-Trauth *et al.*, 1996). Comparisons of the coding region of *tub* in C57BL/6J and CAST/Ei mice, revealed that variant alternative splicing of the intron preceeding exon five results in that intron being shorter in CAST/Ei mice (Kleyn *et al.*, 1996). As discussed by York (York *et al.*, 1999), other possible candidate genes include the insulin-like growth factor-1 receptor (*Igf1r*), and the sulfonylurea receptor gene (*Sur*), which have been found to be linked to obesity in an obese human population of French Caucasians (Hani *et al.*, 1997). According to York (York *et al.*, 1999), the gene for

proprotein convertase subtilisin/kexin type-3 (Pcsk3), which is responsible for the conversion of precursors of peptide hormones and neuropeptides to their biologically active forms (Nakayama, 1997), could also be another possible candidate. Furthermore, other genes as of yet not characterized could also account for the differential phenotype ensuing from the presence of the congenic segment within the B6 background.

In conclusion, although we were unable to conclusively determine the cause of the observed resistance to obesity of the B6-CAST congenic mice fed a high fat diet, this mouse model remains very interesting. It seems clear from this research that the difference between the two groups lies on the energy expenditure side of the energy balance equation, since these mice do not have a reduced energy intake when compared to B6 control mice. More sensitive and precise methods of measuring energy expenditure may be required, since the differences in energy expenditure required to explain the differences in adiposity appear to be quite small. One option could be to examine total body energy expenditure using doubly-labeled water, though accuracy is difficult to achieve in small rodents. While the possibility remains that allelic variations in the UCP2 and/or UCP3 genes may be responsible to some extent for the decrease in fat deposition, the contribution of other genes within the congenic segment cannot be excluded. Efforts are now being focused on shortening the length of the congenic segment thus decreasing the number of possible candidate genes, and increasing the chances of being able to attribute the obesity resistant phenotype to one (or possibly more) specific gene(s), or to interactions between two or more specific genes.

REFERENCES

Argyropoulos G., Brown A.M., Willi S.M., Zhu J., He Y., Reitman M., Gevao S.M., Spruill I., and Garvey W.T. (1998) Effects of mutations in the human uncoupling protein 3 gene on the respiratory quotient and fat oxidation in severe obesity and type 2 diabetes. *J. Clin. Invest.*, **102:** (7), 1345-1351.

Bancroft J.D. (1975) Histochemical techniques. Butterworths, London

Bhattacharya S.K., Thakar J.H., Johnson P.L., and Shanklin D.R. (1991) Isolation of skeletal muscle mitochondria using an ionic medium containg ethylenediarninetetraacetic acid and Nagarse. *Anal. Biochem.*, **192:** 344-349.

Bianco A.C., Sheng X.Y., and Silva J.E. (1988) Triiodothyronine amplifies norepinephrine stimulation of uncoupling protein gene transcription by a mechanism not requiring protein synthesis. *J. Biol. Chem.*, **263:** (34), 18168-18175.

Birmingham C.L., Muller J.L., Palepu A., Spinelli J.J., and Anis A.H. (1999) The cost of obesity in Canada. *CMAJ*, **160:** (4), 483-488.

Blaxter K. (1989) Energy metabolism in animals and man. Cambridge University Press, Cambridge

Boss O., Samec S., Paoloni-Giacobino A., Rossier C., Dulloo A., Seydoux J., Muzzin P., and Giacobino J.-P. (1997) Uncoupling protein-3: A new member of the mitochondrial carrier family with tissue-specific expression. *FEBS Lett.*, **408:** (1), 39-42.

Bouchard C. (1991) Current understanding of the etiology of obesity: Genetic and non-genetic factors. *Am. J. Clin. Nutr.*, **53:** 1561S-1565S.

Bouchard C. (1997) Genetics of human obesity - Recent results from linkage studies. *J. Nutr.*, **127:** (9), S1887-S1890.

Bouchard C., Despres J.-P., and Tremblay A. (1991) Genetics of obesity and human energy metabolism. *Proc. Nutr. Soc.*, **50:** 139-147.

Bouchard C., and Perusse L. (1988) Heredity and body fat. *Annu. Rev. Nutr.*, **8:** 259-277.

Bouchard C., Perusse L., Chagnon Y.C., Warden C., and Ricquier D. (1997) Linkage between markers in the vicinity of the uncoupling protein 2 gene and resting metabolic rate in humans. *Hum. Mol. Genet.*, **6:** (11), 1887-1889.

Bouchard C., and Tremblay A. (1997) Genetic influences on the response of body fat and fat distribution to positive and negative energy balances in human identical twins. *J. Nutr.*, **127:** (Suppl 5), S943-S947.

Bouillaud F., Weissenbach J., and Ricquier D. (1986) Complete cDNA-derived amino acid sequence of rat brown fat uncoupling protein. *J. Biol. Chem.*, **261:** (4), 1487-1490.

Brand M.D. (1990) The contribution of the leak of protons across the mitochondrial inner membrane to standard metabolic rate. *J. Theoret. Biol.*, **145:** 267-286.

Brand M.D. (1994) The stoeichiometry of proton pumping and ATP synthesis in mitochondria. *The Biochemist*, **Aug/Sept:** 20-24.

Brand M.D. (1995) Measurement of mitochondrial protonmotive force. In *Bioenergetics: A Practical Approach*, Edited by: G.C. Brown and C.E. Cooper., IRL Press., Oxford., pp. 39-62.

Brand M.D., Chien L.-F., Ainscow E.K., Rolfe D.F.S., and Porter R.K. (1994) The causes and functions of mitochondrial proton leak. *Biochim. Biophys. Acta.*, **1187:** 132-139.

Brand M.D., Couture P., Else P.L., Withers K.W., and Hulbert A.J. (1991) Evolution of energy metabolism: Proton permeability of the inner membrane of liver mitochondria is greater in a mammal than in a reptile. *Biochem. J.*, **275:** 81-86.

Brand M.D., and Murphy M.P. (1987) Control of electron flux through the respiratory chain in mitochondria and cells. *Biol. Rev. Camb. Philos. Soc.*, **62:** (2), 141-193.

Brand M.D., Steverding D., Kadenbach B., Stevenson P.M., and Hafner R.P. (1992) The mechanism of the increase in mitochondrial proton permeability induced by thyroid hormones. *Eur. J. Biochem.*, **206:** 775-781.

Brindley D.N., and Rolland Y. (1989) Possible connections between stress, diabetes, obesity, hypertension and altered lipoprotein metabolism that may result in atherosclerosis. *Clinical Science*, **77:** 453-461.

Brody S. (1945) Bioenergetics and Growth. Reinhold, New York

Brookes P.S., Rolfe D.F.S., and Brand M.D. (1997) The proton permeability of liposomes made from mitochondrial inner membrane phospholipids - comparison with isolated mitochondria. *J. Memb. Biol.*, **155:** (2), 167-174.

Brown G.C. (1985) Control of mitochondrial respiration. In *Recent advances in biological membrane studies*, Edited by: L. Packer., Plenum., New York., pp. 463-477.

Brown G.C. (1992a) Control of respiration and ATP synthesis in mammalian mitochondria and cells. *Biochem. J.*, **284:** 1-13.

Brown G.C. (1992b) The leaks and slips of bioenergetic membranes. *FASEB J.*, **6:** 2961-2965.

Brown G.C., and Brand M.D. (1986) Changes in the permeability to protons and other cations at high proton motive force in rat liver mitochondria. *Biochem. J.*, **234:** 75-81.

Brown G.C., Hafner R.P., and Brand M.D. (1990a) A 'top-down' approach to the determination of control coefficients in metabolic control theory. *Eur. J. Biochem.*, **188:** 321-325.

Brown G.C., Lakin-Thomas P.L., and Brand M.D. (1990b) Control of mitochondrial respiration and ATP synthesis in isolated rat liver cells. *Eur. J. Biochem.*, **192:** 355-362.

Bukowiecki L.J., Follea N., Lupien J., and Paradis A. (1981) Metabolic relationships between lipolysis and respiration in rat brown adipocytes: The role of long chain fatty acids as regulators of mitochondrial respiration and feedback inhibitors of lipolysis. *J. Biol. Chem.*, **256:** (24), 12840-12848.

Buttgereit F., Brand M.D., and Muller M. (1992) ConA-induced changes in energy metabolism of rat thymocytes. *Biosci. Rep.*, **12:** 381-386.

Buttgereit F., Muller M., and Rapoport S.M. (1991) Quantification of ATP-producing and consuming processes in quiescent pig spleen lymphocytes. *Biochem. Int.*, **24:** 59-67.

Cassard-Doulcier A.M., Gelly C., Fox N., Schrementi J., Raimbault S., Klaus S., Forest C., Bouillaud F., and Ricquier D. (1993) Tissue-specific and beta-adrenergic regulation of the mitochondrial uncoupling protein gene: control by cis-acting elements in the 5'-flanking region. *Molecular Endocrinology*, **7:** (4), 497-506.

Cassard-Doulcier A.M., Larose M., Matamala J.C., Champigny O., Bouillaud F., and Ricquier D. (1994) In vitro interactions between nuclear proteins and uncoupling protein gene promoter reveal several putative transactivating factors including Ets1, retinoid X receptor, thyroid hormone receptor, and a CACCC box-binding protein. *J. Biol. Chem.*, **269:** (39), 24335-24342.

Chaffee R.R., and Roberts J.C. (1971) Temperature acclimation in birds and mammals. *Annu. Rev. Physiol.*, **33:** 155-202.

Chagnon Y.C., and Bouchard C. (1996) Genetics of obesity - Advances from rodent studies. *Trends in Genetics,* **12:** (11), 441-444.

Chagnon Y.C., Perusse L., and Bouchard C. (1998) The human obesity gene map - The 1997 update. *Obesity Research,* **6:** (1), 76-92.

Challoner D.R. (1968) Respiration in myocardium. *Nature,* **217:** 78-79.

Chen R.F. (1967) Removal of fatty acids from serum albumin by charcoal treatment. *J. Biol. Chem.,* **242:** 173-181.

Coleman D.L., Eicher E.M., and Southard J.L. (1978) Tubby (tub). *Mouse News Lett.,* **59:** 25.

DeBry R.W., and Seldin M.F. (1996) Human/mouse homology relationships. *Genomics,* **33:** 337-351.

Desautels M., Zaror-Behrens G., and Himms-Hagen J. (1978) Increased purine nucleotide binding, altered polypeptide composition, and thermogenesis in brown adipose tissue mitochondria of cold-acclimated rats. *Can. J. Biochem.,* **56:** (6), 378-383.

Diolez P., Kesseler A.K., Haraux F., Valerio M., Brinkmann K., and Brand M.D. (1993) Regulation of oxidative phosphorylation in plant mitochondria. *Biochem. Soc. Trans.,* **21:** 769-773.

Else P.L., and Hulbert A.J. (1985) Mammals: an allometric study of metabolism at the tissue and mitochondrial level. *Am. J. Physiol.,* **248:** R415-R421.

Enerback S., Jacobsson A., Simpson E.M., Guerra C., Yamashita H., Harper M.E., and Kozak L.P. (1997) Mice lacking mitochondrial uncoupling protein are cold sensitive but not obese. *Nature,* **387:** (6628), 90-94.

Fell D.A. (1992) Metabolic control analysis: A survey of its theoretical and experimental development. *Biochem. J.,* **286:** 313-330.

Fernandez M., Nicholls D.G., and Rial E. (1987) The uncoupling protein from brown-adipose-tissue mitochondria. Chymotrypsin-induced structural and functional modifications. *Eur. J. Biochem.,* **164:** (3), 675-680.

Figlewicz D.P., Schwartz M.W., and Seeley R.J. (1996) Endocrine regulation of food intake and body weight. *J. Lab. Clin. Med.,* **127:** 328-332.

Fleury C., Neverova M., Collins S., Raimbault S., Champigny O., Levi-Meyrueis C., Bouillard F., Seldin M.F., Surwit R.S., Ricquier D., and Warden C.H. (1997) Uncoupling protein-2: A novel gene linked to obesity and hyperinsulinemia. *Nature Genetics,* **15:** 269-272.

Flier J.S. (1995) The adipocyte: Storage depot or node on the energy information superhighway? *Cell,* **80:** 15-18.

Flier J.S., and Lowell B.B. (1997) Obesity research springs a proton leak. *Nature Genetics,* **15:** (3), 223-224.

Friedman M.I., Tordoff M.G., and Ramirez I. (1986) Integrated metabolic control of food intake. *Brain Res. Bull.,* **17:** 855-859.

Garby L., and Lammert O. (1994a) Between-subjects variation in energy expenditure: estimation of the effect of variation in organ size. *Eur. J. Clin. Nutr.,* **48:** 376-378.

Garby L., and Lammert O. (1994b) Estimation of the sources of the between-subjects variation in energy metabolism. *Eur. J. Clin. Nutr.,* **48:** 303-304.

Garruti G., and Ricquier D. (1992) Analysis of uncoupling protein and its mRNA in adipose tissue deposits of adult humans. *International Journal of Obesity & Related Metabolic Disorders,* **16:** (5), 383-390.

Gimeno R.E., Dembski M., Weng X., Deng N., Shyjan A.W., Gimeno C.J., Iris F., Ellis S.J., Woolf E.A., and Tartaglia L.A. (1997) Cloning and characterization of an uncoupling protein homolog: a potential molecular mediator of human thermogenesis. *Diabetes,* **46:** (5), 900-906.

Gong D.W., He Y., Karas M., and Reitman M. (1997) Uncoupling protein-3 is a mediator of thermogenesis regulated by thyroid hormone, beta3-adrenergic agonists, and leptin. *J. Biol. Chem.,* **272:** (39), 24129-32.

Gornall A.G., Bardawil C.J., and David M.M. (1949) Determination of serum proteins by means of the biuret reaction. *J. Biol. Chem.,* **177:** 751-766.

Groen A.K., Wanders R.J.A., Westerhoff H.V., Van Der Meer R., and Tager J.M. (1982) Quantification of the contribution of various steps to the control of mitochondrial respiration. *J. Biol. Chem.,* **257:** 2754-2757.

Guerra C., Roncero C., Porras A., Fernandez M., and Benito M. (1996) Triiodothyronine induces the transcription of the uncoupling protein gene and stabilizes its mRNA in fetal rat brown adipocyte primary cultures. *J. Biol. Chem.,* **271:** (4), 2076-2081.

Gustafsson R., Tata J.R., Lindberg O., and Ernster L. (1965) The relationship between the structure and activity of rat skeletal muscle mitochondria after thyroidectomy and thyroid hormone treatment. *J. Cell. Biol.*, **26:** 555-578.

Hafner R.P., Brown G.C., and Brand M.D. (1990) Analysis of the control of respiration rate, phosphorylation rate, proton leak rate and protonmotive force in isolated mitochondria using the 'top-down' approach of metabolic control theory. *Eur. J. Biochem.*, **188:** 313-319.

Hani E.H., Clement K., Velho G., Vionnet N., Hager J., Philippi A., Dina C., Inoue H., Permutt M.A., Basdevant A., North M., Demenais F., Guy-Grand B., and Froguel P. (1997) Genetic studies of the sulfonylurea receptor gene locus in NIDDM and morbid obesity among French Caucasians. *Diabetes,* **46:** 688-694.

Harper M.-E. (1997) Obesity research continues to spring leaks. *Clin. Invest. Med.*, **20:** (4), 239-244.

Harper M.-E., and Brand M.D. (1993) The quantitative contributions of mitochondrial proton leak and ATP turnover reactions to the changed respiration rates of hepatocytes isolated from rats of different thyroid hormone status. *J. Biol. Chem.*, **268:** 14850-14860.

Harper M.-E., and Brand M.D. (1995) Use of top-down elasticity analysis to identify sites of thyroid hormone-induced thermogenesis. *Proc. Soc. Exp. Biol. Med.*, **208:** 228-237.

Hashimoto L., Habita C., Beressi J.P., Delepine M., Besse C., Cambon-Thomsen A., Deschamps I., Rotter J.I., Djoulah S., and James M.R. (1994) Genetic mapping of a susceptibility locus for insulin-dependent diabetes mellitus on chromosome 11q. *Nature,* **371:** 161-164.

Heaton G.M., Wagenvoord R.J., Kemp A., and Nicholls D.G. (1978) Brown adipose tissue mitochondria: photoafinity labelling of the regulatory site of energy dissipation. *Eur. J. Biochem.*, **82:** 515-521.

Heinrich R., and Rapoport T.A. (1973) A linear steady state treatment of enzymatic chains: General properties, control, and effector strenght. *Eur. J. Biochem.*, **42:** 97-105.

Himms-Hagen J. (1976) Cellular thermogenesis. *Annu. Rev. Physiol.*, **38:** 315-351.

Himms-Hagen J. (1989) Brown adipose tissue thermogenesis and obesity. *Prog. Lipid Res.*, **28:** 67-115.

Himms-Hagen J. (1990) Brown adipose tissue thermogenesis: Role in thermoregulation, energy regulation and obesity. In *Thermoregulation: Physiology and Biochemistry.*, Edited by: E. Schonbaum and P. Lomax., Pergamon Press Inc., New York., pp. 327-414.

Himms-Hagen J., Cerf J., Desautels M., and Zaror-Behrens G. (1978) Thermogenic mechanisms and their control. In *Effectors of Thermogenesis*, Edited by: L. Girardier and J. Seydoux., Birhauser Verlag., Basel., pp. 119-134.

Himms-Hagen J., and Desautels M. (1978) A mitochondrial defect in brown adipose tissue of the obese (ob/ob) mouse: reduced binding of purine nucleotides and a failure to respond to cold by an increase in binding. *Biochem. Biophys. Res. Commun.*, **83:** 628-634.

Hulbert A.J. (1985) A comparative study of thyroid function in reptiles and mammals. In *The Endocrine System and the Environment*, Edited by: B.K. Follit, S. Ishii, and A. Chandola., Japan Sci. Soc. Press., Tokyo., pp. 105-115.

Jansky L. (1973) Non-shivering thermogenesis and its thermoregulatory significance. *Biol. Rev. Camb. Philos. Soc.*, **48:** (1), 85-132.

Jung R.T. (1997) Obesity as a disease. *British Medical Bulletin*, **53:** (2), 307-321.

Kacser H., and Burns J.A. (1973) The control of flux. *Symp. Soc. Exp. Biol.*, **32:** 65-104.

Kacser H., and Burns J.A. (1995) The control of flux: 21 years on. *Biochem. Soc. Trans.*, **23:** 341-366.

Kacser H., and Porteous J.W. (1987) Control of metabolism: What do we have to measure? *TIBS*, **12:** 5-13.

Kamo N., Muratsugu M., Hongoh R., and Kobatake Y. (1979) Membrane potential of mitochondria measured with an electrode sensitive to tetraphenyl phosphonium and relationship between proton electrochemical potential and phosphorylation potential in steady state. *J. Memb. Biol.*, **49:** 105-121.

Kesseler A.K., Diolez P., Brinkmann K., and Brand M.D. (1992) Characterization of the control of respiration in potato tuber mitochondria using the top-down approach of metabolic control analysis. *Eur. J. Biochem.*, **210:** 775-784.

Kleyn P.W., Fan W., Duyk G.M., and Moore K.J. (1996) Identification and characterization of the mouse obesity gene tubby: A member of a novel gene family. *Cell*, **85:** 281-290.

Kopecky J., Hodny Z., Kolarova P., Horakova M., and Kolenovska R. (1997) Ontogenic changes in uncoupling protein 1 in white fat of the ap2-Ucp transgenic and nontransgenic mice: post-transcriptional control of gene expression. *Obesity Research,* **5:** S65.

Kozak U.C., and Kozak L.P. (1994) Norepinephrine-dependent selection of brown adipocyte cell lines. *Endocrinology,* **134:** (2), 906-913.

Krebs H.A. (1950) Body size and tissue respiration. *Biochim. Biophys. Acta,* **4:** 249-269.

Krishnamoorthy G., and Hinkle P.C. (1984) Non-ohmic proton conductance of mitochondria and liposomes. *Biochem.,* **23:** 1640-1645.

Kuczmarski R.J., Flegal K.M., Campbell S.M., and Johnson C.L. (1994) Increasing prevalence of overweight among US adults. *JAMA,* **272:** 205-211.

Lander E.S., and Botstein D. (1989) Mapping mendelian factors underlying quantitative traits using RFLP linkage maps. *Genetics,* **121:** 185-199.

LaNoue K.F., Strzelecki T., Strzelecka D., and Koch C. (1986) Regulation of the uncoupling protein in brown adipose tissue. *J. Biol. Chem.,* **261:** (1), 298-305.

Larose M., Cassard-Doulcier A.M., Fleury C., Serra F., Champigny O., Bouillaud F., and Ricquier D. (1996) Essential cis-acting elements in rat uncoupling protein gene are in an enhancer containing a complex retinoic acid response domain. *J. Biol. Chem.,* **271:** (49), 31533-31542.

Letellier T., Malgat M., and Mazat J.-P. (1993) Control of oxidative phosphorylation in rat muscle mitochondria: Implications for mitochondrial myopathies. *Biochim. Biophys. Acta,* **1141:** 58-64.

Lew E.A., and Garfinkel L. (1979) Variations in mortality by weight among 750,000 men and women. *J. Chronic Dis.,* **32:** 563-576.

Lillie R.D., and Fulmer H.M. (1976) Histopathological technique and practical histochemistry. McGraw-Hill, New York

Lin C.S., and Klingenberg M. (1982) Characteristics of the isolated purine nucleotide binding protein from brown fat mitochondria. *Biochem.,* **21:** (12), 2950-2956.

Locke R.M., Rial E., Scott I.D., and Nicholls D.G. (1982) Fatty acids are acute regulators of the proton conductance of hamster brown fat mitochondria. *Eur. J. Biochem.,* **129:** 373-380.

Lowell B.B., Susulic V.S., Hamann A., Lawitts J.A., Himms-Hagen J., Boyer B.B., Kozak L.P., and Flier J.S. (1993) Development of obesity in transgenic mice after genetic ablation of brown adipose tissue. *Nature*, **366:** (6457), 740-742.

Lowry O.H., Rosenbrough N.J., Farr A.L., and Randal R.J. (1951) Protein measurement with Folin phenol reagent. *J. Biol. Chem.*, **193:** 265-275.

Mao W., Yu X.X., Li W., Brush J., Sherwood S.W., Adams S.H., and Pan G. (1999) UCP4, a novel brain-specific mitochondrial protein that reduces membrane potential in mammalian cells. *FEBS Lett.*, **443:** (3), 326-330.

Matsuda J., Hosoda K., Itoh H., Son C., Doi K., Tanaka T., Fukunaga Y., Inoue G., Nishimura H., Yoshimasa Y., Yamori Y., and Nakao K. (1997) Cloning of rat uncoupling protein-3 and uncoupling protein-2 cDNAs: their gene expression in rats fed a high-fat diet. *FEBS Lett.*, **418:** (1-2), 200-204.

Melnyk A., Harper M.-E., and Himms-Hagen J. (1997) Raising at thermoneutrality prevents obesity and hyperphagia in BAT-ablated transgenic mice. *Am. J. Physiol.*, **272:** (4 Pt 2), R1088-R1093.

Miller A.T., and Blyth C.S. (1953) Lean body mass as a metabolic reference standard. *J. Appl. Physiol.*, **5:** 311-316.

Millet L., Vidal H., Andreelli F., Larrouy D., Riou J.P., Ricquier D., Laville M., and Langin D. (1997) Increased uncoupling protein-2 and -3 mRNA expression during fasting in obese and lean humans. *J. Clin. Invest.*, **100:** (11), 2665-2670.

Mitchell P., and Moyle J. (1967) Respiration-driven proton translocation in rat liver mitochondria. *Biochem. J.*, **105:** 1147-1162.

Moody D.E., Pomp D., and Nielsen M.K. (1997) Variability in metabolic rate, feed intake and fatness among selection and inbred lines of mice. *Genetical Research*, **70:** (3), 225-235.

Nakayama K. (1997) Furin: A mammalian subtilisin/Kex2p-like endoprotease involved in processing a wide variety of precursor proteins. *Biochem. J.*, **327:** 625-635.

Nicholls D., Cunningham S., and Wiesinger H. (1986) Mechanisms of thermogenesis in brown adipose tissue. *Biochem. Soc. Trans.*, **14:** 223-225.

Nicholls D.G. (1974) The influence of respiration and ATP hydrolysis on the proton-electrochemical gradient across the inner membrane of rat liver mitochondria as determined by ion distribution. *Eur. J. Biochem.*, **50:** 305-315.

Nicholls D.G., Bernson V.S.M., and Heaton G.M. (1978) The identification of the component in the inner membrane responsible for regulating energy dissipation. In *Effectors of Thermogenesis*, Edited by: L. Girardier and J. Seydoux., Birkhauser Verlag., Basel., pp. 89-93.

Nicholls D.G., and Locke R.M. (1984) Thermogenic mechanisms in brown fat. *Physiol. Rev.*, **64:** (1), 1-64.

Noben-Trauth K., Naggert J.K., North M.A., and Nishina P.M. (1996) A candidate gene for the mouse mutation tubby. *Nature*, **380:** 534-538.

Nobes C.D., Brown G.C., Olive P.N., and Brand M.D. (1990) Non-ohmic proton conductance of the mitochondrial inner membrane in hepatocytes. *J. Biol. Chem.*, **265:** 12903-12909.

Pi-Sunyer X. (1993) Medical hazards of obesity. *Ann. Intern. Med.*, **119:** 657-660.

Porter R.K., and Brand M.D. (1993) Body mass dependence of H+ leak in mitochondria and its relevance to metabolic rate. *Nature*, **362:** 628-630.

Porter R.K., and Brand M.D. (1995a) Causes and differences in respiration rate of hepatocytes from mammals of different body mass. *Am. J. Physiol.*, **269:** R1213-R1224.

Porter R.K., and Brand M.D. (1995b) Cellular oxygen consumption depends on body mass. *Am. J. Physiol.*, **269:** R226-R228.

Porter R.K., Hulbert A.J., and Brand M.D. (1996) Allometry of mitochondrial proton leak - Influence of membrane surface area and fatty acid composition. *Am. J. Physiol.*, **40:** (6), R1550-R1560.

Rabelo R., Reyes C., Schifman A., and Silva J.E. (1996) A complex retinoic acid response element in the uncoupling protein gene defines a novel role for retinoids in thermogenesis. *Endocrinology*, **137:** 3488-3496.

Reynafarje B., Costa L.E., and Lehniger A.L. (1985) O2 solubility in aqueous media determined by a kinetic method. *Anal. Biochem.*, **145:** 406-418.

Rial E., Poustie A., and Nicholls D.G. (1983) Brown-adipose-tissue mitochondria: the regulation of the 32000-MW uncoupling protein by fatty acids and purine nucleotides. *Eur. J. Biochem.*, **137:** 197-203.

Ricquier D., Bouillaud F., Toumelin P., Mory G., Bazin R., Arch J., and Penicaud L. (1986) Expression of uncoupling protein mRNA in thermogenic or weakly thermogenic brown adipose tissue. Evidence for a rapid beta-adrenoreceptor-mediated and transcriptionally regulated step during activation of thermogenesis. *J. Biol. Chem.*, **261:** (30), 13905-13910.

Ricquier D., and Kader J.-C. (1978) Mitochondrial protein alteration in active brown fat: a sodium dodecyl sulfate-polyacrylamide gel electrophoretic study. *Biochem. Biophys. Res. Commun.*, **73:** 577-583.

Rohlfs E.M., Daniel K.W., Premont R.T., Kozak L.P., and Collins S. (1995) Regulation of the uncoupling protein gene (Ucp) by beta 1, beta 2, and beta 3-adrenergic receptor subtypes in immortalized brown adipose cell lines. *J. Biol. Chem.*, **270:** (18), 10723-10732.

Rohner-Jeanrenaud F., and Jeanrenaud B. (1997) Central nervous system and body weight regulation. *Annales d'Endocrinologie*, **58:** (2), 137-142.

Rolfe D.F.S., and Brand M.D. (1996a) Contribution of mitochondrial proton leak to skeletal muscle respiration and to standard metabolic rate. *Am. J. Physiol.*, **270:** C1380-C1389.

Rolfe D.F.S., and Brand M.D. (1996b) Proton leak and control of oxidative phosphorylation in perfused, resting rat skeletal muscle. *Biochim. Biophys. Acta*, **1276:** (1), 45-50.

Rolfe D.F.S., and Brand M.D. (1997) The physiological significance of mitochondrial proton leak in animal cells and tissues. *Bioscience Reports*, **17:** (1), 9-16.

Rolfe D.F.S., and Brown G.C. (1997) Cellular energy utilization and molecular origin of standard metabolic rate in mammals. *Physiol. Rev.*, **77:** (3), 731-758.

Rolfe D.F.S., Hulbert A.J., and Brand M.D. (1994) Characteristics of mitochondrial proton leak and control of oxidative phosphorylation in the major oxygen-consumming tissues of the rat. *Biochim. Biophys. Acta*, **1188:** 405-416.

Rosenbaum M. (1997) Medical progress - Obesity. *N. Eng. J. Med.*, **337:** (6), 396-407.

Rothwell N.J., and Stock M.J. (1979) A role for brown adipose tissue in diet-induced thermogenesis. *Nature*, **281:** 31-35.

Samec S., Seydoux J., and Dulloo A.G. (1998) Role of UCP homologues in skeletal muscles and brown adipose tissue: mediators of thermogenesis or regulators of lipids as fuel substrate? *FASEB J.*, **12:** (9), 715-724.

Sanchis D., Fleury C., Chomiki N., Goubern M., Huang Q., Neverova M., Gregoire F., Easlick J., Raimbault S., Levi-Meyrueis C., Miroux B., Collins S., Seldin M., Richard D., Warden C., Bouillaud F., and Ricquier D. (1998) BMCP1, a novel mitochondrial carrier with high expression in the central nervous system of humans and rodents, and respiration uncoupling activity in recombinant yeast. *J. Biol. Chem.*, **273:** (51), 34611-34615.

Schacterle G., and Pollack R. (1973) A simplified method for the quantitative assay of small amounts of protein in biological material. *Anal. Biochem.*, **51:** 654-655.

Schmidt-Nielsen K. (1984). "Scaling: Why is animal size so important?" Cambridge University Press, Cambridge, UK, 183.

Schutz Y. (1995) The basis of direct and indirect calorimetry and their potentials. *Diabetes Metab. Rev.*, **11:** 383-408.

Seldin M.F., Mott D., Bhat D., Petro A., Kuhn C.M., Kingsmore S.F., Bogardus C., Opara E., Feinglos M.N., and Surwit R.S. (1994) Glycogen synthase: A putative locus for diet-induced hyperglycemia. *J. Clin. Invest.*, **94:** 269-276.

Shinohara Y., Shima A., Kamida M., and Terada H. (1991) Uncoupling protein is expressed in liver mitochondria of cold-exposed and newborn rats. *FEBS Lett.*, **293:** (1-2), 173-174.

Silva J.E. (1995) Thyroid hormone control of thermogenesis and energy balance. *Thyroid*, **5:** (6), 481-492.

Silva J.E., and Rabelo R. (1997) Regulation of the uncoupling protein gene expression. *Eur. J. Endocrinol.*, **136:** (3), 251-264.

Silver L.M. (1995) Mouse Genetics: Concepts and Applications. Oxford University Press, New York., pp. 362

Slinde E., Pederson J.I., and Flatmark T. (1975) Sedimentation coefficient and buoyant density of brown adipose tissue mitochondria from guinea pig. *Anal. Biochem.*, **65:** 581-585.

Smith R.E., and Hock R.J. (1963) Brown fat: thermogenic effector of arousal in hibernators. *Science*, **140:** 199-200.

Smith R.E., and Horwitz B.A. (1969) Brown fat and thermogenesis. *Physiol. Rev.*, **49:** (2), 330-425.

Solanes G., Vidal-Puig A., Grujic D., Flier J.S., and Lowell B.B. (1997) The human uncoupling protein-3 gene: Genomic structure, chromosomal localization, and genetic basis for short and long form transcripts. *J. Biol. Chem.*, **272:** (41), 25433-25436.

Surwit R.S., Wang S.Y., Petro A.E., Sanchis D., Raimbault S., Ricquier D., and Collins S. (1998) Diet-induced changes in uncoupling proteins in obesity-prone and obesity-resistant strains of mice. *Proc. Nat. Acad. Sci.*, **95:** (7), 4061-4065.

Susulic V.S., Frederich R.C., Lawitts J., Tozzo E., Kahn B.B., Harper M.-E., Himms-Hagen J., Flier J.S., and Lowell B.B. (1995) Targeted disruption of the β3-adrenergic receptor gene. *J. Biol. Chem.*, **270:** (49), 29483-29492.

Tata J.R. (1964) Basal metabolic rate and thyroid hormones. In *Advances in Metabolic Disorders*, Edited by: R. Levine and R. Luft., Academic., New York., pp. 153-189.

Taylor B.A., and Phillips S.J. (1996) Detection of obesity QTLs on mouse chromosomes 1 and 7 by selective DNA pooling. *Genomics*, **34:** 389-398.

Taylor B.A., and Phillips S.J. (1997) Obesity QTLs on mouse chromosomes 2 and 17. *Genomics*, **43:** (3), 249-257.

Vidal-Puig A., Solanes G., Grujic D., Flier J.S., and Lowell B.B. (1997) UCP3: An uncoupling protein homologue expressed preferentially and abundantly in skeletal muscle and brown adipose tissue. *Biochem. Biophys. Res. Commun.*, **235:** (1), 79-82.

Walder K., Norman R.A., Hanson R.L., Schrauwen P., Neverova M., Jenkinson C.P., Easlick J., Warden C.H., Pecqueur C., Raimbault S., Ricquier D., Silver M.H.K., Shuldiner A.R., Solanes G., Lowell B.B., Chung W.K., Leibel R.L., Pratley R., and Ravussin E. (1998) Association between uncoupling protein polymorphisms (UCP2/UCP3) and energy metabolism: Obesity in Pima Indians. *Hum. Mol. Genet.*, **9:** (7), 1431-1435.

Warden C.H., and Fisler J.S. (1994) Identification of genes underlying polygenic obesity in animal models. In *The Genetics of Obesity*, Edited by: C. Bouchard., CRC Press., Boca Raton, Florida., pp. 181-197.

Warden C.H., Fisler J.S., Shoemaker S.M., Wen P.-Z., Svenson K.L., Pace M.J., and Lusis A.J. (1995) Identification of four chromosmal loci determining obesity in a multifactorial mouse model. *J. Clin. Invest.*, **95:** 1545-1552.

Weigle D.S., Selfridge L.E., Schwartz M.W., Seeley R.J., Cummings D.E., Havel P.J., Kuijper J.L., and BeltrandelRio H. (1998) Elevated free fatty acids induce uncoupling protein 3 expression in muscle: a potential explanation for the effect of fasting. *Diabetes,* **47:** (2), 298-302.

West D.B., Truett G.E., Goudey-Lefevre J., and York B. (1995) Loci of chromosomes 4, 7, 9, 12 and 15 control a significant proportion of dietary obesity phenotype in the mouse. *FASEB J.,* **9:** A722.

York B., Lei K., and West D.B. (1996) Sensitivity to dietary obesity linked to a locus on chromosome 15 in a Cast/Ei x C57BL/6J F2 intercross. *Mamm. Gen.,* **7:** 677-681.

York B., Truett A.A., Monteiro M.P., Barry S.J., Warden C.H., Naggert J.K., Maddatu T.P., and West D.B. (1999) Gene-environment interaction: a significant diet-dependent obesity locus demonstrated in a congenic segment on mouse chromosome 7. *Mamm. Gen.,* **10:** 457-462.

York D.A. (1996) Lessons from animal models of obesity. *Endocrinology & Metabolism Clinics of North America,* **25:** (4), 781 ff.

Manon Danielle Gagné

Permanent Address:
318 Marleau Rd
Sturgeon Falls, ON
P0H 2G0
Tel: (705) 753-0629

Local Address:
15 Spindle Way
Stittsville, ON
K2S 1J4
Tel: (613) 831-1246

Lab: (613) 562-5800 x 8230
email: ***manon.gagne@sympatico.ca***

EDUCATION

1997- Present — **M.Sc. Biochemistry**
University of Ottawa, Ottawa (Ontario)
Expected: July 1999

1993-1997 — **B.Sc. Hon. Biochemistry**
Summa Cum Laude
University of Ottawa, Ottawa (Ontario)
Conferred: June 1997

1988-1993 — **O.S.S.D (Ontario Secondary School Diploma)**
École Secondaire Franco-Cité, Sturgeon Falls (Ontario)
Conferred: June 1993

SCHOLARSHIPS AND DISTINCTIONS

- «Fondation Baxter & Alma Ricard» – post-graduate fellowship (1999)
  Awarded to French Canadians living in a linguistic minority situation
  Value: $19,000/yr (renewable for up to three years)

- Eva Princz Award - Travel grant from the Department of Biochemistry (1998)
  Prize: $500

Manon Danielle Gagné
Tel: (613) 831-1246
Lab: (613) 562-5800 x 8230
email: manon.gagne@sympatico.ca

- North American Association for the Study of Obesity (NAASO) Travel Grant (1998)
  Young Investigator Award finalist
  Prize: $ 1,000 to attend the 8th International Congress on Obesity and present research results at the 8th International Congress on Obesity symposium "Genetic and Molecular basis of Obesity" August 25th to September 3rd 1998 , in Paris, France.

- Natural Sciences and Engineering Research Council (NSERC) Scholarship (1997- 1999)
  Location of Tenure: Mary-Ellen Harper's Laboratory, Department of Biochemistry, Microbiology and Immunology, University of Ottawa
  Value: 1997-1998 → $15,700
  1998-1999 → $17,300

- University of Ottawa Excellence Scholarship (1997)
  NSERC recipient award
  Prize: $2,000

- University of Ottawa Excellence Scholarship (1997-1999)
  Tuition waiver for duration of Masters studies
  Prize: over $5,000

- Plaque of the Department of Biochemistry (1997)
  For graduating with the highest CGPA

- Plaque from The Chemical Institute of Canada (Biochemistry) (1997)

- Dean's Honour List (1993-1997)

- University of Ottawa Admission Scholarship (1993-1997)
  Undergraduate studies
  Prize: $1,500/yr for 3yrs; $1,800/yr for 1yr

- Canada Scholarships in Science and Engineering (1993-1997)
  Prize: $2,500/yr for 4yrs

- Scholarship to study in French (1993)
  Prize: $2,000

- Governor General medal (1993)
  For having achieved the highest mark of my graduating class

- High School Academic Bursaries (1992-1993)
  Plaques and monetary awards for excellence in subjects such as English, Physics, Chemistry, Biology, Calculus and All Around Academic Excellence

Manon Danielle Gagné
Tel: (613) 831-1246
Lab: (613) 562-5800 x 8230
email: manon.gagne@sympatico.ca

ABSTRACTS AND PRESENTATIONS

1) **Manon Danielle Gagné,** Barbara York, David B. West, and Mary-Ellen Harper. (1998) *Congenic mice at UCP2 and UCP3 show no differences in body fat or skeletal muscle mitochondrial uncoupling on a low-fat diet.* **Poster presentation** at the Genetic and Molecular Bases of Obesity satellite symposium of the 8th International Congress on Obesity, August 26-28th, 1998, Paris, France.

2) **Manon Danielle Gagné,** Barbara York, David B. West, and Mary-Ellen Harper. (1999) *Les souris congéniques en UCP2/3 sont résistantes à l'obésité induite par un régime hyperlipidique, mais possèdent dans leurs muscles une fuite de protons mitochondriale normale.* **Affiche présentée** au 67e Congrès de l'ACFAS (Association canadienne-française pour l'avancement des sciences), du 10-14 mai 1999, Ottawa, Ontario.

EMPLOYMENT HISTORY

1997- Present — **INDUSTRY CANADA – CIPO (Canadian Intellectual Property Office)**
Hull (Québec)
Representative Drawing Identifier
- Worked on the Patent Representative Drawing Backcapture Project aimed at generating an on-line abbreviated version of all patent applications including those pending approval
- Supervised and trained new personnel
- Utilised the Canadian Patent Data base, a proprietary type software called Techsource
- Conducted quality control and quality assurance analyses

Supervisor: Gale Connah (819) 994-6704

1997-1998 — **UNIVERSITY OF OTTAWA - Biochemistry Department**
Ottawa (Ontario)
Teacher's Assistant / Laboratory Demonstrator
- Demonstrated proper and safe use of laboratory equipment
- Guided, assisted, and evaluated students' work
- Marked laboratory reports and final laboratory exams
- Translated exam questions
- Proctored and supervised final exams

Lab Co-ordinator: Dr. Miguel Rodriguez (613) 562-5800 x 6803

Manon Danielle Gagné
Tel: (613) 831-1246
Lab: (613) 562-5800 x 8230
email: manon.gagne@sympatico.ca

1996 and 1994 (May-August)

FUND RAISER PRODUCTS
Ottawa (Ontario)
Administrative Assistant

- Performed daily administrative and secretarial work including word processing, typing, filing, preparing legal documents, data entry and assisting callers
- Participated in the development of the company's Nevada Management System designed to administer every aspect of the business including placement and tracking of orders, accounts payable, accounts receivable etc...

Employer: Georges Robert, President (613) 724-6040

1995 (May-August)

REVENUE CANADA -- Client Services Directorate
Ottawa (Ontario)
Clerk

- Provided administrative and clerical support to the Division, and receptionist services to the Directorate
- Underwent government security screening at the level of "Enhanced Reliability Check"
- Passed the Second Language Evaluation with levels of C in Reading, C in Writing and EX in Oral Interaction

Employer: Janice Parent
A/Manager, Finance & Administration
Client Services Directorate

1993 and 1992 (Summer)

NIPISSING BOARD OF EDUCATION – Summer School
North Bay (Ontario)
Environmental Science and Outdoors Course Instructor

- Supervised groups of students (ages 9 to 16)
- Made camping and excursion preparations
- Maintained discipline

Employer: Ronald Beauchamp, director (705) 753-3739

SPECIAL SKILLS AND ABILITIES

Computer Skills

Word Processors: WordPerfect, Word
Spreadsheets: Excel, Graph Pad Prism
Presentation Tools: PowerPoint
Other: Windows95, Netscape

Communication Skills

Perfectly bilingual in both official languages of Canada